Department of Pathobiology
University of Veterinary Medicine Vienna

Institute of Immunology
(Head: Univ.-Prof. Dr. Armin Saalmüller)

Phenotypic and functional differentiation of porcine CD8$^+$ cytolytic T cells

PhD thesis submitted for the fulfilment of the requirements for the academic degree of

Doctor of Philosophy (PhD)

University of Veterinary Medicine Vienna

submitted by

Emil Lagumdzic, Mag.med.vet.

Vienna, July 2023

PhD Committee

First Supervisor
Prof. Dr. Armin Saalmüller
Institute of Immunology
Department of Pathobiology
University of Veterinary Medicine Vienna
Veterinärplatz 1
1210 Vienna, Austria
armin.saalmueller@vetmeduni.ac.at

Second Supervisor
Prof. Dr. Till Rümenapf
Institute of Virology
Department of Pathobiology
University of Veterinary Medicine Vienna
Veterinärplatz 1
1210 Vienna, Austria
till.ruemenapf@vetmeduni.ac.at

Oath

I hereby declare under oath that this PhD thesis at the University of Veterinary Medicine Vienna is the product of my own independent work. All content and ideas drawn directly or indirectly from external sources are indicated as such. The thesis has not been submitted to any other examining body and has not been published.

Acknowledgments

I would like to express my deep gratitude to Prof. Dr. Armin Saalmüller, my research supervisor, for his patient guidance, enthusiastic encouragement, and useful critiques of this research work. His expertise and mentorship have been instrumental in shaping the success of this endeavour.

Furthermore, I would also like to thank research fellows for their valuable and constructive suggestions during the planning and development of this research work. Their input has significantly enriched the quality and depth of this work.

I would also like to thank my wife Nejla for her unwavering support, understanding, and love throughout this journey. Her encouragement and belief in me have been pivotal in overcoming challenges and achieving success.

Finally, I must express my very profound gratitude to my parents, Fatima and Safet, and my brother Eli for providing me with unfailing support and continuous encouragement throughout my academic journey and through the process of researching and writing this thesis. This accomplishment would not have been possible without them. Thank you sincerely for everything.

Table of contents

Abstract

The pig, with its anatomical, physiological, and metabolic similarities to humans, holds great potential as a research model for human diseases, pharmacology, and transplantation studies. However, a better understanding of the porcine immune system is essential. In this study, we investigated the transcriptomes of porcine $CD8^+$ T-cell subsets and the response of $CD8^+$ T cells after PRRSV infection.

First, we characterized the gene expression profiles of three distinct subsets of porcine $CD8^+$ T cells based on their CD11a/CD27 expression pattern: naïve (T_n; $CD8\beta^+CD27^+CD11a^{low}$), intermediate ($T_{inter}$; $CD8\beta^+CD27^{dim}CD11a^+$), and terminally differentiated cells (T_{term}; $CD8\beta^+CD27^-CD11a^{high}$). Our analysis revealed significant differences in gene expression between these subsets. T_n displayed a unique gene expression profile associated with early stages of T-cell differentiation, characterized by the upregulation of key transcription factors (*LEF1*, *BACH2*, *TCF7*), lymph node homing receptors (*CCR7*, *SELL*, *CCR9*), and genes involved in maintaining quiescence (*SATB1*, *ZEB1*, *BCL2*). In contrast, T_{term} exhibited a distinct gene expression signature associated with late-stage differentiation, marked by the upregulation of cytolytic genes (*GNLY*, *PRF1*, *GZMB*, *FASL*, *IFNG*, *TNF*) and effector molecules. On the other hand, T_n did not exhibit expression of genes associated with cytolytic activity, even after *in vitro* stimulation. Furthermore, the T_{inter} showed a gene expression profile more closely resembling later stages of T-cell differentiation.

In the second study, we investigated the immune response of porcine $CD8^+$ T cells after PRRSV infection. $CD8^+$ T cells exhibited a strong adaptive immune response, with the highest number of DEGs observed at 21 dpi. This response led to the formation of highly differentiated $CD8^+$ T cells starting from 14 dpi. The gene expression pattern of $CD8^+$ T cells revealed a distinctive profile characterized by the upregulation of effector and cytolytic genes (*PRF1*, *GZMA*, *GZMB*, *GZMK*, *KLRK1*, *KLRD1*, *FASL*, *NKG7*), indicating

their pivotal role in the immune response after PRRSV infection. Temporal clustering analysis of DEGs in $CD8^+$ T cells revealed four clusters, indicating tight transcriptional regulation of the adaptive immune response to PRRSV. The main clusters in $CD8^+$ T cells represented the initial transformation and differentiation of these cells in response to PRRSV infection. GSEA further supported the effector state of $CD8^+$ T cells at 21 dpi, with significant enrichment of gene sets associated with effector $CD8^+$ T cells, IFN-α and IFN-γ responses, inflammatory response, T-cell activation and maintenance of effector $CD8^+$ T cells during infection. Furthermore, the flow cytometry analysis of $CD8^+$ T cells revealed a significant expansion of T_{inter} and T_{term} subsets in the PRRSV-infected animals, indicating the impact of the infection on the $CD8^+$ T-cell differentiation.

These studies provide comprehensive insights into the gene expression profiles and immune responses of porcine $CD8^+$ T cells during PRRSV infection. The findings highlight the dynamic nature of the immune response and provide potential biomarker targets for vaccine and therapeutic development. The combination of these studies expands our understanding of the porcine immune system and its interaction with pathogens, contributing to the advancement of porcine immunology research.

1. Introduction

1.1. CD8$^+$ T cells

The immune system is a complex and highly organized defence network that protects the body against a wide array of pathogens and diseases. Its sophisticated network of cells, tissues, and molecules works together to detect and eliminate foreign antigens, ensuring the body's health and well-being (1). At the forefront of this defence system are antigen-specific T cells, a group of lymphocytes that play a crucial role in adaptive immunity. T cells, along with B cells, form the backbone of the adaptive immune response, which provides long-lasting protection against specific pathogens. While B cells primarily differentiate into plasma cells to produce antibodies (2), T cells exhibit a diverse range of functions critical for effective immune defence. Among the various subsets of T cells, CD8$^+$ T cells hold a prominent position due to their unique capabilities and contributions. CD8$^+$ T cells, often referred to as cytotoxic T lymphocytes (CTLs), express CD8 heterodimer, which is composed of α and β chains connected through disulphide bond (3,4). They possess extraordinary potential in combating infections and eradicating abnormal cells (5) and are armed with specialized receptors and effector mechanisms that allow them to recognize, engage, and eliminate target cells displaying signs of infection or malignancy. Specifically, CD8$^+$ T cells express T cell receptors (TCRs) on their surface and through their specific recognition of antigenic peptides presented by major histocompatibility complex class I (MHC-I) molecules, CD8$^+$ T cells execute their cytotoxic functions with precision, ensuring the removal of infected or abnormal cells (6). In general, cytolytic capacity of CTLs is characterized by two mechanisms, namely membranolytic through the release of cytotoxic granules such as perforin and granzymes or the induction of apoptosis in targeted cell through Fas/Fas-ligand interaction (7–10). Also, in response to infection CTLs produce cytokines (INF-γ) and tumor necrosis factor α (TNF-α) that have antimicrobial and antitumor effects (10,11).

1.2. Development of $CD8^+$ T cell

The development of $CD8^+$ T cells is highly regulated, and it takes place within the thymus during a process called thymic selection or thymocyte development. The process starts with the differentiation of hematopoietic stem cells into common lymphoid progenitor in the bone marrow (12). Lymphoid progenitors migrate to the thymus where they receive a signal from thymic epithelial cells via Notch signalling pathway that initiates commitment to the T-cell lineage (13). Afterwards, lymphoid progenitors give rise to double-negative thymocytes (DN, no CD4 or CD8) and they can be further differentiated into four stages by their expression of CD44 and CD25, namely: DN1 ($CD44^+CD25^-$); DN2 ($CD44^+CD25^+$); DN3 ($CD44^-CD25^+$); and DN4 ($CD44^-CD25^-$) (14).

DN1 or early thymic progenitor cells (ETPs) express high levels of c-Kit and undergo proliferation and rearrangement of their T cell receptor (TCR) genes (15,16). Next, DN1 cells transition to the DN2 or pro-T cells, by undergoing further proliferation and rearrangement of TCR genes. In this phase, the cells begin to express the pre-TCR complex composed of a surrogate α chain (pre-Tα) and a rearranged β chain. The pre-TCR complex plays a crucial role in signalling and subsequent development (17,18). In the DN3 stage, DN cells lose c-Kit expression and undergo β-selection, which involves positive selection of cells that successfully rearrange and express a functional TCRβ chain in association with the pre-Tα chain, encoded by a non-rearranging locus, and this process determines whether the cells can progress to the DP stage (19). DN3 or pre-T cells that successfully undergo β-selection progress to the DN4 stage, where the cells finalize the rearrangement of their TCR genes and undergo proliferation leading to the loss of CD25 expression. Finally, the transition from DN to double-positive (DP) occurs when DN4 cells begin expressing both CD4 and CD8 co-receptors on their surface, becoming DP cells (18).

After the DP stage, the next step in T cell development is positive selection in the thymus, during which DP cells interact with self-peptides presented by major histocompatibility complex (MHC) molecules on thymic epithelial cells (20,21). The majority of DP thymocytes that have inadequate TCR/co-receptor signalling cannot sustain viability and this leads to delayed apoptosis or death by neglect (12). In the medulla most of DP cells undergo rapid negative selection through acute apoptosis, which eliminates T cells with high affinity for self-peptides presented by MHC molecules, preventing the development of auto-reactive T cells (22–24). However, few immature T cells that have a TCR capable of recognizing self-peptides in the context of MHC molecules with appropriate affinity receive survival signals and progress to the next stage. The surviving cells that pass negative selection initiate effective maturation and ultimately differentiate into lineage-specific CD8 single-positive (SP) cells which are then ready to move from the medulla to other peripheral lymphoid tissues. At this stage SP cells express sphingosine 1-phosphate (S1P) receptor known as S1PR, which attracted by high amount of S1P in peripheral blood, induce their egress from thymus into blood where they become part of the circulating naïve T-cell population (25,26).

1.3. Differentiation stages of $CD8^+$ T cells

Generally, naïve $CD8^+$ T cells show limited functional activity and are phenotypically characterized by surface expression of CD45RA, lymph node homing receptors CCR7 and/or CD62L (L-selectin) (27). Once the naïve $CD8^+$ T cells encounter their specific antigen, presented as peptide:MHC complex by conventional dendritic cell, they become activated and undergo rapid differentiation and proliferation resulting in formation of effector $CD8^+$ T cells. Human effector $CD8^+$ T cells can be differentiated into short-lived effector cells (SLEC; $CD127^-KLRG1^+$), which mostly die via apoptosis during the immune contraction phase, or memory-precursor effector cells (MPEC; $CD127^+KLRG1^-$), which are able to form long-lived memory $CD8^+$ T cells (28–30). Moreover, SLEC show a low memory potential, acute dependence on IL-15 for survival, and high IL-12 induced T-bet expression, which drives SLEC formation and commitment. In contrast, MPEC have a memory potential, lower T-bet expression, self-renewal potential, and are dually responsive to IL-7 and IL-15 (31). Also, during acute and chronic infections they express high amounts of CXCR3 and intermediate to high amounts of CX3CR1 as well as high cell plasticity, enabling them to give rise to different memory subsets (32).

After antigen clearance most of effector $CD8^+$ T cells die off in process of controlled apoptosis. However, small fraction of memory-precursor cells develops into long-lived memory T cells, capable of inducing faster and stronger in case of secondary infection (33). A small fraction of minimally differentiated circulating $CD8^+$ T cells with stem cell–like ability to self-renew and the pluripotent potential are known as stem cell memory T cells (T_{SCM}) (34). At first, these T_{SCM} were included in naïve $CD8^+$ T cells, however now they are defined as a unique population that represent the bridge between naïve and memory $CD8^+$ T cells. Even though T_{SCM} express CCR7 and CD62L similar to naïve $CD8^+$ T cells, they additionally express CD95, which is known as typical marker of $CD8^+$ T memory cells (27). Furthermore, T_{SCM} also express CXCR3, IL-2Rβ, CD58 and CD11a and show functional characteristics of memory cells such as rapid proliferation and release of inflammatory cytokines after reencountering antigen (35,36).

Based on the expression CCR7 and CD62L, memory $CD8^+$ T cells can be classified into two populations: central memory T cells (T_{CM}) and effector memory T cells (T_{EM}). In contrast to T_{SCM} with the $CD95^+CD45RA^+CD45RO^-CCR7^+CD62L^+$ profile, central memory T cells show $CD95^+CD45RA^-CD45RO^+CCR7^+CD62L^+$ profile (27). However, effector memory T cells (T_{EM}) lack expression of lymphoid-organ homing markers (CCR7, CD62L) and express highly markers associated with more differentiated status such as T-bet, ZEB2, and BLIMP1 (37,38). Moreover, based on the expression of chemokine receptors CXCR3 and CCR5, T_{EM} are able to migrate to infection sites where they eliminate the pathogen through to cytolytic activity. Once at inflammation site, T_{EM} release effector molecules such as perforin, granzyme B or granulysin (39). In contrary, T_{CM} are more associated with TCF-1, BCL-6, ID3 and STAT3 and are predominantly found in lymph nodes (31,39,40).

Transitional memory (T_{TM}) cells, characterized as $CD45RA^{-}CCR7^{-}$ $CD27^{+}CD28^{+}CD95^{+}$, are specific subset of intermediately differentiated memory T cells between T_{CM} and T_{EM} (41,42). Terminal differentiation of T_{EM} leads to generation of terminally differentiated subset known as T_{TE} or T_{EMRA} that show low proliferation and functional capacity and are defined as $CD45RA^{+}CCR7^{-}CD28^{-}$ (41,43). In humans, frequencies of T_{TE} increase with the age and as a result of chronic infection with human cytomegalovirus (CMV) or immunodeficiency virus (HIV) (44,45).

1.4. Porcine $CD8^{+}$ T-cell differentiation

Even though human and mice share similarities with the porcine immune system, there is still a lack of detailed information on the phenotype and differentiation stages of porcine $CD8^{+}$ T cells (46–48). Over the years a major disadvantage in further characterization of porcine $CD8^{+}$ T cells was due to shortage of specific monoclonal antibodies to describe these cells. In their seminal paper, Pauly et. al defined porcine classical swine fever virus-specific CTLs as $CD4^{-}CD6^{+}CD8^{+}$ MHC class I-restricted T lymphocytes (49). In a major advance in 1999, Saalmüller et. al first reported a high expression of CD8α in $CD4^{-}CD6^{+}CD8^{+}$ cells, representing the viral specific porcine CTLs (50). Furthermore, a number of studies have found that porcine CTLs characterized as $CD2^{+}CD3^{+}CD4^{-}CD5^{high}CD6^{+}CD8\alpha^{high}CD8\beta^{+}$ show cytolytic potential expressed through perforin production (51,52). It has now been demonstrated that naïve $CD8^{+}$ T cells at birth have $CD3^{+}CD8\alpha\beta^{+}CD27^{+}perforin^{-}SLA\text{-}DR^{-}$ profile. Over time, these cells gradually downregulate CD27 expression while simultaneously increasing perforin

expression. Furthermore, an increasing number of $CD27^{dim}SLA\text{-}DR^{+}perforin^{+}$ from week 7 was observed, indicating possible early effector $CD8^{+}$ T cells, which then transitioned into late effector $CD8^{+}$ T cells with $CD27^{-}SLA^{-}DR^{+}perforin^{+}$ phenotype (53).
More recent evidence suggests that high CD11a expression positively correlates with perforin expression in $CD8\beta^{+}$ T cells, whereas $CD8\beta^{+}CD11^{low}$ cells demonstrate reduced perforin induction. Moreover, $CD8\beta^{+}CD11a^{low}$ cells expressed CD45RA and CCR7, while $CD8\beta^{+}CD11a^{high}$ were negative for CD45RA and CCR7 (54). Consistent with prior investigations, these observations provide further evidence that naive $CD8^{+}$ T cells can be classified as $CD11a^{low}CD27^{+}CD45RA^{+}CCR7^{+}SLA\text{-}DR^{-}perforin^{-}$ (55). Building upon previous research, recent study demonstrated that porcine naïve $CD8^{+}$ T cells are $CD45RA^{+}CCR7^{+}$, while postulated effector memory (T_{EM}) and terminally differentiated (T_{TM} or T_{EMRA}) $CD8^{+}$ T cells, predominantly located in mucosal tissues, are $CD45RA^{-}CCR7^{-}$ and $CD45RA^{+}CCR7^{-}$, respectively. Also, the study revealed the presence of potential central memory $CD8^{+}$ T cells (T_{CM}), identified as $CD8^{+}CD45RA^{-}CCR7^{+}$, in PBMCs, spleen and tracheo-bronchial lymph nodes. Upon PMA/Ionomycin stimulation, blood-sorted T_{CM} and T_{EM} showed the highest production of IFN-γ and TNF-α, whereas naïve $CD8^{+}$ T cells and T_{TM} demonstrated lower capacity for cytokine production (56). When looked at T-bet and Eomes expression, $T\text{-}bet^{+}CD8$ T cells had a $CD27^{dim/-}perforin^{+}$ phenotype with the capacity for IFN-γ production, suggesting effector or effector memory profile. On other hand, $CD8^{+}$ T cells that expressed Eomes were largely $CD27^{high}perforin^{-}$ and their number declined with the age, indicating a predominantly naïve profile (57). As outlined by previous review (58), unlike humans and mice, the more detailed description of porcine $CD8^{+}$ T-cell subsets, including the identification of the additional differentiation markers and stages, is a critical problem that can be effectively addressed through the utilization of novel technologies such as RNA sequencing. Up to now, most of transcriptomic studies in swine have focused on gene expression alterations in PBMCs alone (59–61). Consequently, our understanding of the transcriptome profile of porcine $CD8^{+}$ T cells remains largely constrained by limited data.

1.5. Porcine $CD8^+$ T cells after PRRSV infection

Over the past two decades, porcine reproductive and respiratory syndrome (PRRS) has become a widespread disease that poses a significant challenge in the swine industry worldwide and leads to huge economic losses (62). PRRSV's striking ability to suppress the host immune system increases the susceptibility to secondary infections by other viral and bacterial pathogens and thus cause higher mortality rates (63–66).

$CD8^+$ T cells play a critical part of adaptive immunity against viral or bacterial infections. Once activated, they rapidly proliferate and differentiate into effector $CD8^+$ T cells known for their strong cytolytic activity (31,67). Previous studies showed that PRRSV infection leads to T-cell mediated immune response within 2 to 4 weeks. T-cell immune response to PRRSV has been confirmed through different assays including *in vitro* proliferation assays, *in vitro* IFN-γ ELISpot assays and *in vivo* delayed type hypersensitivity assays (68–71). Moreover, several studies demonstrated the *in vitro* stimulation with PRRSV increases the number of INF-γ^+CD8^+ T cells in multiple tissues such as PBMCs, lung, BAL and tracheo-bronchial lymph nodes (72–75). However, a previous study revealed the impairment of CTL activity upon *in vitro* restimulation with PRRSV Lelystad virus strain, despite the proliferation of $CD3^+CD8^{high}$ cells from 14 dpi (71). A possible explanation is that the time point of blood sampling plays significant role in the detection of CTLs and their direct effector activity in the PBMCs, as the time window for virus-specific CTL activity is rather short (76,77). Also, considering that the infection with different PRRSV strains results in varying severity of pathology, there is still considerable uncertainty with regard to these findings on CTL activity (78). In one study, Lena strain caused severe pathology at 5 weeks post-infection, leading to increase of $CD8^+$ T cells as well as of IFN-γ-producing cells in the BAL of infected animals (79). Moreover, another study demonstrated the presence of PRRSV-specific T cells already at 2 weeks post-infection. However, the efficacy of CTLs in controlling primary PRRSV infection remains uncertain, as anti-PRRSV-targeted CTLs were only observed following the clearance of viremia (71). Nevertheless, more recent evidence underscores the importance of $CD8\alpha^{+}CD27^{dim}$ early effector $CD8\beta^{+}$ T cells, as they demonstrated the strongest response against PRRSV-1 infections in comparison to other lymphocyte subsets (80). Several researchers have underscored the importance of exploring novel methodologies for the examination of CTLs in swine infected with PRRSV, indicating the demand for fresh perspectives in experimental analysis (81).

Future studies on the current topic are therefore required in order to elucidate the role of $CD8^{+}$ T cells and their specific subsets involved in adaptive immune response to PRRSV. Moreover, gaining the deeper understanding of underlying immune mechanisms and functions holds remarkable potential for the identification of biomarker targets valuable for the development of more effective vaccines and therapeutics.

As outlined by Loving et al. (82), the advancements in this field have widespread implications and will be beneficial in enhancing our understanding of immunity to other swine infectious diseases as well.

2. Aims and hypotheses

As outlined above, little is known about the differentiation stages of porcine $CD8^+$ T cells.

The following hypotheses were addressed:

- Transcriptional profiles of subsets defined by their CD11a/CD27 expression pattern, represent three differentiation stages of porcine $CD8\beta^+$ T-cell subsets: naïve (T_n; $CD8\beta^+CD27^+CD11a^{low}$), intermediate differentiated (T_{inter}; $CD8\beta^+CD27^{dim}CD11a^+$), and terminally differentiated cells (T_{term}; $CD8\beta^+CD27^-CD11a^{high}$).

- The activation of $CD8^+$ T cells during the early phase of PRRSV infection leads to their differentiation into highly specialized effector cells with strong effector and cytolytic capabilities by 21 dpi. These highly differentiated $CD8^+$ T cells are likely to be key players in the immune defence against PRRSV, contributing to the control of viral replication and the elimination of infected cells.

3. Publications

- Lagumdzic E, Pernold C, Viano M, Olgiati S, Schmitt MW, Mair KH, Saalmüller A (2022) **Transcriptome profiling of porcine naïve, intermediate and terminally differentiated CD8⁺ T cells**. Front. Immunol. 13:849922. doi: 10.3389/fimmu.2022.849922

- Lagumdzic E, Pernold P.S. C, Ertl R, Palmieri N, Stadler M, Sawyer S, Stas M R., Kreutzmann H, Rümenapf T, Ladinig A, Saalmüller A (2023) **Gene expression of peripheral blood mononuclear cells and CD8⁺ T cells from gilts after PRRSV infection.** Front. Immunol. 14: 1159970. doi: 10.3389/fimmu.2023.1159970

Additional publications not included in this thesis:

- Pernold CPS, Lagumdzic E, Stadler M, Mair KH, Jäckel S, Schmitt MW, Ladinig A, Knecht C, Dürlinger S, Kreutzmann H, Martin V, Sawyer S, Saalmüller A (2022) **Characterization of the immune system of Ellegaard Göttingen Minipigs - An important large animal model in experimental medicine**. Front. Immunol. 13:1003986. doi: 10.3389/fimmu.2022.1003986

- Pernold CPS, Lagumdzic E, Stadler M, Mair KH, Dolezal M, Jäckel S, Schmitt MW, Saalmüller A (2023) **Comparison of the reactivity of PBMCs from human and Göttingen Minipigs after in vitro stimulation and treatment with immune modulating drugs.**

frontiers in Immunology

ORIGINAL RESEARCH
published: 21 February 2022
doi: 10.3389/fimmu.2022.849922

Transcriptome Profiling of Porcine Naïve, Intermediate and Terminally Differentiated CD8⁺ T Cells

*Emil Lagumdzic[1], Clara Pernold[1], Marta Viano[2], Simone Olgiati[2], Michael W. Schmitt[3], Kerstin H. Mair[1,4] and Armin Saalmüller[1]**

[1] Department of Pathobiology, Institute of Immunology, University of Veterinary Medicine, Vienna, Austria, [2] Istituto di Ricerche Biomediche "A. Marxer" RBM S.p.A., Torino, Italy, [3] Merck Healthcare KGaA, Chemical & Preclinical Safety, Darmstadt, Germany, [4] Christian Doppler Laboratory for Optimized Prediction of Vaccination Success in Pigs, Department of Pathobiology, Institute of Immunology, University of Veterinary Medicine, Vienna, Austria

The pig has the potential to become a leading research model for human diseases, pharmacological and transplantation studies. Since there are many similarities between humans and pigs, especially concerning anatomy, physiology and metabolism, there is necessity for a better understanding of the porcine immune system. In adaptive immunity, cytotoxic T lymphocytes (CTLs) are essential for host defense. However, most data on CTLs come from studies in mice, non-human primates and humans, while detailed information about porcine $CD8^+$ CTLs is still sparse. Aim of this study was to analyze transcriptomes of three subsets of porcine $CD8\beta^+$ T-cell subsets by using next-generation sequencing technology. Specifically, we described transcriptional profiles of subsets defined by their CD11a/CD27 expression pattern, postulated as naïve ($CD8\beta^+CD27^+CD11a^{low}$), intermediate differentiated ($CD8\beta^+CD27^{dim}CD11a^+$), and terminally differentiated cells ($CD8\beta^+CD27^-CD11a^{high}$). Cells were analyzed in *ex vivo* condition as well as upon *in vitro* stimulation with concanavalin A (ConA) and PMA/ionomycin. Our analyses show that the highest number of differentially expressed genes was identified between naïve and terminally differentiated $CD8^+$ T-cell subsets, underlining their difference in gene expression signature and respective differentiation stages. Moreover, genes related to early (*IL7-R*, *CCR7*, *SELL*, *TCF7*, *LEF1*, *BACH2*, *SATB1*, *ZEB1* and *BCL2*) and late (*KLRG1*, *TBX21*, *PRDM1*, *CX3CR1*, *ZEB2*, *ZNF683*, *BATF*, *EZH2* and *ID2*) stages of $CD8^+$ T-cell differentiation were highly expressed in the naïve and terminally differentiated $CD8^+$ T-cell subsets, respectively. Intermediate differentiated $CD8^+$ T-cell subsets shared a more comparable gene expression profile associated with later stages of T-cell differentiation. Genes associated with cytolytic activity (*GNLY*, *PRF1*, *GZMB*, *FASL*, *IFNG* and *TNF*) were highly expressed in terminally and intermediate differentiated $CD8^+$ T-cell subsets, while naïve $CD8^+$ T cells lacked expression even after *in vitro* stimulation. Overall, PMA/ionomycin stimulation induced much stronger upregulation of genes compared to stimulation with ConA. Taken together, we provided comprehensive results showing transcriptional profiles of three differentiation stages of porcine $CD8^+$ T-cell subsets. In addition, our study provides a powerful toolbox for the identification of candidate markers to characterize porcine immune cell subsets in more detail.

Keywords: CD8+ T cells, RNA-Seq, transcriptome, swine, T-cell differentiation

OPEN ACCESS

Edited by:
*Enric M. Mateu,
Universitat Autònoma de Barcelona, Spain*

Reviewed by:
*Simon Paul Graham,
The Pirbright Institute, United Kingdom
Karl Kai McKinstry,
University of Central Florida, United States*

****Correspondence:***
*Armin Saalmüller
armin.saalmueller@vetmeduni.ac.at*

Specialty section:
This article was submitted to Comparative Immunology, a section of the journal Frontiers in Immunology

Received: *06 January 2022*
Accepted: *02 February 2022*
Published: *21 February 2022*

Citation:
Lagumdzic E, Pernold C, Viano M, Olgiati S, Schmitt MW, Mair KH and Saalmüller A (2022) Transcriptome Profiling of Porcine Naïve, Intermediate and Terminally Differentiated CD8⁺ T Cells. Front. Immunol. 13:849922. doi: 10.3389/fimmu.2022.849922

INTRODUCTION

$CD8^+$ T cells play a key role in immune responses against intracellular pathogens by killing infected cells. Previous studies also identified their involvement in the destruction of tumor cells whereby an increased number of $CD8^+$ T cells in colorectal, ovarian and gastric cancer was associated with a better overall survival (1–3). Furthermore, activated $CD8^+$ T cells are responsible for major histocompatibility complex class I (MHC I) mediated allograft rejection (4). $CD8^+$ T cells recognize peptide antigens presented by MHC class I molecules with their T-cell receptors (TCRs) and due to their striking feature of killing infected cells they are designated as cytotoxic T lymphocytes (CTLs). Their cytolytic activity is mediated through the release of cytotoxic granules, containing perforin and granzymes or Fas/Fas-Ligand interaction, leading to apoptosis of the target cells. Second, CTLs also produce cytokines such as interferon-γ (IFN-γ) and tumor necrosis factor (TNF), which show antimicrobial and antitumor properties (5, 6). Conventionally, differentiation stages of $CD8^+$ T cells in the murine immune system can be delineated by CD44 and CD62L surface markers. Naïve $CD8^+$ T cells (T_n) are defined as $CD44^{low}CD62L^{high}$ cells, whereas effector $CD8^+$ T cells (T_{eff}) show a $CD44^{high}CD62L^{low}$ phenotype. Based on CD127 and KLRG1 expression, effector $CD8^+$ T cells can be further differentiated into short-lived effector cells (SLEC) and memory precursor effector cells (MPEC) showing $CD127^-$ $KLRG1^+$ and $CD127^+KLRG1^-$ phenotypes, respectively (7, 8). Moreover, low expression of CD11a and high expression of CD27 is associated with T_n, while T_{eff} show high expression of CD11a and low expression of CD27. Expression levels of CD11a enable the identification of antigen-experienced $CD8^+$ T cells and correlates positively with cytolytic activity and SLEC generation, whereas its absence favors formation of MPEC (9, 10). Different populations of $CD8^+$ memory T-cells can be identified by using CD44, CD62L, CD69, CXCR1 and CD49d markers. Bach2 has been identified as being a transcription factor expressed on T_n, while T-bet, Id2 and Blimp-1 are found on more differentiated T cells such as T_{eff} (11, 12). In the human immune system differentiation stages of $CD8^+$ T cells are described based on the expression of four main surface markers, namely: CD45RA, CD27, CD28 and CCR7. With the combination of those markers, $CD8^+$ T cells can be divided into T_n cells ($CD27^+CD28^+CCR7^+CD45RA^+$), early differentiated cells ($CD27^+CD28^+CCR7^-CD45RA^-$), early-like cells ($CD27^-CD28^+CCR7^-CD45RA^-$), intermediately differentiated cells ($CD27^+CD28^-CCR7^-CD45RA^-$), T-effector RA^+ cells ($CD27^-CD28^-CCR7^-CD45RA^+$), T-effector RA^- cells ($CD27^-CD28^-CCR7^-CD45RA^-$) and central memory T cells ($CD27^+CD28^+CCR7^+CD45RA^-$) (13–17). Although the human and murine immune systems share similarities with the porcine immune system, detailed information about the phenotype and the differentiation stages of porcine $CD8^+$ T cells is still sparse (18). Over the years, one of the major drawbacks to further characterizing $CD8^+$ T cells is the absence of specific monoclonal antibodies against the respective differentiation antigens. An initial study on cellular response of porcine virus-specific CTLs against classical swine fever virus (CSFV) infected cells described them as $CD4^-CD5^+CD6^+$ MHC-I restricted T lymphocytes (19). In 1999 Saalmüller et al. described that $CD4^-CD5^+CD6^+$ cells with high expression of CD8α represent porcine CTLs (20). A more recent study defined $CD2^+CD3^+CD4^-CD5^{high}CD6^+$ $CD8\alpha^{high}CD8\beta^+$ cells, which were also capable of perforin production, as porcine CTLs (21, 22). Previous studies by our group showed that naïve $CD8^+$ T cells express CD27 and are negative for perforin, whereas the phenotype of more differentiated $CD8^+$ T-cell subsets correlates with the increase of perforin and the decrease of CD27 expression (23). In this study we followed this hypothesis that the gradual change of CD27 expression, from intermediate to negative, indicates the transition from early to late effector or memory $CD8^+$ T cells. Furthermore, we included CD11a for the discrimination of porcine $CD8^+$ T-cell subsets, based on literature on CTL differentiation in mice (9, 10, 13). To confirm our hypothesis, we combined surface-antigen based cell sorting with transcriptome analysis of the respective subpopulations by using next-generation sequencing (NGS) technologies. We investigated three $CD8^+$ T-cell subsets considered as the differentiation stages of naïve ($CD8\beta^+CD27^+CD11a^{low}$), intermediate differentiated ($CD8\beta^+$ $CD27^{dim}CD11a^+$), and terminally differentiated cells ($CD8\beta^+$ $CD27^-CD11a^{high}$). So far, most of the transcriptomic studies in swine have addressed gene expression changes in peripheral blood mononuclear cells (PBMCs) only, i.e. upon vaccination or infection and our knowledge of the transcriptome profile of porcine $CD8^+$ T-cells is largely based on limited data (24–26). To gain deeper insight into the differentiation of the $CD8^+$ T cells we examined besides the direct *ex vivo* analyses the transcriptome changes after stimulation with different *in vitro* stimuli. Here, we include extensive gene ontology (GO) enrichment and pathway analysis, providing more detailed information about the immunological roles and functions of genes specific for the differentiation stages of porcine $CD8^+$ T-cell subsets. Therefore, this study is an important contribution to the further characterization of the immune system in swine - a species with the potential to become a highly relevant preclinical model for human diseases and pharmacological questions as well as for transplantation studies.

MATERIALS AND METHODS

Animals and Cell Isolation

Blood samples from swine were obtained from a local abattoir. Prior to blood sampling, animals were anesthetized electrically and sacrificed by exsanguination in accordance with Austrian Animal Welfare Slaughter Regulation. PBMCs were isolated from fresh heparinized blood of six animals of approximately six months of age by density gradient centrifugation (Pancoll human, density: 1.077 g/ml, PAN-Biotech, Aidenbach, Germany; 30 min at 920 x g).

Magnetic-Activated Cell Sorting (MACS)

$CD8^+$ T cells were enriched by positive selection of CD8β-labeled PBMCs using magnetic-activated cell sorting (MACS, Miltenyi

Biotec, Bergisch Gladbach, Germany). For enrichment of CD8β$^+$ T cells, freshly isolated PBMCs (1 x 10^9) were stained with an in-house produced primary monoclonal anti-CD8β antibody (clone PPT23, IgG1) for 20 min on ice. Subsequently, cells were washed once with MACS buffer [PBS w/o Ca/Mg + 2% (v/v) FCS (both Gibco^{TM}, Thermo Fisher Scientific) + 2mM EDTA (Carl Roth)], resuspended in 1,5 mL MACS buffer and incubated with magnetically labeled secondary antibody (rat-anti mouse IgG1, Miltenyi Biotec) for 30 min on ice. After a further washing step, cells were resuspended in 3 mL MACS buffer and loaded on pre-wetted LS columns (Miltenyi Biotec). The columns were applied to a magnetic field and unlabeled cells were removed by extensive washing. For final elution of the positive fraction, columns were removed from the magnetic field and CD8β$^+$ T cells were eluted in 5 mL MACS buffer. Finally, sorted cells were resuspended in cold culture medium (RPMI 1640 + 100 IU/mL penicillin + 0.1 mg/mL streptomycin (all PAN Biotech) + 10% (v/v) FCS), centrifuged and counted with a Cell Counter (XP-300 Hematology Analyzer, Sysmex Europe GmbH, Norderstedt). Purity of the positively sorted cells was over 90% (FACSCanto^{TM}II, BD Biosciences, San Jose, CA, USA).

Fluorescence-Activated Cell Sorting (FACS)

In order to further separate MACS-enriched CD8β$^+$ cells into subpopulations, CD8β$^+$ cells were FACS sorted based on surface expression of CD27 and CD11a (**Supplementary Figure S1**).

Upon magnetic-activated cell sorting, CD8β$^+$ cells were washed once with FACS buffer (RPMI 1640 + 100 IU/mL penicillin + 0.1 mg/mL streptomycin + 5% FCS + 5% porcine plasma (in-house preparation) + 2 mM EDTA) and then labeled with a goat anti-mouse IgG1-PE secondary antibody to stain residual CD8β$^+$ cells (Southern Biotech, Birmingham, AL, USA).

Free binding sites of the PE-labeled antibody were blocked with whole mouse IgG molecules (2 µg per sample, ChromPure, Jackson ImmunoResearch, West Grove, PA, USA). Afterwards, cells were incubated with directly labeled primary antibodies: CD27-Alexa647 (b30c7, mouse IgG1, in-house preparation and labeling with Alexa Fluor-647 Protein Labeling Kit, Thermo Fisher Scientific) and CD11a-FITC (BL1H8, mouse IgG2b, BioRad, Hercules, CA, USA).

Cell sorting was performed on a FACSAria (BD Biosciences) and CD8$^+$ T-cell subsets were defined as follows: naïve (CD8β$^+$CD27$^+$CD11a^{low}), intermediate differentiated (CD8β$^+$ CD27^{dim}CD11a$^+$), and terminally differentiated cells (CD8β$^+$ CD27$^-$CD11a^{high}). Subsets were sorted with an average purity greater than 96%.

In Vitro Stimulation

To identify transcriptomic differences between the CD8$^+$ T-cell subsets as well as between *ex vivo* and stimulated cells within the same CD8$^+$ T-cell subset, cells from each sorted subpopulations with at least 5 x 10^5 sorted cells were cultivated at 37°C and 5% CO_2 under following conditions: (i) 16 hours, unstimulated in culture medium, (ii) cultivation in culture medium for 14 hours followed by stimulation for two hours with phorbol 12-myristate 13-acetate (PMA, 50 ng/mL, Sigma-Aldrich, Schnelldorf, Germany) and ionomycin (500 ng/mL, Sigma-Aldrich), (iii) stimulated with concanavalin A (ConA) (5 µg/mL, Amersham Biosciences, Uppsala, Sweden) for 16 hours. Both stimulation protocols are established in our laboratory and used as high controls for proliferation experiments and cytokine induction in ELISpot assays (ConA) and as positive control for intracellular cytokine staining in flow cytometry (PMA/ionomycin). Furthermore, each CD8$^+$ T-cell subset with 5 x 10^5 was used immediately after sorting for RNA isolation without any further cell culture (*ex vivo*). Altogether four different conditions for each CTL subset were applied: cultivation in medium, stimulation with PMA/ionomycin or ConA and *ex vivo* isolation. Therefore, 72 samples (3 subsets x 4 conditions x 6 animals) were generated.

RNA Extraction, Library Preparation and Sequencing

Total RNA was isolated from the samples mentioned above using RNeasy Mini Kit with on-column DNase treatment using the RNAse-Free DNase Set (both Qiagen, Hilden, Germany), following manufacturer's protocol. Quantification and quality control of isolated RNA were assessed with both Qubit 3.0 fluorometer (RNA HS assay kit, ThermoFisher, Massachusetts, MA, USA) and Agilent 2100 Bioanalyzer (Agilent RNA 6000 Pico Kit, Agilent Technologies, Palo Alto, CA, USA). Samples with both a final yield comprised between 0.03 – 1.25 ng/µl and a RIN of 9 were prepared for sequencing with the SMARTer Stranded Total RNA-Seq v2 – Pico Input Mammalian Kit (Takara Bio Inc., Shiga, Japan). Fully automated library preparation was performed on a Microlab Star Hamilton robotic station (Hamilton Company, Reno, NV, USA). Briefly, 8 µl per sample were used for the cDNA synthesis *via* the SMART® technology (SMART technology, Clontech, USA). Thereafter, each sample was amplified to generate Illumina-compatible libraries according to the manufacturer's guidance. Libraries were validated using the Agilent 2100 Bioanalyzer (Agilent High Sensitivity DNA Kit, Agilent Technologies, Palo Alto, CA) and the Qubit 3.0 fluorometer (DNA HS assay kit, ThermoFisher, Massachusetts, MA, USA). Libraries were paired-end sequenced on two SP flow cell on NovaSeq 6000 system (Illumina Inc., San Diego, CA, USA).

Mapping and Differential Gene Expression Analysis (DGE)

Standard raw sequencing data in BCL format was converted to FASTQ files using the software bcl2fastq v2.19.1.403. After importing the FASTQ files into CLC Genomics Workbench 21.0.3 (Qiagen, Aarhus, Denmark), the reads were adapter- and quality trimmed. Prior to mapping, sequence reads were trimmed using quality score (Phred score ≤ 25) and with maximum number of 2 ambiguous nucleotides allowed. Next, the adapter sequences were trimmed off according to the Illumina Adapter List. Reads shorter than 35 and longer than 75 nucleotides were discarded.

The filtered reads were mapped to the Sus scrofa 11.1 reference genome from NCBI database (GCA_000003025.6) using default parameters of CLC Genomics RNA-Seq Analysis tool (mismatch cost = 2, insertion cost = 3, deletion cost = 3, length fraction = 0.8 and similarity fraction = 0.8). For principal component analysis (PCA), mapped reads were TMM normalized, log CPM values calculated and Z-normalization performed. For the *ex vivo* condition, differential gene expression test for differences between all pairs of CD8+ T-cell subsets using Wald test was performed. Therefore, three pairwise comparisons were made: (i) naïve vs. terminally differentiated, (ii) intermediate vs. terminally differentiated, and (iii) naïve vs. intermediate differentiated. To assess the effect of stimulation on gene expression profiles of CD8+ T-cell subsets, Wald test with medium condition as control group was used. Correspondingly, that yielded two pairwise comparisons for each CD8+ T-cell subset: (i) ConA stimulation vs. medium and (ii) PMA/ionomycin stimulation vs. medium. As criteria to define differentially expressed genes (DEGs), fold-change > |2|, maximum of the average reads per kilobase per million mapped reads (RPKM's) > 2 and a false discovery rate corrected p-value < 0.01 (FDR) were used. Venn diagram and heat map visualization of DEGs were constructed using ggvenn and pheatmap packages in R software version 4.0.2 (R Core Team, GNU General Public License). Bar charts were visualized with Tableau Desktop 2020.3 (Tableau Software Inc.).

Gene Ontology Enrichment and Pathway Analysis

For DEGs, gene ontology (GO) and enrichment analysis for immune system processes were executed using the ClueGO v.2.5.8 plug-in in the bioinformatic software Cytoscape 3.8.2. version (https://cytoscape.org). The analysis was performed for upregulated genes between CD8+ T-cell subsets and based on GO data for Sus scrofa. Following cut-off thresholds were set: at least 3 genes per GO term, two-sided hypergeometric statistical testing corrected with the Bonferroni step-down method ($p < 0.05$) and a Kappa score of 0.4. Moreover, organism-specific pathway analysis of DEGs were constructed by using KEGG mapper based on Kyoto Encyclopedia of Genes and Genomes (KEGG) pathway database with KEGG Orthology (KO) assignment.

RESULTS

Gene Expression Profiles of *Ex Vivo* Sorted CD8+ T-Cell Subsets

Based on our hypothesis that within the CD8β+ T-cell subpopulation three subsets with distinct differentiation stages can be defined, we analyzed the presumable naïve (T_n; CD8β+CD27+CD11a^{low}), intermediate differentiated (T_{inter}; CD8β+CD27^{dim}CD11a+), and terminally differentiated cells (T_{term}; CD8β+CD27-CD11a^{high}).

In total 3.59 billion paired-end reads were generated by sequencing 72 libraries. Overall, the percentage of mapping reads to the reference genome was between 90.44% and 94.87% (mean = 93.1%) with approximately 50 million paired-end reads per sample. PCA of gene expression data from all *ex vivo* CD8+ T-cell subsets revealed distinguishable differences between CTL subsets as PCA plot clustered data into three distinct groups (**Figure 1A**).

For hierarchical cluster analysis, we selected 1439 genes, which were significantly expressed in at least one pairwise comparison between CD8+ T-cell subsets (as defined in the Methods section). Afterwards, a heat map based on their gene expression values was generated. Notably, the hierarchical clustering of selected genes identified three well-defined groups of samples. The first contained all T_n samples, the second all T_{term} samples and the third all T_{inter} samples (**Figure 1B**). Genes highly expressed in T_n were downregulated in T_{term} and vice versa. This clear separation regarding gene expression could indicate transcriptional switch that CD8+ T cells undergo while differentiating from naïve to terminally differentiated CD8+ T cells. In comparison to T_n and T_{term}, T_{inter} showed upregulation of genes expressed in both groups. However, Venn diagram analysis showed that T_{inter} and T_{term} share more DEGs (n=386) than T_{inter} and T_n (n=130) (**Figure 1C**). In contrast, only one upregulated DEGs was shared between the T_n and T_{term} when compared to T_{inter}. Next, using Wald test for pairwise comparison, 575 and 709 DEGs were identified as upregulated in T_n and T_{term}, respectively (**Supplementary Table S1**). The number of upregulated DEGs was smaller in T_{inter} vs. T_{term} comparison than T_n vs. T_{inter} comparison. A higher number of upregulated DEGs (n = 492) was observed in T_{inter} compared to T_n (n = 215) CD8+ T cells. Also, higher numbers of upregulated DEGs were discovered in T_{inter} (n = 208) than in T_{term} (n = 132). To obtain further information about each stage of CD8 T-cell differentiation, gene expression profiles were compared between T_n, T_{inter} and T_{term}. We found that genes related to early stages of CD8 T-cell differentiation were highly expressed in the T_n (**Table 1**). Expression of several genes encoding transcription factors associated with naïve lymphocytes (27), including *LEF1*, *BACH2*, *TCF7* (TCF1), *SATB1*, *ZEB1* and *BCL2* were markedly increased in the T_n. In contrast, genes encoding transcription factors associated with terminally differentiated effector cells, such as *TBX21* (T-bet), *PRDM1* (Blimp-1), *ZEB2*, *ZNF683* (Hobit), *BATF*, *EZH2* and *ID2* were highly upregulated in the T_{term}.

Furthermore, T_{term} showed high expression of several genes involved in cell adhesion and migration including *CX3CR1*, *CCR5*, *CCL4* and *CCL5*. Moreover, higher expression of adhesion genes *ITGAM* (CD11b) and *ITGAL* (CD11a) (28) was observed among T_{term} compared with T_n and T_{inter}. Expression of *ITGA4* (CD49d), which together with CD44 is expressed in effector T cells and effector memory T cells (13), was upregulated in T_{inter} and T_{term}. In addition, expression of *CD44* was increased in both T_{inter} and T_{term} but not in the T_n (**Supplementary Table S1**). Conversely, genes encoding lymph node homing receptor molecules such as *CCR7*, *SELL* (CD62L) and *CCR9* were highly upregulated in the T_n. Sphingosine-1-Phosphate Receptor 1 (*S1PR1*), important for lymphocyte trafficking and upregulated in human naïve T cells (29), was also increased in the porcine T_n. Also, T_n showed high expression of genes encoding CD27 and CD28 molecules, the former in accordance with cell surface expression used for the sorting strategy.

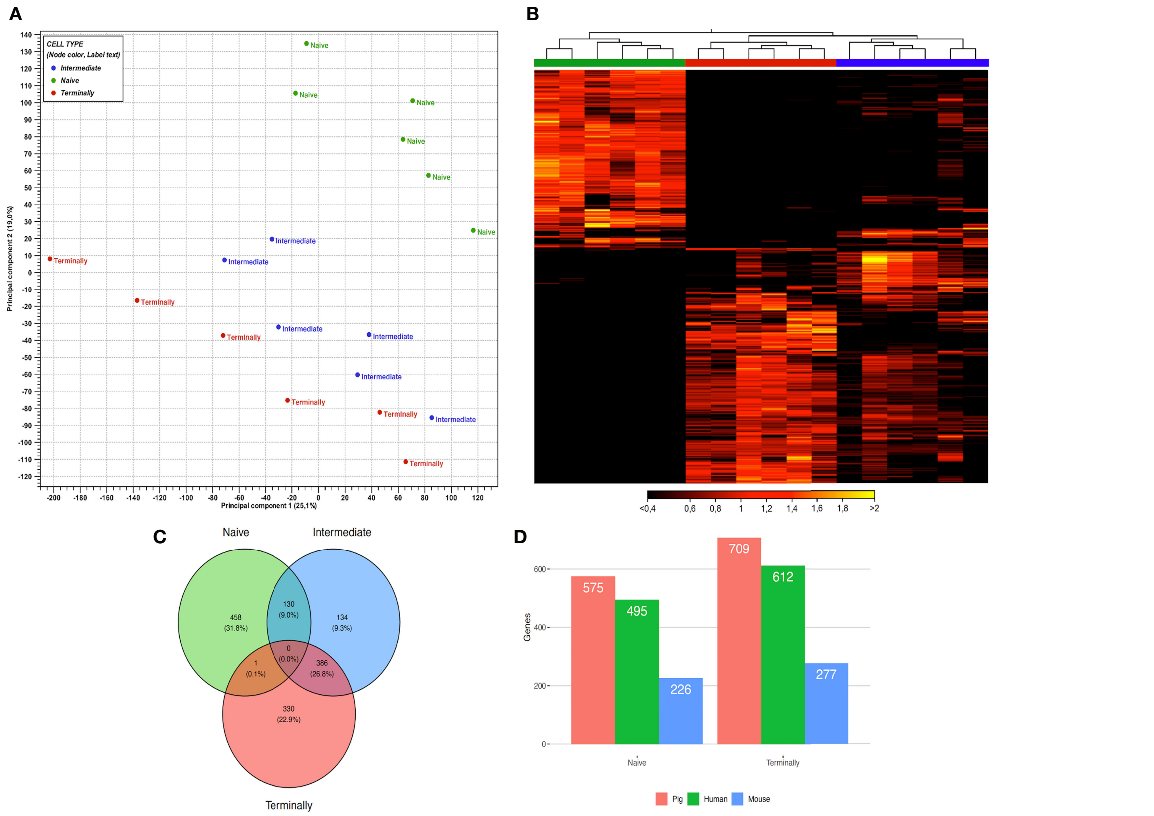

FIGURE 1 | Gene expression profiles of *ex vivo* sorted CD8$^+$ T-cell subsets. **(A)** PCA plot of expression data derived from 18 *ex vivo* CD8$^+$ T-cell subsets of six animals. Colors indicate three CD8$^+$ T-cell subsets: green, naïve CD8$^+$ T cells; blue, intermediate differentiated CD8$^+$ T cells; red, terminally differentiated CD8$^+$ T cells. PC1 explains 25.1% and PC2 explains 19% of the observed variance in data. **(B)** Heat map with hierarchical clustering of 1439 selected genes between *ex vivo* CD8$^+$ T-cell subsets. Figure illustrates clustering of three CD8$^+$ T-cell subsets based on gene expression values. Rows represent genes and columns samples, with yellow indicating high and black low expression. The dendrogram on the top indicates the correlation between samples. Colors underneath the dendrogram represent three CD8$^+$ T-cell subsets, namely: naïve (green), terminally (red) and intermediate (blue). **(C)** Venn diagram showing the overlap of 1439 DEGs between *ex vivo* CD8$^+$ T-cell subsets. Colors indicate three main CD8$^+$ T-cell subsets: green, naïve CD8$^+$ T cells; blue, intermediate differentiated CD8$^+$ T cells; red, terminally differentiated CD8$^+$ T cells. **(D)** Orthologous genes from DEGs in porcine naïve and terminally differentiated CD8$^+$ T-cell subsets compared to human and mouse.

We observed that several genes involved in T-cell effector functions and cytolytic killing, including *GNLY* (Granulysin), *PRF1* (Perforin), *GZMB* (Granzyme B), *FAS*, *FASL*, *IFNG* and *TNF*, were highly increased in T_{term} in comparison to T_n or T_{inter}. Notably, T_{term} expressed the *GNLY* 1457-fold higher in comparison to T_n. Moreover, T_{term} showed high expression of *KLRG1*, *KLRD1* and *KLRK1*, whereas T_n displayed high mRNA levels of *IL-7R* (CD127). In mouse a selective expression of *IL-7R* (CD127) is used for the discrimination between MPEC and SLEC, with the high expression specific for MPEC (8). In addition to the high expression of *IL-7R*, human MPEC show low expression of *KLRG1*, while SLEC show upregulation of *KLRG1* and low expression of *IL7R* (13).

We found higher expression of co-inhibitory molecule *PDCD1* (PD-1) in T_{inter} and T_{term} when compared to the T_n. Previous research suggests that high expression of *PDCD1* (PD-1) is specific for SLEC formation, whereas low *PDCD1* expression contributes to the T effector memory generation (30). Several genes encoding cytokine receptors associated with effector T cells were increased in the T_{term}, including *IL2RB* (CD122), *IL2RG* (CD132), *IL12RB1* and *IL12RB2*. In comparison to the T_n, T_{inter} and T_{term} showed high expression of *IRF8*, which supports the transition from naïve to effector CD8$^+$ T cells in independent matter to T-bet and Eomes (31). Furthermore, upregulation in transcript levels of *ITGB2* (CD18) and *ANXA2*, known to be increased in CD8$^+$ effector T cells (32), as well as *LGALS1*, which is expressed only on activated CD8$^+$ effector T cells but not resting CD8$^+$ T cells (33), were observed in T_{inter} and T_{term}. Additionally, genes strongly linked to cytotoxic T cells such as *S1PR5* and *ADGRG1* were substantially upregulated in the T_{term}. By contrast, T_n showed high expression of genes, which enforce quiescence state of naïve T cells (*MYB*, *FOXP1*, *KLF9* and *SOCS3*). In comparison to T_n, we found other members of SOCS family, namely SOCS1 and SOCS7, highly expressed in T_{term}. Furthermore, expression of *MKI67*, encoding proliferation marker Ki-67, was upregulated in T_{inter} and T_{term}. Both *TNFRSF1A* (TNFR1) and *TNFRSF1B* (TNFR2) were upregulated in T_{inter} and T_{term}. While transcripts of *TNFSF12*

TABLE 1 | Selected differentially expressed genes between *ex vivo* T_n, T_{inter} and T_{term}.

	T_n vs. T_{term}			T_n vs. T_{inter}			T_{inter} vs. T_{term}		
Gene name	**Fold change**		**p-value**	**Fold change**		**p-value**	**Fold change**		**p-value**
CCR7	535.18	–	4.2E-118	5.73	–	8.0E-17	93.32	–	5.8E-60
LEF1	95.23	–	8.7E-104	6.04	–	9.7E-17	15.77	–	3.4E-37
MYB	76.28	–	1.1E-72	11.64	–	1.9E-35	–	–	–
SELL	62.31	–	7.4E-35	4.97	–	1.1E-05	12.54	–	1.5E-12
IL7R	40.14	–	8.6E-72	2.38	–	1.3E-04	16.89	–	4.5E-41
CD27	29.30	–	6.5E-54	2.20	–	8.1E-04	13.34	–	9.4E-31
TCF7	26.40	–	4.0E-79	2.17	–	6.7E-05	12.14	–	6.9E-45
ZEB1	18.13	–	7.3E-78	2.23	–	3.2E-07	8.11	–	2.5E-39
MYC	14.95	–	5.0E-51	2.81	–	8.7E-08	5.32	–	8.9E-19
KLF9	12.43	–	3.9E-12	3.53	–	9.2E-04	–	–	–
CD28	12.12	–	9.1E-21	–	–	–	12.30	–	5.2E-20
CCR9	9.82	–	1.6E-16	2.47	–	2.8E-03	3.98	–	1.0E-05
BACH2	8.44	–	2.6E-33	3.80	–	3.0E-13	–	–	–
BCL2	8.13	–	7.8E-18	2.65	–	3.0E-04	3.06	–	5.7E-05
SATB1	8.04	–	1.7E-26	3.00	–	1.3E-07	2.68	–	9.4E-06
HIF1A	5.52	–	2.0E-21	–	–	–	3.79	–	2.0E-12
TNFRSF25	4.24	–	1.3E-10	–	–	–	5.68	–	7.7E-10
S1PR1	4.15	–	2.7E-23	–	–	–	3.23	–	4.6E-15
SOCS3	3.69	–	1.3E-03	–	–	–	8.91	–	3.5E-08
FOXP1	3.01	–	9.2E-19	2.35	–	3.6E-11	–	–	–
GNLY	–	1457.47	1.1E-230	–	372.87	1.1E-151	–	3.91	8.3E-11
ADGRG1	–	996.20	6,5E-221	–	285.90	1,4E-147	–	3.48	1,7E-09
CX3CR1	–	582.11	5,2E-46	–	193.70	4,3E-31	–	–	–
ZEB2	–	458.99	1,2E-239	–	143.51	3,0E-156	–	3.20	2,6E-15
S1PR5	–	377.46	3,9E-100	–	110.16	5,6E-62	–	3.43	1,0E-08
ITGAM	–	207.10	4,9E-48	–	200.19	9,5E-47	–	–	–
PRDM1	–	173.10	5,9E-114	–	73.37	2,9E-78	–	2.36	4,5E-04
GZMB	–	120.37	9,2E-65	–	58.46	4,5E-46	–	–	–
FASLG	–	118.25	1,2E-25	–	61.36	1,1E-18	–	–	–
CCL5	–	103.94	1,0E-67	–	72.50	4,2E-57	–	–	–
KLRD1	–	99.05	9,9E-49	–	–	–	–	2.56	2,7E-03
TBX21	–	87.10	1,3E-60	–	38.71	4,0E-40	–	–	–
KLRG1	–	77.32	8,5E-77	–	23.61	1,6E-39	–	3.28	3,8E-12
IFNG	–	41.96	4,3E-19	–	33.40	2,0E-16	–	–	–
KLRK1	–	37.58	4,7E-36	–	28.56	2,2E-30	–	–	–
GZMA2	–	34.53	1,3E-34	–	50.00	1,4E-41	–	–	–
SLC1A5	–	33.96	1,9E-34	–	21.16	2,7E-25	–	–	–
LGALS1	–	32.25	1,3E-38	–	25.96	2,3E-33	–	–	–
TNFAIP2	–	30.51	1,3E-23	–	10.66	2,9E-11	–	–	–
IL2RB	–	23.10	1,5E-52	–	15.97	2,1E-40	–	–	–
CCR5	–	20.13	3,6E-20	–	27.82	3,4E-24	–	–	–
ZNF683	–	19.64	3,5E-46	–	12.24	2,9E-32	–	–	–
BATF	–	14.91	2,5E-23	–	10.04	1,1E-16	–	–	–
TNF	–	14.20	2,6E-16	–	–	–	–	2.74	4,7E-03
TNFSF12	–	13.51	5,1E-42	–	7.50	1,4E-24	–	–	–
CCL4	–	11.64	2,7E-09	–	15.43	4,4E-11	–	–	–
PRF1	–	9.63	2,9E-32	–	5.39	1,2E-17	–	–	–
PDCD1	–	9.23	5,2E-13	–	8.01	3,9E-11	–	–	–
ANXA2	–	9.14	1,1E-22	–	9.13	3,2E-22	–	–	–
ITGAL	–	7.54	1,4E-29	–	4.31	2,5E-15	–	–	–
IL12RB2	–	7.22	8,3E-24	–	4.49	1,5E-13	–	–	–
MKI67	–	6.80	2,7E-11	–	19.78	3,8E-26	2.91	–	1,5E-03
TNFRSF1B	–	6.23	5,1E-19	–	5.38	8,6E-16	–	–	–
FAS	–	5.41	7,1E-28	–	5.73	2,7E-29	–	–	–
NFKBIE	–	4.52	6,3E-12	–	3.23	3,9E-07	–	–	–
IRF8	–	4.47	1,1E-08	–	6.08	5,3E-12	–	–	–
ITGB2	–	4.39	9,8E-27	–	2.73	3,0E-12	–	–	–
TNFRSF1A	–	4.24	4,0E-12	–	2.28	3,2E-04	–	–	–
RUNX3	–	4.05	1,4E-22	–	2.39	7,4E-09	–	–	–
SOCS1	–	3.66	8,5E-19	–	–	–	–	2.02	1,6E-05
ID2	–	3.62	2,2E-14	–	–	–	–	2.08	1,4E-04

(Continued)

TABLE 1 | Continued

	T_n vs. T_{term}			T_n vs. T_{inter}			T_{inter} vs. T_{term}		
Gene name	**Fold change**		**p-value**	**Fold change**		**p-value**	**Fold change**		**p-value**
TNFSF10	–	3.46	9,3E-10	–	2.51	2,1E-05	–	–	–
EZH2	–	2.92	1,0E-09	–	3.80	2,4E-14	–	–	–
ARNTL	–	2.88	6,3E-15	–	2.05	6,9E-07	–	–	–
GZMM	–	2.82	3,4E-11-	–	–	–	–	–	–
IL12RB1	–	2.77	6,6E-06	–	2.39	2,5E-04	–	–	–
ITGA4	–	2.58	4,9E-12	–	2.24	1,3E-08	–	–	–
SOCS7	–	2.29	6,5E-14	–	–	–	–	–	–
STAT4	–	2.28	7,1E-12	–	–	–	–	–	–
IL2RG	–	2.15	7,0E-07	–	2.36	3,7E-08	–	–	–

(TWEAK) and *TNFSF10* (TRAIL) were upregulated in T_{inter} and T_{term}, expression of costimulatory *TNFRSF25* (DR3) was highly induced in the T_n. Only T_{term} expressed high levels of *GZMM* and *STAT4*, on the other hand T_{inter} showed upregulation of *GZMA2*. Notably, the expression of *RUNX3*, which is important for the acquisition and maintenance of cytolytic functions of $CD8^+$ effector T cells (34), was upregulated in T_{inter} and T_{term}. Furthermore, T_{inter} and T_{term} showed increased levels of *TNFAIP2* and *NFKBIE*. Regarding genes involved in metabolism, we observed high expression of *ARNTL* and *SLC1A5* in more differentiated CTL subsets, whereas expression of *HIF1A* was upregulated in the T_n. Interestingly, when compared to T_n and T_{term}, T_{inter} shared a more comparable gene expression profile associated with later stages of T-cell differentiation. In particular, most of genes highly expressed in T_{term} were also upregulated in T_{inter}. However, the difference in expression of genes related to early stages of T-cell differentiation was substantially smaller between T_n and T_{inter} than T_n and T_{term}. Also, those genes were higher expressed in T_{inter} than T_{term}.

Identification of Swine Orthologous Genes in Human and Mice

For better understanding of the relationship between porcine, human and mouse $CD8^+$ T cells we assessed the orthology of their genes expressed in $CD8^+$ T cells in corresponding subsets publicly available on GEO Data sets (NCBI) under GDS3834 and GDS592. Here, we have focused on the analysis of DEGs in T_n and T_{term}, which cover the vast majority of DEGs generated from porcine $CD8^+$ T-cell subsets. When compared to DEGs in porcine T_n, we found 495 (86.1%) orthologs in human and 226 (39.3%) in mouse data set. In case of T_{term}, out of 709 DEGs, 612 (86.3%) were recorded in human, and 277 (39.1%) in mouse data set (**Figure 1D**).

Gene Signature of *In Vitro* Stimulated $CD8^+$ T-Cell Subsets

In order to further highlight the heterogeneity in gene expression between $CD8^+$ T-cell subsets, cells were analyzed upon stimulation with ConA and PMA/ionomycin and compared to cells cultured in medium control. Overall, a substantially higher number of upregulated DEGs in all three $CD8^+$ T-cell subsets was observed in response to PMA/ionomycin compared to ConA stimulation. Additionally, gene expressions of all PMA/ionomycin-stimulated $CD8^+$ T-cell subsets are clearly distinct from all other $CD8^+$ T-cell subsets as showed in PCA plot (**Figure 2A**). Further investigation of $CD8^+$ T-cell subsets stimulated with PMA/ionomycin revealed the highest number of upregulated DEGs in the T_{term} (1717), followed by the T_{inter} (1667) and the T_n (1383). Conversely, in $CD8^+$ T-cell subsets stimulated with ConA, the highest number of DEGs was found in the T_n (100), followed by the T_{inter} (35) and the T_{term} (36) (**Supplementary Table S1**). In order to obtain a more detailed view upon PMA/ionomycin stimulation, PCA was performed additionally only on PMA/ionomycin-stimulated $CD8^+$ T-cell subsets (**Figure 2B**). Interestingly, $CD8^+$ T-cell subsets clustering is unaltered to PMA/ionomycin stimulation, resulting again in the three distinct groups of T_n, T_{inter} and T_{term}. Despite this separate clustering, Venn diagram analysis revealed high number of DEGs shared between PMA/ionomycin-stimulated $CD8^+$ T-cell subsets (903), indicating that all three subsets acquire more similar cell properties following PMA/ionomycin stimulation. In case of ConA-stimulated $CD8^+$ T-cell subsets, we found much smaller number of shared DEGs (**Figure 2C, D**).

Several genes encoding cytokines involved in T-cell response were differentially expressed between $CD8^+$ T-cell subsets (**Figure 3A**). Looking at the expression of *IFNG* (IFN-γ) and *TNF*, we observed overexpression in all three $CD8^+$ T-cell subsets following PMA/ionomycin stimulation, but only moderate expression in T_{inter} with ConA stimulation. Porcine T_n and T_{inter} showed high expression of *IL2* and its receptor chains *IL2RA* (CD25) and *IL2RG* (CD132) as well as *IRF7* when stimulated with PMA/ionomycin. It was reported that IL2 and its receptor chains IL2RA (CD25) and IL2RG (CD132) are involved in terminal effector differentiation but also in memory development of $CD8^+$ T cells (37). Moreover, expression of *IL4*, *IL17A*, *IL18RAP* and *IL22* was induced only in the T_{inter} stimulated with PMA/ionomycin. In contrary, *IL12RB1*, *IL27RA* and *ILF3* were only expressed by the T_{term}. Nevertheless, both $CD8^+$ T-cell subsets showed high expression of *IL10* and *IRF2BP2* after PMA/ionomycin stimulation. Although the expression of *IRF4* was upregulated in all three $CD8^+$ T-cell subsets following PMA/ionomycin and ConA stimulations, the highest expression was induced by PMA/ionomycin-stimulated T_n followed by T_{inter} and T_{term}. Consistently, studies in mice showed that IRF4 contributes to expansion and maintenance of effector functions of CTL as well

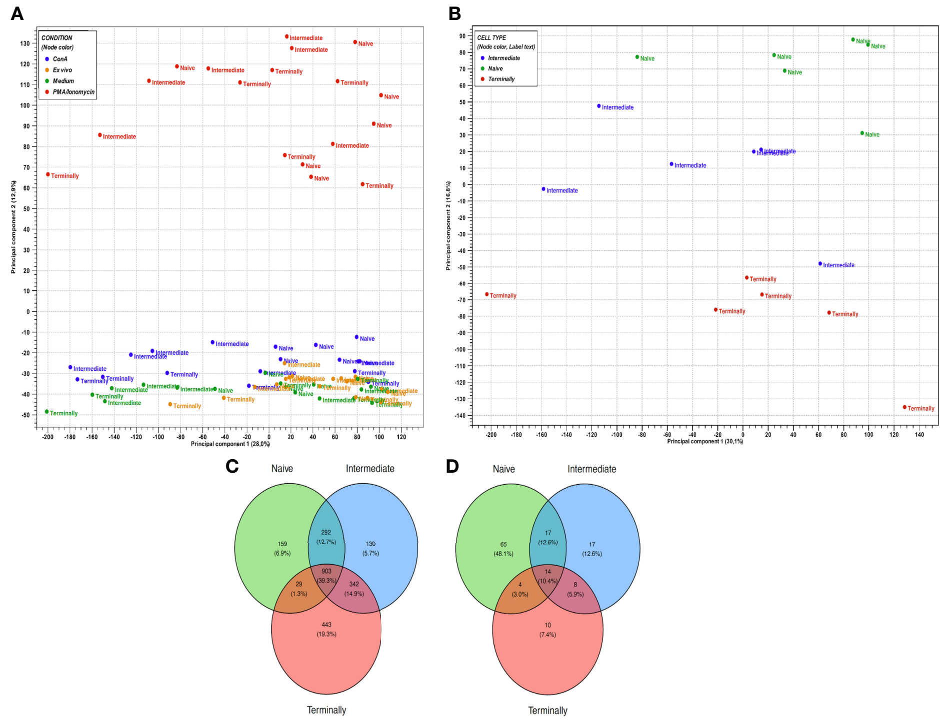

FIGURE 2 | Gene expression profiles of *in vitro* stimulated CD8+ T-cell subsets. **(A)** PCA plot of expression data derived from 72 CD8+ T-cell subsets of six animals. Colors indicate four conditions: blue, ConA stimulation; orange, *ex vivo* condition; green, medium control; red, PMA/ionomycin stimulation. Cross, X symbol and square shape represent naïve, intermediate and terminally differentiated CD8+ T-cell subsets, respectively. PC1 explains 28% and PC2 explains 12.9% of the observed variance in data. **(B)** PCA plot of expression data derived from 18 PMA/ionomycin-stimulated CD8+ T-cell subsets of six animals. Colors indicate three CD8+ T-cell subsets: green, naïve CD8+ T cells; blue, intermediate differentiated CD8+ T cells; red, terminally differentiated CD8+ T cells. PC1 explains 30.1% and PC2 explains 16.8% of the observed variance in data. **(C)** Venn diagram showing the overlap of DEGs between PMA/ionomycin-stimulated CD8+ T-cell subsets. **(D)** Venn diagram showing the overlap of DEGs between ConA-stimulated CD8+ T-cell subsets.

as to memory formation of CTL (36). In case of *IRF8* transcript, we found similar expression between CD8+ T-cell subsets stimulated with PMA/ionomycin. In comparison, ConA stimulation induced a much smaller extent expression of *IRF8* in T_{inter} and T_{term}. Expression of both genes, *IL6ST* and *ILF2* were similarly increased in all three CD8+ T-cell subsets upon PMA/ionomycin stimulation. Remarkably, the highest expression of *IL4R*, *IL15RA* and *IRF1* was recorded in the T_n followed by T_{inter} and T_{term}. Of interest, we found three genes of TNF-induced proteins, namely *TNFAIP2*, *TNFAIP3* and *TNFAIP8* highly expressed in CD8+ T-cell subsets following PMA/ionomycin stimulation. Moreover, expression of *TNFAIP2* and *TNFAIP3*, both inhibiting canonical NF-kB signaling pathway and thus negatively effecting cytokine production, was highest in the T_n (38, 39). Apart from its aforementioned functions, *TNFAIP3*, also highly expressed on naïve T cells, restricts MAP kinases and CD8+ T cell proliferation (40).

Chemokines and chemokine receptors play a pivotal role in attracting and guiding the naïve and effector T cells to lymph nodes and sites of inflammation, respectively (41). Overall, in all three CD8+ T-cell subsets the PMA/ionomycin stimulation induced stronger expression of genes associated with chemokines than after ConA stimulation (**Figure 3B**). Expression of *CCL4* (MIP-1ß) and *XCL1* (ATAC/lymphotactin), the inflammatory chemokines secreted by activated CD8+ T cell (42), was induced in all three CD8+ T-cell subsets upon both stimulations, although with significantly higher increase in PMA/ionomycin-stimulated CD8+ T-cell subsets. All three PMA/ionomycin-stimulated CTL subsets showed similar expression of *CCL3L1*, while following ConA stimulation it was increased in T_{inter} and T_{term}. Interestingly, only T_{inter} stimulated with PMA/ionomycin showed significant increase in *CCL20*, *CXCL8* and *CXCL10* expression, later known as one of interferon-inducible ligands of CXCR3 (43). The PMA/ionomycin stimulation induced also transcriptional upregulation of *CCL5* (RANTES) and *CXCL16* in all three CD8+ T-cell subsets. Furthermore, transcription of *CCL1* was increased in T_{inter} and T_{term} upon PMA/ionomycin stimulation.

Transition from naïve T cell to activated effector T cell is accompanied by metabolic adjustment necessary for specific cellular functions (44). Overall, the PMA/ionomycin stimulation induced stronger expression of genes linked to T-cell metabolism in comparison to the ConA stimulation. T_n and T_{inter} upregulated *BCAT1* and *GCLC* upon PMA/ionomycin stimulation, while T_{term} were enriched in transcripts for *LDHA* and *TPI1* gene. Both T_{inter} and T_{term} induced high expression of

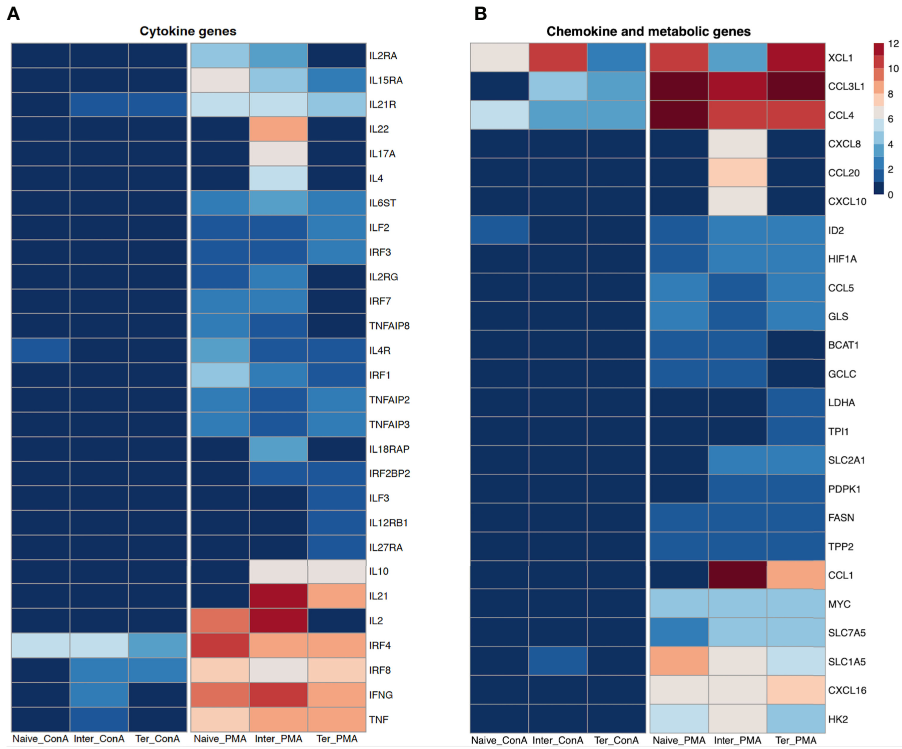

FIGURE 3 | Transcription profiles of naïve, intermediate and terminally differentiated CD8+ T-cell subsets. Data derived from 18 ConA and 18 PMA/ionomycin-stimulated CD8+ T-cell subsetsof six animals. As criteria to define DEGs, fold-change > |2| compared to medium control, maximum of the average RPKM's > 2 and a false discovery rate corrected p-value < 0.01 (FDR) were used. **(A)** Expression of cytokine genes as log2 fold-change between ConA- and PMA/ionomycin-stimulated CD8+ T-cell subsets and their unstimulated control. **(B)** Expression of chemokine and metabolic genes as log2 fold-change between ConA- and PMA/ionomycin-stimulated CD8+ T-cell subsets and their unstimulated control.

PDPK1 and *SLC2A1*, whereas *FASN*, *GLS* and *TPP2* were similarly expressed by all three $CD8^+$ T-cell subsets following PMA/ionomycin stimulation. In comparison to T_n, we recorded higher expression of *HIF1A* and *SLC7A5* in T_{inter} and T_{term}. Upon PMA/ionomycin stimulation, the highest levels of *SLC1A5*, *HK2* and *MYC* were expressed in T_n, T_{inter} and T_{term}, respectively. The ConA stimulation induced upregulation of ID2 expression in T_n and *SLC1A5* in T_{inter} only. Contrary, the PMA/ionomycin stimulation induced upregulation of *ID2* in all three $CD8^+$ T-cell subsets (**Figure 3B**).

Next, we examined the impact of stimulation with PMA/ionomycin and ConA on expression of transcription factor genes in $CD8^+$ T-cell subsets (**Figure 4A**). Several genes encoding transcription factors associated with terminally differentiated effector cells, including *BATF*, *BATF3*, *EZH2*, *MYC* and *TBX21* were upregulated in all three $CD8^+$ T-cell subsets upon PMA/ionomycin stimulation but not after ConA stimulation. While the highest expression of *BATF3*, *EZH2* and *MYC* was observed in the T_{term}, highest upregulation of TBX21 which encodes the T-bet, the master regulator of cytotoxic T-cell development (45), was observed in the T_n compared to T_{inter} and T_{term}. Interestingly, upregulation of *EOMES* and *ID3* was limited only to the ConA-stimulated T_n. T_{inter} and T_{term} displayed upregulation of *FOXO1*, *FOXP1*, *PRDM1* (Blimp-1), *SATB1* and *SREBF2* following PMA/ionomycin stimulation. Recent studies in mice and human have shown that Blimp-1, encoded by *PRDM1*, enhances formation of SLECs, production of IL-10 and cytotoxic functions of $CD8^+$ T cells (46). Along the PMA/ionomycin-stimulated differentiation subsets, we observed a gradual increase of expression of EGR family of zinc-finger transcription factors, including *EGR1*, *EGR2* and *EGR3*, which are upregulated upon TCR activation. Similar expression was recorded in case of *NAB2*, a coactivator and corepressor of T-cell function (47). Also, transcriptions of *NR4A2* and *NR4A3*, two members of the Nuclear receptor 4A (NR4A) family known for their important role during acute and chronic $CD8^+$ T cell response (48), were highly expressed along the differentiation subsets. Moreover, stimulation with PMA/ionomycin induced the highest expression of both genes in T_{term}, followed by T_{inter} and T_n. In contrary, the highest expression of *NR4A2* and *NR4A3* in ConA-stimulated subsets was recorded in T_n. Recently it has been reported that NR4A3 increases early expression of transcription factors involved in the SLEC differentiation and its absence favors differentiation of MPEC and central memory $CD8^+$ T cells (49). Notably, T_n and T_{inter} but not T_{term} expressed high levels of *BCL2* upon PMA/ionomycin and ConA stimulation. These results are in accordance with the recent findings which show that naïve T cells highly express *BCL2* and

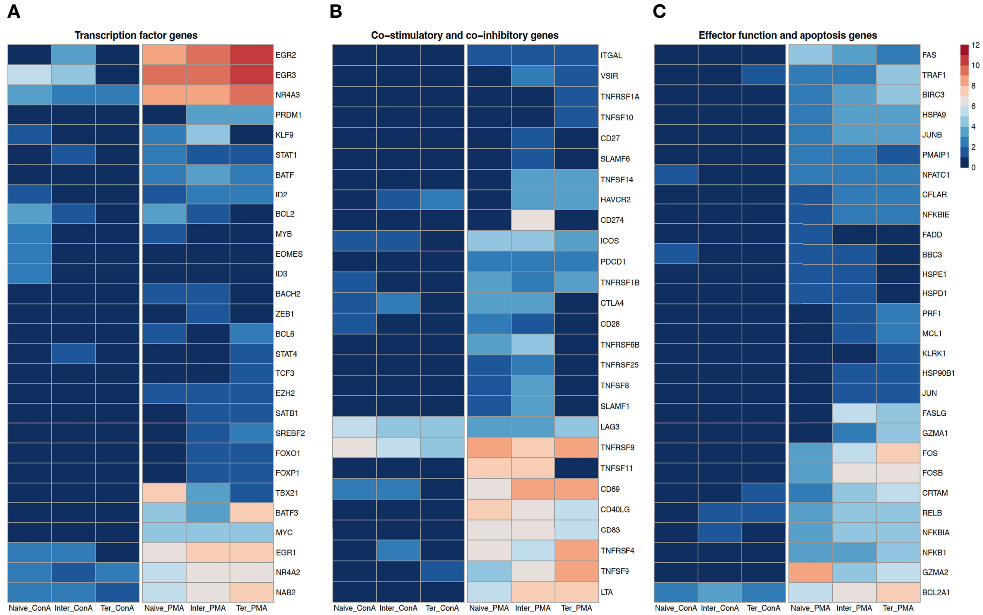

FIGURE 4 | Transcription profiles of naïve, intermediate and terminally differentiated CD8+ T-cell subsets. Data derived from 18 ConA and 18 PMA/ionomycin-stimulated CD8+ T-cell subsets of six animals. As criteria to define DEGs, fold-change > |2| compared to medium control, maximum of the average RPKM's > 2 and a false discovery rate corrected p-value < 0.01 (FDR) were used. **(A)** Expression of transcription factor genes as log2 fold-change between ConA- and PMA/ionomycin-stimulated CD8+ T-cell subsets and their unstimulated control. **(B)** Expression of co-stimulatory and co-inhibitory genes as log2 fold-change between ConA- and PMA/ionomycin-stimulated CD8+ T-cell subsets and their unstimulated control and **(C)** Expression of genes associated with effector functions and apoptosis as log2 fold-change between ConA- and PMA/ionomycin-stimulated CD8+ T-cell subsets and their unstimulated control.

are more dependent on it for survival than effector and memory T cells (50). The transcription factor *MYB* promotes formation of stem-like memory cell and restrains terminal effector differentiation by inducing expression of *BCL-2* and *TCF7* as well as inhibition of *ZEB2* (51). While T_n strongly expressed *MYB* following PMA/ionomycin and ConA stimulation, no upregulation was induced by T_{inter} or T_{term}. Also, expression of *BACH2*, described as transcriptional repressor of terminal differentiation that restrains formation of short-lived effector cells (52, 53), was upregulated in T_n and T_{inter} but not T_{term} after PMA/ionomycin stimulation. Furthermore, the PMA/ionomycin stimulation induced the expression of *ZEB1* and *TCF3* in T_{inter} and T_{term}, respectively. Studies in mice showed that *STAT1* and *STAT4* are important transcription factors for the clonal expansion and promotion of antigen-activated CD8+ T cells. Whereas *STAT1* effects type I IFN-dependent clonal expansion of CD8+ T cells, *STAT4* contributes to proliferation and effector maturation of CD8+ T cells triggered by IL-12-mediated signaling (54, 55). In fact, the PMA/ionomycin stimulation induced high expression of *STAT1* in all three CD8+ T-cell subsets, while the ConA stimulation induced the upregulation only in the T_{inter}. In case of *STAT4* expression, we observed upregulation in the T_{inter} stimulated with ConA and T_{term} stimulated with PMA/ionomycin. Notably, while *BCL6* was highly expressed in T_n and T_{term} following PMA/ionomycin stimulation, expression of *ID2*, a transcriptional regulator upregulated by activated CD8+ T cells late in effector phase which can also influence their differentiation into memory cells (56), was upregulated in all three CD8+ T-cell subsets stimulated with PMA/ionomycin. Moreover, expression of *ID2* was also increased in the T_n following ConA stimulation. Transcription of *KLF9* in the T_n was increased with ConA and PMA/ionomycin stimulation as well as in PMA/ionomycin-stimulated T_{inter}.

Looking at co-stimulatory genes, we found that expression of *CD27* (TNFRSF7), expressed mostly on naïve T cells and also required for T-cell memory in mice (35), was upregulated only in T_{inter} stimulated with PMA/ionomycin (**Figure 4B**). Also, another co-stimulatory gene *CD28*, which is absent from human effector CTLs (14), was upregulated in T_n and T_{inter} stimulated with PMA/ionomycin as well as in T_n stimulated with ConA. Furthermore, upon PMA/ionomycin stimulation all three CD8+ T-cell subsets expressed *ITGAL* (CD11a), a β2 integrin reported to be important for homing of T cells and generation of antigen-specific T cells (9). In all three CD8+ T-cell subsets PMA/ionomycin stimulation induced high expression of *CD40LG*, a member of the tumor necrosis factor superfamily transiently expressed on activated CD8+ T cells that promotes expansion and differentiation in a cell-extrinsic manner (57), and *CD83*, a member of the immunoglobulin superfamily. Expression of *CD69*, an early activation marker, was highly expressed in all three CD8+ T-cell subsets stimulated with PMA/ionomycin, and to a much smaller extent in T_n and

T_{inter} upon ConA stimulation. These differences in transcripts of *CD69* concerning different stimulations can be explained with the fact that the *CD69* expression is upregulated already after 30 to 60 minutes after activation and declines promptly after 4-6 hours (58). Furthermore, transcription of the inducible T cell co-stimulator (*ICOS*), a member of the immunoglobulin family structurally close to CD28 and rapidly expressed on activated T cells (59), was highly increased in all three CD8$^+$ T-cell subsets following PMA/ionomycin and to a lesser extent in T_n and T_{inter} after ConA stimulation. In addition, all three CTL subsets stimulated with PMA/ionomycin showed high increase of the lymphotoxin alpha (*LTA*), described to positively affect antigen-specific T-cell response during an acute LCMV infection through increase of IFN-γ production (60). Two members of the signaling lymphocytic activation molecule family (SLAMF), namely, *SLAMF1* and *SLAMF6*, were induced in T_n and T_{inter} after PMA/ionomycin stimulation. Highest expression of SLAMF1 and SLAMF6 has been reported on central memory and effector memory subsets of CD8$^+$ T cells (61).

In case of co-inhibitory genes, known to inhibit T-cell activation, cytolytic function and cytokine production (62), we observed that expression of *PDCD1* (PD-1) was induced in all three CD8$^+$ T-cell subsets stimulated with PMA/ionomycin, whereas its ligand *CD274* (PD-L1) was only expressed on T_{inter}. Moreover, both T_n and T_{inter} showed upregulation of cytotoxic T lymphocyte antigen-4 (CTLA4) upon stimulations, with PMA/ionomycin stimulation inducing stronger expression. It has been shown that CTLA4 is closely related to CD28, binds to the same ligands (CD80 and CD86) and inhibits T cell response (63). Next, we found that expression of lymphocyte activation gene-3 (LAG3) was induced in all three CD8$^+$ T-cell subsets after both stimulations. This is in accordance with previous research in mice suggesting that naïve CD8$^+$ T cell show low expression of LAG3, but increase its expression in response to stimulation (64). Notably, expression of *HAVCR2*, which encodes T-cell immunoglobulin and mucin domain-3 (Tim-3) inhibitory molecule, was upregulated only in T_{inter} and T_{term}. The tumor necrosis factor superfamily (TNFSF) and its corresponding receptor superfamily (TNFRSF) were differently expressed among porcine CD8$^+$ T-cell subsets.

In case of TNFSFs, PMA/ionomycin stimulation induced expression of *TNFSF8* (CD30L) and *TNFSF11* (RANKL) in T_n and T_{inter}, whereas transcript of *TNFSF14* (LIGHT) was upregulated in T_{inter} and T_{term}. The highest expression of *TNFSF9* (4-1BBL) could be observed in T_{term}, followed by T_{inter} and T_n. In addition, the ConA stimulation induced its expression only in T_{term}. Also, only T_{term} showed increased upregulation of *TNFSF10* (TRAIL) upon PMA/ionomycin stimulation. Regarding TNFRSFs, transcript of *TNFRSF1A* (TNFR1) was enriched in T_{term}, while *TNFRSF1B* (TNFR2) was expressed in all three CD8$^+$ T-cell subsets following PMA/ionomycin stimulation. Both T_n and T_{inter} expressed *TNFRSF6B* (DCR3) and *TNFRSF25* (DR3) after PMA/ionomycin stimulations. Notably, expression of *TNFRSF9* (4-1BB) was strongly induced in all CD8$^+$ T-cell subsets upon both stimulations. Similarly, the PMA/ionomycin stimulation induced high expression of *TNFRSF18* (GITR) and *TNFRSF4* (OX40), an intermediate activation marker, in all CD8$^+$ T-cell subsets, while stimulation with ConA induced the upregulation of these two genes in T_{inter} but only *TNFRSF18* in T_{term}.

Genes associated with effector functions of CTLs were primarily highly expressed by T_{term}, followed by T_{inter} and in just few cases by T_n following PMA/ionomycin stimulation (**Figure 4C**). Moreover, the ConA stimulation had almost no effect on upregulation of those genes in CD8$^+$ T-cell subsets. Several genes linked to cytolytic activity, including *GZMA1*, *PRF1* (Perforin), *FASLG*, *JUN*, *MCL1* and *HSP90B1*, were upregulated only in T_{inter} and T_{term} following PMA/ionomycin stimulation. Also, the highest expression of genes belonging to Jun (*JUN*, *JUNB*) and Fos (*FOS*, *FOSB*) families was detected in the T_{term}, followed by T_{inter} and T_n. Similarly, expression of several other genes involved in effector function and apoptosis, including *BIRC3*, *CFLAR*, *CRTAM*, *HSPA9*, *NFATC1*, *NFKB1* and *NFKBIE* was induced among CD8$^+$ T-cell subsets. Notably, only T_n and T_{inter} showed upregulation of *BBC3*, *HSPD1* and *HSPE1*. While killer cell lectin like receptor k1 (*KLRK1*) gene was upregulated in the T_{term}, transcript of *FADD* was induced only in T_n. Compared to T_{inter} and T_{term}, we found higher expression of *GZMA2* and *PMAIP* in T_n stimulated with PMA/ionomycin. Interestingly, both ConA and PMA/ionomycin stimulation induced upregulation of *BCL2A1* in all CD8$^+$ T-cell subsets, although with markedly stronger expression after PMA/ionomycin stimulation and in T_{term}. What is more, the highest expression of *TRAF1* and *RELB* was observed in the T_{term}, followed by T_{inter} and T_n. In case of T_{term}, expression of *TRAF1* and *RELB* was also induced by the ConA stimulation, whereas T_{inter} showed only the upregulation of *RELB* transcript. Expression of another IkB family gene linked to apoptosis (65), namely the *NFKBIA*, was highest in the T_{inter} stimulated with PMA/ionomycin.

GO and Pathway Analysis of *Ex Vivo* CD8$^+$ T-Cell Subsets

To extend the understanding of the immunological roles and functions of genes across different *ex vivo* CD8$^+$ T-cell subsets, we performed GO term enrichment analysis. For GO terms related to immune system, most of the upregulated DEGs in the T_{term} were assigned to lymphocyte activation involved in immune response (42.39%) (**Figure 5A**). In contrast, upregulated DEGs in the T_n were mostly associated with T-cell differentiation (42.31%), T-cell receptor signaling pathway (23.08%) and V(D)J recombination (11.54%). The majority of upregulated DEGs in the T_{inter} compared to naïve subsets were related to T-cell differentiation involved in immune response (27.69%), T-cell cytokine production (27.69%) and alpha-beta T-cell differentiation (23.08%). On the other side, upregulated DEGs in the T_{inter} compared to T_{term} were mainly linked to the regulation of T-cell differentiation (90.0%). When compared to T_{inter}, most of the upregulated DEGs in T_n were enriched for V(D)J recombination (55.17%), regulation of T-cell receptor signaling pathway (17.24%) and T-cell differentiation (17.24%), whereas within the T_{term} they were associated with regulation of

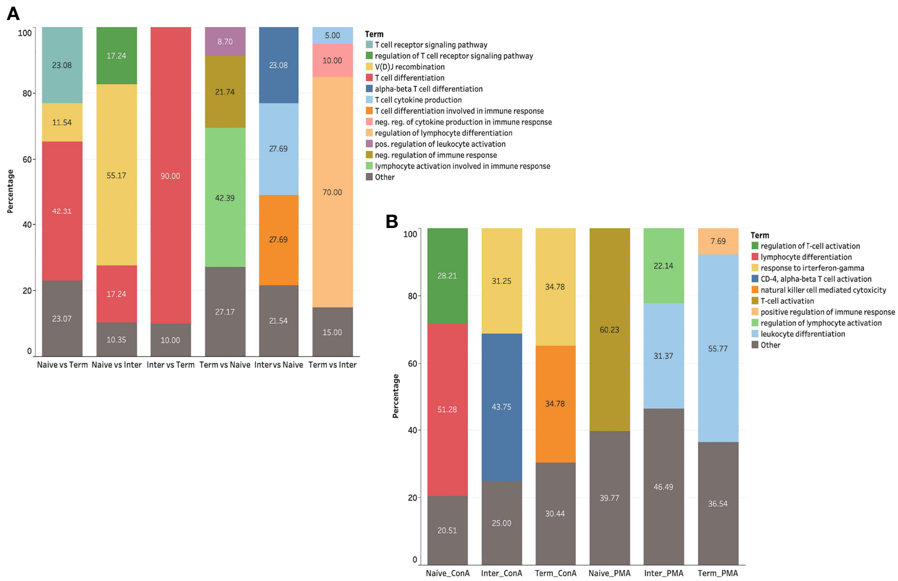

FIGURE 5 | GO term analysis of *ex vivo* and *in vitro* stimulated CD8$^+$ T-cell subsets **(A)** GO terms related to immune system of DEGs in *ex vivo* CD8$^+$ T-cell subsets. **(B)** GO terms related to immune system of DEGs in CD8$^+$ T-cell subsets upon ConA and PMA/ionomycin stimulation.

lymphocyte differentiation (70.0%) (**Supplementary Table S2,** and **Figure S2**).

KEGG pathway analysis revealed that upregulated DEGs in the T_{term} compared to T_n were assigned to 272 pathways, including 21 pathways related to the immune system. Within immune-related pathways, the highest number of upregulated DEGs were enriched in chemokine signaling and T-cell receptor signaling pathways. Additionally, upregulated DEGs were linked to metabolic, MAPK signaling and cytokine-cytokine receptor interaction pathways. Compared to T_{term}, DEGs within T_n were associated with 278 pathways, with 20 immune-related pathways, as well as metabolic and MAPK signaling pathways. When compared to T_{inter}, DEGs of T_n and T_{term} were enriched in 192 and 167 pathways, respectively. Furthermore, DEGs of both T_n and T_{term} were enriched in 15 immune-related pathways. In comparison to T_n and T_{term}, DEGs within T_{inter} were enriched in 268 and 235 pathways, respectively. All pathways including corresponding genes retrieved through KEGG pathway analysis were listed in **Supplementary Table S3**.

GO and Pathway Analysis of *In Vitro* Stimulated CD8$^+$ T-Cell Subsets

To further explore DEGs of *in vitro* stimulated CD8$^+$ T-cell subsets, we conducted GO term enrichment analysis for immune system processes using previously mentioned bioinformatic software and plug-in package. The results demonstrated that the DEGs of PMA/ionomycin-stimulated T_n compared to medium control were mostly associated with the regulation of T-cell activation (60.23%) (**Figure 5B**). In contrast, the DEGs in PMA/ionomycin-stimulated T_{term} were differently linked to the leukocyte differentiation (55.77%). For the DEGs of PMA/ionomycin-stimulated T_{inter}, we found enrichment in GO terms associated with the leukocyte differentiation (31.37%) and the regulation of lymphocyte activation (22.14%). Next, we investigated GO terms for immune processes in different CD8$^+$ T-cell subsets stimulated with ConA, showing that the lymphocyte differentiation and the regulation of T-cell activation were more related with the T_n upon stimulation, while response to interferon-gamma term was typically associated with T_{inter} and T_{term} (**Supplementary Table S2** and **Supplementary Figure S2**).

We next performed KEGG pathway analysis of each CD8$^+$ T-cell subset upon PMA/ionomycin and ConA stimulation as described above. Upregulated DEGs within PMA/ionomycin-stimulated T_n were assigned to 302 pathways in KEGG pathway database. Similar observations were made with T_{inter} (318 pathways) and T_{term} (305 pathways) CD8$^+$ T-cell subsets. Although similar number of pathways related to immune system were observed among PMA/ionomycin-stimulated CD8$^+$ T-cell subsets, a much higher number of DEGs was found from T_{inter} and T_{term} than T_n. Furthermore, T_{inter} showed the highest number of DEGs enriched in T-cell receptor signaling pathway (36), followed by T_{term} (33) and T_n (25). Looking at the chemokine signaling pathway, T_{inter} and T_{term} showed same number of DEGs enriched in the pathway (26), whereas T_n had only 18 DEGs involved. Besides immune-related pathways, DEGs from all PMA/ionomycin-stimulated CD8$^+$ T-cell subsets were highly enriched in metabolic, MAPK-signaling and cytokine-cytokine receptor interaction pathways. Interestingly, number of DEGs enriched in MAPK-signaling pathway was gradually increased along the $CD8^+$ T-cell subsets. Based on upregulated DEGs upon ConA stimulation, we recorded 175 pathways in case of T_n, 120 pathways for T_{inter} and only 43 pathways for T_{term}. Also, upregulated DEGs within the T_n showed the highest number of immune-related pathways. In contrast to PMA/ionomycin-stimulated $CD8^+$ T-cell subsets, ConA stimulation induced a limited number of genes associated with metabolic and MAPK-signaling pathways. Moreover, in all $CD8^+$ T-cell subsets only few DEGs were enriched in T-cell receptor signaling, chemokine signaling and cytokine-cytokine receptor interaction pathways after ConA stimulation (**Supplementary Table S3**).

DISCUSSION

In the present study we assessed the transcriptome of three subsets within the $CD8\beta^+$ T-cell population we hypothesize to represent distinct differentiation stages through RNA-Seq analysis. We aimed to identify differences in gene expression profiles between subsets as well as upon *in vitro* stimulation with ConA and PMA/ionomycin. Based on surface expression of CD11a and CD27, we defined differentiation stages of $CD8\beta^+$ T-cells as follows: naïve (T_n; $CD8\beta^+CD27^+CD11a^{low}$), intermediate differentiated (T_{inter}; $CD8\beta^+CD27^{dim}CD11a^+$), and terminally differentiated cells (T_{term}; $CD8\beta^+CD27^-CD11a^{high}$). To the best of our knowledge, this is the first study which comprehensively describes the transcriptomes of porcine $CD8^+$ T-cell subsets.

Differential gene expression analysis of *ex vivo* $CD8^+$ T-cell subsets revealed significant differences between subsets regarding expression of genes associated with early and late stages of differentiation. By comparing T_n and T_{term} *ex vivo*, we found 575 and 709 DEGs upregulated, respectively. In particular, T_n highly expressed a set of genes encoding transcription factors, such as *LEF1*, *BACH2*, *TCF7* (TCF1), *SATB1*, *ZEB1* and *BCL2*, which maintain quiescence state (11, 12). In contrast, T_{inter} and T_{term} showed upregulation of transcription genes that drive terminally effector cell differentiation including *TBX21* (T-bet), *PRDM1* (Blimp-1), *ZEB2*, *ZNF683* (Hobit), *ID2* and *STAT4* (12, 30, 66). Moreover, we observed upregulation of genes related to effector function, cytokines and chemokines along the differentiation gradient. For example, expression of CX3CR1, receptor of Fractalkine/CX3C ligand 1 which expression correlates with the grade of effector $CD8^+$ T differentiation (67), was highly induced on T_{term} and T_{inter}. In previous studies in human and mice, Gerlach et al. identified three distinct effector subpopulations based on expression of CX3CR1, namely $CX3CR1^-$, $CX3CR1^{int}$ and $CX3CR1^{hi}$. $CX3CR1^{hi}$ $CD8^+$ T effector cells were characterized as $CD27^-$, $CD127^-$, $KLRG^+$, produced the smallest amount of IL2 and showed at least 50% higher expression of T-bet in comparison to $CX3CR1^-$ and $CX3CR1^{int}$ cells (68). Moreover, these values have been found to be typical for terminally differentiated T effector cells (7, 67) and are consistent with our findings of porcine T_{term}.

In adult mice, naïve $CD8^+$ T cell subpopulations are phenotypically characterized as $CD11a^{low}CD44^{low}CD27^+KLRG^-CD62L^+CD122^-$, while terminally differentiated effector cells (TTDE) are defined as $CD11a^{high}CD44^{high}CD27^-KLRG^+CD62L^-CD122^-$ (13). Besides expression of CD122 (*IL2RB*) in T_{term}, this fits well with our findings on porcine T_n and T_{term}. In addition, naïve $CD8^+$ T cell subpopulations in mice show absence of *ITGA4* (CD49d), while it is highly expressed in more differentiated subpopulation such as $CD8^+$ effector T cells, central and effector memory $CD8^+$ T cells. Our values for *ITGA4* (CD49d) expression in T_{inter} and T_{term} correlate favorably with these previous reports and further support the idea of high *ITGA4* expression in more differentiated $CD8^+$ T-cell subsets. In addition to the CD49d, mice antigen-experienced CTLs following LMCV infection express also CD11a (*ITGAL)* and Ki67 (*MKI67*) markers (10). Likewise, our data demonstrate high upregulation of *ITGAL* (CD11a) and *MKI67* (Ki67) in T_{inter} and T_{term} but not in the T_n. A possible explanation for the differential expression of *MKI67* among porcine subsets is that T_{inter} and T_{term} are in the expansion phase of activated $CD8^+$ T cells, which is accompanied by induced expression of the proliferation gene *MKI67*. Following expansion, antigen-experienced $CD8^+$ T cells differentiate into SLEC ($CD127^-$ $KLRG1^+$) or MPEC ($CD127^+KLRG1^-$) exhibiting distinct functional profiles (7, 8). Whereas T_n showed high expression of *IL7R* (CD127) and low of *KLRG1*, we found the exact opposite expression of these genes in porcine T_{inter} and T_{term}. Thus, between T_{inter} and T_{term}, the expression of *KLRG1* was more than three times higher in T_{term}, suggesting their more differentiated state. On the other hand, the expression of *IL7R* (CD127) was significantly higher in T_{inter} than T_{term}. It can thus be reasonably assumed that T_{inter} and T_{term} may represent porcine MPEC and SLEC, respectively.

Our findings on high expression of *CD27*, *CCR7* and *CD28* in the T_n fit well with the four-dimensional model to address T-cell differentiation stages in human (13). In contrast, we found all three genes downregulated in the T_{term}. Compared to T_{term}, T_{inter} expressed *CD27* and *CD28*, but no *CCR7*, and based on this 4D model in humans they could represent in swine early-differentiated $CD8^+$ T cells.

CTLs perform their main killing function through the release of granzymes and perforin as well as Fas ligand expression which induces apoptosis on the target cells (69). As expected, our analysis showed high expression of genes associated with cytolytic activity in the T_{term} and to lesser extent in T_{inter}. Further analyses showed the highest upregulation of *GNLY*, *PRF1* (Perforin), *GZMB*, *FASL*, *INFG* and *TNF* in the T_{term} followed by the T_{inter}. Moreover, our data confirmed an absence of these genes in *ex vivo* T_n. Taken together, these results offer crucial evidences for different gene signatures of distinct $CD8^+$ T-cell subsets.

As indicated by previous comparative studies on porcine, mice and human genome and transcriptome concerning immune system (70, 71), we also found higher numbers of orthologous genes shared between pig and human than shared by pig and mouse. In particular, from DEGs in T_n and T_{term} we found around 86% orthologs in human and 39% in mouse data sets of $CD8^+$ T cells. These differences can be explained in part by the fact that pig and human share more orthologs, while mice show the highest number of unique immune response genes that are not present in human and pig (71–73). Therefore, our results provide additional support for the similarity between human and pig genome on immune level, highlighting the pig as an appropriate model for human immunology research.

In a parallel approach, we showed gene expression changes in CD8$^+$ T-cell subsets upon stimulation with ConA and PMA/ionomycin. Generally, PMA/ionomycin stimulation induced much stronger upregulation of genes compared to stimulation with ConA. These additional results demonstrate two things. First, following PMA/ionomycin stimulation, CD8$^+$ T-cell subsets acquired more similar gene expression profiles as indicated by high number of DEGs shared between CD8$^+$ T-cell subsets. It is very likely that upon stimulation all three CD8$^+$ T-cell subsets switch to an activated state and this is accompanied by functional changes in gene expression. Second evidence, although all three CD8$^+$ T-cell subsets upregulated several genes associated with CD8$^+$ T-cell activation and differentiation upon stimulation, the differences in gene expression profiles remained and they clustered into three distinct subsets again. Even though stimulated T_n expressed some genes associated with the T-cell activation and differentiation, including *TBX21*, *ID2*, *BATF* and *EZH2*, they still showed no expression of *GNLY*, *PRF1*, *GZMB* and *FASL* even after PMA/ionomycin stimulation. In some cases, they even induced upregulation of several genes linked to early stages of differentiation e.g. *BACH2* and *BCL6*, which negatively correlates with granzyme B expression in effector CD8$^+$ T cells (74). Contrary to the findings on *in vitro* stimulated T_n, we found even higher expression of late-stage differentiation genes in T_{term} and T_{inter} following *in vitro* stimulation. It may be assumed that T_n require more time to reach full cytotoxic potential, whereas T_{inter} and T_{term} promptly show cytotoxic activity and effectively produce cytokines upon *in vitro* stimulation.

GO term enrichment analysis of *ex vivo* CD8$^+$ T-cell subsets revealed that most of DEGs were involved in immunological processes associated with T-cell differentiation. Once stimulated, T_{inter} and T_{term} were mostly enriched in same GO terms, whereas T_n were linked to other GO terms related to the immune system. Nevertheless, DEGs of T_n stimulated with ConA and PMA/ionomycin were enriched in differentiation and T-cell activation, respectively. This GO term enrichment analysis implies that T_{inter} and T_{term} share more comparable gene expression profile and functions compared to T_n.

Furthermore, KEGG pathway analysis of DEGs in the *ex vivo* T_n and T_{term} were assigned to 278 and 272 pathways, respectively. Although DEGs of T_n and T_{term} were involved in similar number of immune-related pathways, we found higher number of DEGs of T_{term} represented in those pathways, including T-cell receptor and chemokine signaling pathways. In contrast, the lowest number of KEGG pathways obtained from DEGs between two subsets were found in case of T_{inter} and T_{term}. In our view the results emphasize the differences in gene expression profiles among *ex vivo* CD8$^+$ T-cell subsets, with biggest difference between T_n and T_{term} and smallest between T_{inter} and T_{term}. As anticipated, PMA/ionomycin-stimulated CD8$^+$ T-cell subsets were involved in much higher number of pathways than after ConA stimulation. Interestingly, for the T_{term}, over seven times more KEGG pathways were obtained after PMA/ionomycin stimulation in comparison to ConA stimulation. In addition, a higher number of DEGs from T_{inter} and T_{term} were enriched in immune-related pathways than T_n, which confirmed our initial findings on *ex vivo* CD8$^+$ T-cell subsets. On the other hand, following ConA stimulation, the highest number of KEGG pathways was recorded in the T_n, followed by T_{inter}. Whereas CD8$^+$ T-cell subsets showed high enrichment in T-cell receptor, chemokine signaling and cytokine-cytokine receptor interaction pathways upon PMA/ionomycin stimulation, the number of those pathways was substantially smaller once CD8$^+$ T-cell subsets were stimulated with ConA. Thus, our findings show clearly that PMA/ionomycin stimulation of CD8$^+$ T-cell subsets induces much stronger cytolytic T-cell response than ConA stimulation and that the response was earlier and stronger in more differentiated than naïve CD8$^+$ T cells.

In the present study we investigated transcriptomes of *ex vivo* CD8$^+$ T-cell subsets and after *in vitro* stimulation. We obtained comprehensive results showing that substantial gene expression differences exist among phenotypically defined porcine CD8$^+$ T-cell subsets. Therefore, this work can serve as valuable reference for gene expression profiling of differentiation stages of porcine CD8$^+$ T-cell subsets. The findings will support future *in vivo* gene expression studies in healthy as well as in infected or vaccinated animals in order to get a more complete picture of differentiation stages of porcine CD8$^+$ T-cell subsets, especially after antigen-specific activation. We are aware of the limitation of this study since only gene expression was analyzed without validation of protein expression data. This is due to the lack of specific monoclonal antibodies. Nevertheless, the present findings identified specific targets and thus help to solve the problem of non-existing monoclonal antibodies against the respective differentiation antigens.

DATA AVAILABILITY STATEMENT

The datasets presented in this study can be found in online repositories. The names of the repository/repositories and accession number(s) can be found below: https://www.ncbi.nlm.nih.gov/, PRJNA761916.

ETHICS STATEMENT

Ethical review and approval was not required for the animal study because porcine blood was collected from abattoir in accordance with Austrian Animal Welfare Slaughter Regulation.

AUTHOR CONTRIBUTIONS

EL, MS, KM, and AS designed the project. EL performed lymphocyte isolation, *in vitro stimulation*, magnetic-activated cell sorting and RNA isolation. KM organized fluorescence-activated cell sorting. MV and SO prepared library and sequenced the samples. EL performed in-depth bioinformatic analysis. EL and AS analyzed the experiments and wrote the manuscript. CP assisted with interpretation of the data. All authors contributed to the article and approved the submitted version.

FUNDING

This work was financially supported by intramural funds of the University of Veterinary Medicine Vienna.

ACKNOWLEDGMENTS

We thank Maria Stadler for the PBMC isolation as well as Anna Hoog for the assistance with the FACS.

SUPPLEMENTARY MATERIAL

The Supplementary Material for this article can be found online at: https://www.frontiersin.org/articles/10.3389/fimmu.2022.849922/full#supplementary-material

REFERENCES

1. Pagès F, Berger A, Camus M, Sanchez-Cabo F, Costes A, Molidor R, et al. Effector Memory T Cells, Early Metastasis, and Survival in Colorectal Cancer. *N Engl J Med* (2005) 353:2654–66. doi: 10.1056/NEJMoa051424
2. Zhang L, Conejo-Garcia JR, Katsaros D, Gimotty PA, Massobrio M, Regnani G, et al. Intratumoral T Cells, Recurrence, and Survival in Epithelial Ovarian Cancer. *N Engl J Med* (2003) 348:203–13. doi: 10.1056/NEJMoa020177
3. Kim K-J, Lee KS, Cho HJ, Kim YH, Yang HK, Kim WH, et al. Prognostic Implications of Tumor-Infiltrating FoxP3+ Regulatory T Cells and CD8+ Cytotoxic T Cells in Microsatellite-Unstable Gastric Cancers. *Hum Pathol* (2014) 45:285–93. doi: 10.1016/j.humpath.2013.09.004
4. Le Moine A, Goldman M, Abramowicz D. Multiple Pathways to Allograft Rejection. *Transplantation* (2002) 73:1373–81. doi: 10.1097/00007890-200205150-00001
5. Actor JK. T Lymphocytes: Ringleaders of Adaptive Immune Function. In: *Introductory Immunology, 2nd ed.* London: Academic Press (2019). p. 45–62.
6. Badovinac VP, Tvinnereim AR, Harty JT. Regulation of Antigen-Specific CD8 + T Cell Homeostasis by Perforin and Interferon-γ. *Science* (2000) 290:1354–7. doi: 10.1126/science.290.5495.1354
7. Joshi NS, Cui W, Chandele A, Lee HK, Urso DR, Hagman J, et al. Inflammation Directs Memory Precursor and Short-Lived Effector CD8+ T Cell Fates *via* the Graded Expression of T-Bet Transcription Factor. *Immunity* (2007) 27:281–95. doi: 10.1016/j.immuni.2007.07.010
8. Kaech SM, Tan JT, Wherry EJ, Konieczny BT, Surh CD, Ahmed R. Selective Expression of the Interleukin 7 Receptor Identifies Effector CD8 T Cells That Give Rise to Long-Lived Memory Cells. *Nat Immunol* (2003) 4:1191–8. doi: 10.1038/ni1009
9. Bose TO, Pham Q-M, Jellison ER, Mouries J, Ballantyne CM, Lefrançois L. CD11a Regulates Effector CD8 T Cell Differentiation and Central Memory Development in Response to Infection With Listeria Monocytogenes. *Infect Immun* (2013) 81:1140–51. doi: 10.1128/IAI.00749-12
10. Masopust D, Murali-Krishna K, Ahmed R. Quantitating the Magnitude of the Lymphocytic Choriomeningitis Virus-Specific CD8 T-Cell Response: It Is Even Bigger Than We Thought. *J Virol* (2007) 81:2002–11. doi: 10.1128/JVI.01459-06
11. Tsukumo S-I, Unno M, Muto A, Takeuchi A, Kometani K, Kurosaki T, et al. Bach2 Maintains T Cells in a Naive State by Suppressing Effector Memory-Related Genes. *Proc Natl Acad Sci* (2013) 110:10735–40. doi: 10.1073/pnas.1306691110
12. Kaech SM, Cui W. Transcriptional Control of Effector and Memory CD8+ T Cell Differentiation. *Nat Rev Immunol* (2012) 12:749–61. doi: 10.1038/nri3307
13. Cossarizza A, Chang H, Radbruch A, Acs A, Adam D, Adam-Klages S, et al. Guidelines for the Use of Flow Cytometry and Cell Sorting in Immunological Studies (Second Edition). *Eur J Immunol* (2019) 49:1457–973. doi: 10.1002/eji.201970107
14. Hamann D, Baars PA, Rep MHG, Hooibrink B, Kerkhof-Garde SR, Klein MR, et al. Phenotypic and Functional Separation of Memory and Effector Human CD8+ T Cells. *J Exp Med* (1997) 186:1407–18. doi: 10.1084/jem.186.9.1407
15. Appay V, Dunbar PR, Callan M, Klenerman P, Gillespie GMA, Papagno L, et al. Memory CD8+ T Cells Vary in Differentiation Phenotype in Different Persistent Virus Infections. *Nat Med* (2002) 8:379–85. doi: 10.1038/nm0402-379
16. Sallusto F, Lenig D, Förster R, Lipp M, Lanzavecchia A. Two Subsets of Memory T Lymphocytes With Distinct Homing Potentials and Effector Functions. *Nature* (1999) 401:708–12. doi: 10.1038/44385
17. van Aalderen MC, Remmerswaal EBM, Verstegen NJM, Hombrink P, ten Brinke A, Pircher H, et al. Infection History Determines the Differentiation State of Human CD8 + T Cells. *J Virol* (2015) 89:5110–23. doi: 10.1128/JVI.03478-14
18. Overgaard NH, Fan TM, Schachtschneider KM, Principe DR, Schook LB, Jungersen G. Of Mice, Dogs, Pigs, and Men: Choosing the Appropriate Model for Immuno-Oncology Research. *ILAR J* (2018) 59:247–62. doi: 10.1093/ilar/ily014
19. Pauly T, Elbers K, König M, Lengsfeld T, Saalmüller A, Thiel H-J. Classical Swine Fever Virus-Specific Cytotoxic T Lymphocytes and Identification of a T Cell Epitope. *J Gen Virol* (1995) 76:3039–49. doi: 10.1099/0022-1317-76-12-3039
20. Saalmüller A, Pauly T, Höhlich B-J, Pfaff E. Characterization of Porcine T Lymphocytes and Their Immune Response Against Viral Antigens. *J Biotechnol* (1999) 73:223–33. doi: 10.1016/S0168-1656(99)00140-6
21. Denyer MS, Wileman TE, Stirling CMA, Zuber B, Takamatsu H-H. Perforin Expression Can Define CD8 Positive Lymphocyte Subsets in Pigs Allowing Phenotypic and Functional Analysis of Natural Killer, Cytotoxic T, Natural Killer T and MHC Un-Restricted Cytotoxic T-Cells. *Vet Immunol Immunopathol* (2006) 110:279–92. doi: 10.1016/j.vetimm.2005.10.005
22. Pauly T, Weiland E, Hirt W, Dreyer-Bux C, Maurer S, Summerfield A, et al. Differentiation Between MHC-Restricted and Non-MHC-Restricted Porcine Cytolytic T Lymphocytes. *Immunology* (1996) 88:238–46. doi: 10.1111/j.1365-2567.1996.tb00010.x
23. Talker SC, Käser T, Reutner K, Sedlak C, Mair KH, Koinig H, et al. Phenotypic Maturation of Porcine NK- and T-Cell Subsets. *Dev Comp Immunol* (2013) 40:51–68. doi: 10.1016/j.dci.2013.01.003
24. Zhao F-R, Xie Y-L, Liu Z-Z, Shao J-J, Li S-F, Zhang Y-G, et al. Transcriptomic Analysis of Porcine PBMCs in Response to FMDV Infection. *Acta Trop* (2017) 173:69–75. doi: 10.1016/j.actatropica.2017.05.009
25. Yang T, Zhang F, Zhai L, He W, Tan Z, Sun Y, et al. Transcriptome of Porcine PBMCs Over Two Generations Reveals Key Genes and Pathways Associated With Variable Antibody Responses Post PRRSV Vaccination. *Sci Rep* (2018) 8:2460. doi: 10.1038/s41598-018-20701-w
26. Zhang J, Zheng Y, Xia X-Q, Chen Q, Bade SA, Yoon K-J, et al. High-Throughput Whole Genome Sequencing of Porcine Reproductive and Respiratory Syndrome Virus From Cell Culture Materials and Clinical Specimens Using Next-Generation Sequencing Technology. *J Vet Diagn Investig* (2017) 29:41–50. doi: 10.1177/1040638716673404
27. Bennett TJ, Udupa VAV, Turner SJ. Running to Stand Still: Naive CD8+ T Cells Actively Maintain a Program of Quiescence. *Int J Mol Sci* (2020) 21:9773. doi: 10.3390/ijms21249773
28. Shukla AK, McIntyre LL, Marsh SE, Schneider CA, Hoover EM, Walsh CM, et al. CD11a Expression Distinguishes Infiltrating Myeloid Cells From Plaque-Associated Microglia in Alzheimer's Disease. *Glia* (2019) 67:844–56. doi: 10.1002/glia.23575
29. Drouillard A, Neyra A, Mathieu A-L, Marçais A, Wencker M, Marvel J, et al. Human Naive and Memory T Cells Display Opposite Migratory Responses to

Sphingosine-1 Phosphate. *J Immunol* (2018) 200:551–7. doi: 10.4049/jimmunol.1701278

30. Chen Y, Zander R, Khatun A, Schauder DM, Cui W. Transcriptional and Epigenetic Regulation of Effector and Memory CD8 T Cell Differentiation. *Front Immunol* (2018) 9:2826. doi: 10.3389/fimmu.2018.02826
31. Miyagawa F, Zhang H, Terunuma A, Ozato K, Tagaya Y, Katz SI. Interferon Regulatory Factor 8 Integrates T-Cell Receptor and Cytokine-Signaling Pathways and Drives Effector Differentiation of CD8 T Cells. *Proc Natl Acad Sci* (2012) 109:12123–8. doi: 10.1073/pnas.1201453109
32. Kaech SM, Hemby S, Kersh E, Ahmed R. Molecular and Functional Profiling of Memory CD8 T Cell Differentiation. *Cell* (2002) 111:837–51. doi: 10.1016/S0092-8674(02)01139-X
33. Blaser C, Kaufmann M, Müller C, Zimmermann C, Wells V, Mallucci L, et al. β-Galactoside-Binding Protein Secreted by Activated T Cells Inhibits Antigen-Induced Proliferation of T Cells. *Eur J Immunol* (1998) 28:2311–9. doi: 10.1002/(SICI)1521-4141(199808)28:08<2311::AID-IMMU2311>3.0.CO;2-G
34. Shan Q, Zeng Z, Xing S, Li F, Hartwig SM, Gullicksrud JA, et al. The Transcription Factor Runx3 Guards Cytotoxic CD8 + Effector T Cells Against Deviation Towards Follicular Helper T Cell Lineage. *Nat Immunol* (2017) 18:931–9. doi: 10.1038/ni.3773
35. Hendriks J, Gravestein LA, Tesselaar K, van Lier RAW, Schumacher TNM, Borst J. CD27 Is Required for Generation and Long-Term Maintenance of T Cell Immunity. *Nat Immunol* (2000) 1:433–40. doi: 10.1038/80877
36. Huber M, Lohoff M. IRF4 at the Crossroads of Effector T-Cell Fate Decision. *Eur J Immunol* (2014) 44:1886–95. doi: 10.1002/eji.201344279
37. Kalia V, Sarkar S. Regulation of Effector and Memory CD8 T Cell Differentiation by IL-2—A Balancing Act. *Front Immunol* (2018) 9:2987. doi: 10.3389/fimmu.2018.02987
38. Jia L, Shi Y, Wen Y, Li W, Feng J, Chen C. The Roles of TNFAIP2 in Cancers and Infectious Diseases. *J Cell Mol Med* (2018) 22:5188–95. doi: 10.1111/jcmm.13822
39. Das T, Chen Z, Hendriks RW, Kool M. A20/Tumor Necrosis Factor α-Induced Protein 3 in Immune Cells Controls Development of Autoinflammation and Autoimmunity: Lessons From Mouse Models. *Front Immunol* (2018) 9:104. doi: 10.3389/fimmu.2018.00104
40. Just S, Nishanth G, Buchbinder JH, Wang X, Naumann M, Lavrik I, et al. A20 Curtails Primary But Augments Secondary CD8+ T Cell Responses in Intracellular Bacterial Infection. *Sci Rep* (2016) 6:39796. doi: 10.1038/srep39796
41. Stein JV, Nombela-Arrieta C. Chemokine Control of Lymphocyte Trafficking: A General Overview. *Immunology* (2005) 116:1–12. doi: 10.1111/j.1365-2567.2005.02183.x
42. Dorner BG, Scheffold A, Rolph MS, Huser MB, Kaufmann SHE, Radbruch A, et al. MIP-1, MIP-1, RANTES, and ATAC/lymphotactin Function Together With IFN- as Type 1 Cytokines. *Proc Natl Acad Sci* (2002) 99:6181–6. doi: 10.1073/pnas.092141999
43. Groom JR, Luster AD. CXCR3 in T Cell Function. *Exp Cell Res* (2011) 317:620–31. doi: 10.1016/j.yexcr.2010.12.017
44. Buck MD, O'Sullivan D, Pearce EL. T Cell Metabolism Drives Immunity. *J Exp Med* (2015) 212:1345–60. doi: 10.1084/jem.20151159
45. Kallies A, Good-Jacobson KL. Transcription Factor T-Bet Orchestrates Lineage Development and Function in the Immune System. *Trends Immunol* (2017) 38:287–97. doi: 10.1016/j.it.2017.02.003
46. Fu S-H, Yeh L-T, Chu C-C, Yen BL-J, Sytwu H-K. New Insights Into Blimp-1 in T Lymphocytes: A Divergent Regulator of Cell Destiny and Effector Function. *J BioMed Sci* (2017) 24:49. doi: 10.1186/s12929-017-0354-8
47. Collins S, Wolfraim LA, Drake CG, Horton MR, Powell JD. Cutting Edge: TCR-Induced NAB2 Enhances T Cell Function by Coactivating IL-2 Transcription. *J Immunol* (2006) 177:8301–5. doi: 10.4049/jimmunol.177.12.8301
48. Odagiu L, May J, Boulet S, Baldwin TA, Labrecque N. Role of the Orphan Nuclear Receptor NR4A Family in T-Cell Biology. *Front Endocrinol* (2021) 11:624122. doi: 10.3389/fendo.2020.624122
49. Odagiu L, Boulet S, Maurice De Sousa D, Daudelin J-F, Nicolas S, Labrecque N. Early Programming of CD8 + T Cell Response by the Orphan Nuclear Receptor NR4A3. *Proc Natl Acad Sci* (2020) 117:24392–402. doi: 10.1073/pnas.2007224117
50. Zhan Y, Carrington EM, Zhang Y, Heinzel S, Lew AM. Life and Death of Activated T Cells: How Are They Different From Naïve T Cells? *Front Immunol* (2017) 8:1809. doi: 10.3389/fimmu.2017.01809
51. Gautam S, Fioravanti J, Zhu W, Le Gall JB, Brohawn P, Lacey NE, et al. The Transcription Factor C-Myb Regulates CD8+ T Cell Stemness and Antitumor Immunity. *Nat Immunol* (2019) 20:337–49. doi: 10.1038/s41590-018-0311-z
52. Yao C, Lou G, Sun H-W, Zhu Z, Sun Y, Chen Z, et al. BACH2 Enforces the Transcriptional and Epigenetic Programs of Stem-Like CD8+ T Cells. *Nat Immunol* (2021) 22:370–80. doi: 10.1038/s41590-021-00868-7
53. Roychoudhuri R, Clever D, Li P, Wakabayashi Y, Quinn KM, Klebanoff CA, et al. BACH2 Regulates CD8+ T Cell Differentiation by Controlling Access of AP-1 Factors to Enhancers. *Nat Immunol* (2016) 17:851–60. doi: 10.1038/ni.3441
54. Li Q, Eppolito C, Odunsi K, Shrikant PA. IL-12-Programmed Long-Term CD8 + T Cell Responses Require Stat4. *J Immunol* (2006) 177:7618–25. doi: 10.4049/jimmunol.177.11.7618
55. Quigley M, Huang X, Yang Y. STAT1 Signaling in CD8 T Cells Is Required for Their Clonal Expansion and Memory Formation Following Viral Infection *In Vivo*. *J Immunol* (2008) 180:2158–64. doi: 10.4049/jimmunol.180.4.2158
56. Cannarile MA, Lind NA, Rivera R, Sheridan AD, Camfield KA, Wu BB, et al. Transcriptional Regulator Id2 Mediates CD8+ T Cell Immunity. *Nat Immunol* (2006) 7:1317–25. doi: 10.1038/ni1403
57. Tay NQ, Lee DCP, Chua YL, Prabhu N, Gascoigne NRJ, Kemeny DM. CD40L Expression Allows CD8+ T Cells to Promote Their Own Expansion and Differentiation Through Dendritic Cells. *Front Immunol* (2017) 8:1484. doi: 10.3389/fimmu.2017.01484
58. Cibrián D, Sánchez-Madrid F. CD69: From Activation Marker to Metabolic Gatekeeper. *Eur J Immunol* (2017) 47:946–53. doi: 10.1002/eji.201646837
59. Wikenheiser DJ, Stumhofer JS. ICOS Co-Stimulation: Friend or Foe? *Front Immunol* (2016) 7:304. doi: 10.3389/fimmu.2016.00304
60. Suresh M, Lanier G, Large MK, Whitmire JK, Altman JD, Ruddle NH, et al. Role of Lymphotoxin α in T-Cell Responses During an Acute Viral Infection. *J Virol* (2002) 76:3943–51. doi: 10.1128/JVI.76.8.3943-3951.2002
61. Karampetsou MP, Comte D, Kis-Toth K, Kyttaris VC, Tsokos GC. Expression Patterns of Signaling Lymphocytic Activation Molecule Family Members in Peripheral Blood Mononuclear Cell Subsets in Patients With Systemic Lupus Erythematosus. *PloS One* (2017) 12:e0186073. doi: 10.1371/journal.pone.0186073
62. Riley JL. PD-1 Signaling in Primary T Cells. *Immunol Rev* (2009) 229:114–25. doi: 10.1111/j.1600-065X.2009.00767.x
63. McCoy KD, Le Gros G. The Role of CTLA-4 in the Regulation of T Cell Immune Responses. *Immunol Cell Biol* (1999) 77:1–10. doi: 10.1046/j.1440-1711.1999.00795.x
64. Grosso JF, Kelleher CC, Harris TJ, Maris CH, Hipkiss EL, De Marzo A, et al. LAG-3 Regulates CD8+ T Cell Accumulation and Effector Function in Murine Self- and Tumor-Tolerance Systems. *J Clin Invest* (2007) 117:3383–92. doi: 10.1172/JCI31184
65. Wang M, Windgassen D, Papoutsakis ET. A Global Transcriptional View of Apoptosis in Human T-Cell Activation. *BMC Med Genomics* (2008) 1:53. doi: 10.1186/1755-8794-1-53
66. Rutishauser RL, Kaech SM. Generating Diversity: Transcriptional Regulation of Effector and Memory CD8 + T-Cell Differentiation. *Immunol Rev* (2010) 235:219–33. doi: 10.1111/j.0105-2896.2010.00901.x
67. Sarkar S, Kalia V, Haining WN, Konieczny BT, Subramaniam S, Ahmed R. Functional and Genomic Profiling of Effector CD8 T Cell Subsets With Distinct Memory Fates. *J Exp Med* (2008) 205:625–40. doi: 10.1084/jem.20071641
68. Gerlach C, Moseman EA, Loughhead SM, Alvarez D, Zwijnenburg AJ, Waanders L, et al. The Chemokine Receptor CX3CR1 Defines Three Antigen-Experienced CD8 T Cell Subsets With Distinct Roles in Immune Surveillance and Homeostasis. *Immunity* (2016) 45:1270–84. doi: 10.1016/j.immuni.2016.10.018
69. Andersen MH, Schrama D, Thor Straten P, Becker JC. Cytotoxic T Cells. *J Invest Dermatol* (2006) 126:32–41. doi: 10.1038/sj.jid.5700001

70. Dawson HD, Reece JJ, Urban JF. A Comparative Analysis of the Porcine, Murine, and Human Immune Systems. *Vet Immunol Immunopathol* (2009) 128:309. doi: 10.1016/j.vetimm.2008.10.211
71. Dawson HD, Smith AD, Chen C, Urban JF. An in-Depth Comparison of the Porcine, Murine and Human Inflammasomes; Lessons From the Porcine Genome and Transcriptome. *Vet Microbiol* (2017) 202:2–15. doi: 10.1016/j.vetmic.2016.05.013
72. Dawson HD, Loveland JE, Pascal G, Gilbert JG, Uenishi H, Mann KM, et al. Structural and Functional Annotation of the Porcine Immunome. *BMC Genomics* (2013) 14:332. doi: 10.1186/1471-2164-14-332
73. Pabst R. The Pig as a Model for Immunology Research. *Cell Tissue Res* (2020) 380(2):287–304. doi: 10.1007/s00441-020-03206-9
74. Yoshida K, Sakamoto A, Yamashita K, Arguni E, Horigome S, Arima M, et al. Bcl6 Controls Granzyme B Expression in Effector CD8+ T Cells. *Eur J Immunol* (2006) 36:3146–56. doi: 10.1002/eji.200636165

Conflict of Interest: MV and SO are employed by Istituto di Ricerche Biomediche “A. Marxer” RBM S.p.A. MS is employed by Merck Healthcare KGaA. The remaining authors declare that the research was conducted in the absence of any commercial or financial relationships that could be construed as a potential conflict of interest.

Publisher’s Note: All claims expressed in this article are solely those of the authors and do not necessarily represent those of their affiliated organizations, or those of the publisher, the editors and the reviewers. Any product that may be evaluated in this article, or claim that may be made by its manufacturer, is not guaranteed or endorsed by the publisher.

frontiers | Frontiers in Immunology

TYPE Original Research
PUBLISHED 20 June 2023
DOI 10.3389/fimmu.2023.1159970

OPEN ACCESS

EDITED BY
Enric M. Mateu,
Autonomous University of Barcelona, Spain

REVIEWED BY
Jordi Argilaguet,
Centre for Research on Animal Health, Spain
Laura Caldwell Miller,
Kansas State University, United States

*CORRESPONDENCE
Armin Saalmüller
armin.saalmueller@vetmeduni.ac.at

RECEIVED 06 February 2023
ACCEPTED 05 June 2023
PUBLISHED 20 June 2023

CITATION
Lagumdzic E, Pernold CPS, Ertl R, Palmieri N, Stadler M, Sawyer S, Stas MR, Kreutzmann H, Rümenapf T, Ladinig A and Saalmüller A (2023) Gene expression of peripheral blood mononuclear cells and $CD8^+$ T cells from gilts after PRRSV infection.
Front. Immunol. 14:1159970.
doi: 10.3389/fimmu.2023.1159970

Gene expression of peripheral blood mononuclear cells and $CD8^+$ T cells from gilts after PRRSV infection

Emil Lagumdzic[1], Clara P. S. Pernold[1], Reinhard Ertl[2], Nicola Palmieri[3], Maria Stadler[1], Spencer Sawyer[4], Melissa R. Stas[4], Heinrich Kreutzmann[4], Till Rümenapf[5], Andrea Ladinig[4] and Armin Saalmüller[1*]

[1]Institute of Immunology, Department of Pathobiology, University of Veterinary Medicine, Vienna, Austria, [2]VetCore Facility for Research, University of Veterinary Medicine, Vienna, Austria, [3]University Clinic for Poultry and Fish Medicine, Department for Farm Animals and Veterinary Public Health, University of Veterinary Medicine, Vienna, Austria, [4]University Clinic for Swine, Department for Farm Animals and Veterinary Public Health, University of Veterinary Medicine, Vienna, Austria, [5]Institute of Virology, Department of Pathobiology, University of Veterinary Medicine, Vienna, Austria

Porcine reproductive and respiratory syndrome virus (PRRSV) is a positive-stranded RNA virus, which emerged in Europe and U.S.A. in the late 1980s and has since caused huge economic losses. Infection with PRRSV causes mild to severe respiratory and reproductive clinical symptoms in pigs. Alteration of the host immune response by PRRSV is associated with the increased susceptibility to secondary viral and bacterial infections resulting in more serious and chronic disease. However, the expression profiles underlying innate and adaptive immune responses to PRRSV infection are yet to be further elucidated. In this study, we investigated gene expression profiles of PBMCs and $CD8^+$ T cells after PRRSV AUT15-33 infection. We identified the highest number of differentially expressed genes in PBMCs and $CD8^+$ T cells at 7 dpi and 21 dpi, respectively. The gene expression profile of PBMCs from infected animals was dominated by a strong innate immune response at 7 dpi which persisted through 14 dpi and 21 dpi and was accompanied by involvement of adaptive immunity. The gene expression pattern of $CD8^+$ T cells showed a strong adaptive immune response to PRRSV, leading to the formation of highly differentiated $CD8^+$ T cells starting from 14 dpi. The hallmark of the $CD8^+$ T-cell response was the increased expression of effector and cytolytic genes (*PRF1*, *GZMA*, *GZMB*, *GZMK*, *KLRK1*, *KLRD1*, *FASL*, *NKG7*), with the highest levels observed at 21 dpi. Temporal clustering analysis of DEGs of PBMCs and $CD8^+$ T cells from PRRSV-infected animals revealed three and four clusters, respectively, suggesting tight transcriptional regulation of both the innate and the adaptive immune response to PRRSV. The main cluster of PBMCs was related to the innate immune response to PRRSV, while the main clusters of $CD8^+$ T cells represented the initial transformation and differentiation of these cells in response to the PRRSV infection. Together, we provided extensive transcriptomics data explaining gene signatures of the immune response of

PBMCs and CD8$^+$ T cells after PRRSV infection. Additionally, our study provides potential biomarker targets useful for vaccine and therapeutics development.

KEYWORDS

PRRSV, CD8$^+$ T cells, PBMCs, RNA-Seq, transcriptome, swine

1 Introduction

Porcine reproductive and respiratory syndrome (PRRS) is a widespread disease responsible for leading economic losses in the swine industry worldwide (1). Only in U.S.A. estimated losses due to PRRS are approximately $664 million per year (2). One of the most remarkable features of PRRSV is the ability of the virus to suppress the host immune system which increases the susceptibility to other viral and bacterial pathogens leading to secondary infections and higher mortality rates (3–6). Recent findings showed that PRRSV causes poor innate immune response by suppressing the cytotoxic activity of NK cells and the production of cytokines. Consequently, this weakens and delays the activation of the adaptive immunity (7–9).

Despite its general success, PRRSV vaccine development has been slow and unable to prevent numerous outbreaks over the past 30 years. The root cause is attributed to the high variability of PRRSV strains, which facilitates constant evolution and sustains their virulence (10, 11). Previous research has found that modified live virus (MLV) vaccines effectively elicit humoral and cell-mediated immune responses against genetically homologous wild-type PRRSV strains, but provide only partial protection against heterologous strains (12–19). Nevertheless, compared to unvaccinated, MLV-vaccinated animals demonstrated improved immune response, with an early onset and efficient control of inflammation as well as effective cell-mediated immunity in case of infection with heterologous field strain (20, 21). However, a great source of concern is the safety of PRRSV-MLV since reports show possible reversion to virulence and recombination between MLVs and wild-type PRRSV strains (22–26). Contrary to MLV, inactivated PRRSV vaccines show better safety, but also unsatisfactory efficacy since they are unable to induce an effective cell-mediated immune response or increase production of PRRSV-specific neutralizing antibodies to reduce viral load (14, 26). The role of inactivated PRRSV vaccines in the induction of an MHC-class I restricted CD8$^+$ T-cell response is also not clear and would in contrast to live attenuated vaccines postulate cross-presentation of the viral antigens. Therefore, the induction of an MHC class I restricted T-cell response, which leads to CD8 T-cell activation and effector functions such as initiation of apoptosis in virus-infected target cells, antiviral cytokine secretion and generation of vaccine induced CD8$^+$ memory T cells needs to be further elucidated (27). Thus, a better understanding of the CD8$^+$ T-cell response could be a key for better vaccine development and PRRSV control.

In the traditional approach, adaptive immunity and virus elimination is facilitated primarily through antigen-specific cytotoxic T lymphocytes (CTLs); however, the role of CTLs in PRRSV infection remains poorly understood. Several scientists have highlighted the necessity of new approaches in experimental analysis of CTLs in PRRSV-infected swine (28). An innovative solution to this problem is transcriptional profiling, which has the capacity to describe the underlying mechanisms of the immune response of CTLs to PRRSV infection. In the past, the focus of PRRSV research has relied on the quantification of viral load using PCR and an immunological assessment via ELISpot assay, flow cytometry, immunohistochemistry, and ELISA. Few researchers have addressed the question of transcriptional profiling following PRRSV infection. Preliminary work in this field has focused primarily on gene set enrichment of peripheral blood mononuclear cells (PBMCs) at fewer time points (29). Transcriptional profiling has been used to monitor expression changes in other swine tissues after PRRSV infection (30–32). However, the characteristics of gene expression changes in PBMCs as well as in CD8$^+$ T cells upon PRRSV infection over the course of time have not been investigated in-depth.

Emerging in Lower Austria in 2015, the highly pathogenic AUT15-33 strain caused a severe clinical outbreaks (33) and has since been confirmed by studies to induce clinical signs and lung lesions (34), highlighting its virulence and potential advantageous properties. In this study we investigated the transcriptomes of PBMCs and CD8$^+$ T cells in PRRSV-infected gilts at different time points after PRRSV AUT15-33 inoculation to better understand PRRS pathogenesis. Our approach combined time-series clustering analysis, protein-protein interaction (PPI) networks, extensive gene ontology (GO) enrichment, pathway analysis, and gene set enrichment analysis (GSEA) to define the innate and adaptive immunity against PRRSV more accurately. To complement our analysis, we also measured viral loads in serum and conducted flow cytometry analyses. Our aim was to identify specific gene profiles in PBMCs and CD8$^+$ T cells which will provide biomarker targets useful for the development of vaccines and therapeutics. Collectively, our findings improve our understanding of gene expression profiles and kinetics of the host immune response during PRRSV infection.

2 Materials and methods

2.1 Animals and cell isolation

A total of 64 samples from eight one-year old gilts were included in the study. PBMCs and MACS-sorted $CD8^+$ T cells were derived from four PRRSV-infected gilts (infected group, from an infection experiment with PRRSV strain AUT15-33, GenBank Acc. No. MT000052.1) as well as from four non-infected gilts (negative control group). At gestation day 85 (± 1), the experimental infection was induced via intranasal administration of AUT15-33 ($5x10^5$ $TCID_{50}$ per animal in approximately 5 mL into both nostrils). Blood was collected at four different time points, starting at day 0 just prior to experimental infection of the infection group, followed by blood sampling at days 7, 14 and approximately 21 (termination day, 21 ± 2) post infection. Prior to euthanasia, animals were anesthetized by intravenous injection of Ketamine (Narketan® 100 mg/mL, Vetoquinol Österreich GmbH, Vienna Austria, 10 mg/kg body weight) and Azaperone (Stresnil® 40 mg/mL, Elanco GmbH, Cuxhaven, Germany, 1.5 mg/kg body weight) and subsequently euthanized via intracardial injection of T61® (Intervet GesmbH, Vienna, Austria, 1 mL/10 kg body weight). PBMCs were isolated from fresh heparinized blood of eight animals by density gradient centrifugation (Pancoll human, density: 1.077 g/mL, PAN-Biotech, Aidenbach, Germany; 30 min at 920 x g). Subsequently, isolated PBMCs were stored at -150°C in a freezing medium (50% (v/v) RPMI 1640 with stable glutamine (PAN-Biotech), 100 IU/mL penicillin and 0.1 mg/mL streptomycin (PAN-Biotech), 40% (v/v) fetal calf serum (FCS, Gibco™, Thermo Fisher Scientific), and 10% (v/v) DMSO (Sigma-Aldrich). All experiments were approved by institutional ethics and animal welfare committee (Vetmeduni Vienna) and the national authority according to §§26ff. of Animal Experiments Act, Tierversuchsgesetz in Austria – TVG 2012 (BMWFW-2021-0.117.108).

2.2 Magnetic-activated cell sorting

Enriched $CD8^+$ T cells were prepared by positive selection of CD8β-labeled PBMCs using magnetic-activated cell sorting (MACS, Miltenyi Biotec, Bergisch Gladbach, Germany). For purification of $CD8\beta^+$ T cells, thawed PBMCs (1×10^8) were incubated with a primary monoclonal anti-CD8β antibody (clone PPT23, IgG1, in-house) for 20 min on ice. In a next step, cells were washed with MACS buffer (PBS w/o Ca/Mg + 2% (v/v) FCS (both Gibco™, Thermo Fisher Scientific) + 2 mM EDTA (Carl Roth GmbH, Karlsruhe, Germany), resuspended in 1.5 mL MACS buffer and incubated with magnetically labeled secondary antibody (rat-anti mouse IgG1, Miltenyi Biotec) for 30 min on ice. After a washing step, cells were resuspended in 3 mL MACS buffer and transferred onto LS columns (Miltenyi Biotec) pre-wetted with buffer. The columns were applied to a magnetic field and the negative fraction was removed by extensive washing. Afterwards columns were removed from the magnetic field and the positive fraction containing $CD8\beta^+$ T cells was eluted in 5 mL MACS buffer. Lastly, sorted cells were resuspended in cold culture medium (RPMI 1640 + 100 IU/mL penicillin + 0.1 mg/mL streptomycin (all PAN Biotech) + 10% (v/v) FCS) and counted using a Cell Counter (XP-300 Hematology Analyzer, Sysmex Europe GmbH, Norderstedt, Germany). The purity of the positively sorted cells was above 90% (FACSCanto™II, BD Biosciences, San Jose, CA, U.S.A.).

2.3 RNA extraction, library preparation and sequencing

Total RNA was isolated from the samples mentioned above using RNeasy Mini Kit with on-column DNase treatment using the RNAse-Free DNase Set (both Qiagen, Hilden, Germany), following manufacturer's protocol. Quantification and quality control of isolated RNA were assessed with Agilent 2100 Bioanalyzer (Agilent RNA 6000 Pico Kit, Agilent Technologies, Palo Alto, CA, U.S.A.). Samples with both a final yield comprised between 3.4 – 36.5 ng/μL and an average RIN value of 8.5 were prepared for sequencing with Lexogen's Poly(A)RNA Selection Kit V1.5 and CORALL™ Total RNA-Seq Kit with UDIs (Lexogen GmbH, Vienna, Austria) to generate Illumina-compatible libraries according to the manufacturer's guidance. Libraries were validated using the Agilent 4200 TapeStation (High Sensitivity D1000 ScreenTape Assay, Agilent Technologies) and the Qubit 3.0 fluorometer (DNA HS assay kit, ThermoFisher, Massachusetts, MA, U.S.A.). Libraries were sequenced on a S4 XP flow cell on a NovaSeq 6000 system (Illumina Inc., San Diego, CA, U.S.A.) implementing paired-end 150-bp reads. The sequencing was performed by the Next Generation Sequencing Facility at Vienna BioCenter Core Facilities (VBCF), member of the Vienna BioCenter (VBC), Austria.

2.4 Mapping and differential gene expression analysis

Standard raw sequencing data in BCL format were converted to FASTQ files using the bcl2fastq2 Conversion Software v2.20 (Illumina Inc.). Afterwards, the FASTQ files were imported into CLC Genomics Workbench 22.0.1 (Qiagen, Aarhus, Denmark) and the reads were subjected to adapter and quality trimming. Only reads with a Phred score of at least 25, a read length between 35 and 75 nucleotides, and no more than two ambiguous nucleotides were retained. Finally, all trimmed reads were mapped to the reference genome of *Sus scrofa* 11.1 from NCBI database (GCA_000003025.6) using default parameters of CLC Genomics RNA-Seq Analysis tool (mismatch cost = 2, insertion cost = 3, deletion cost = 3, length fraction = 0.8 and similarity fraction = 0.8). Principal component analysis (PCA) was performed using TMM adjusted mapped reads after log CPM transformation and z-score normalization. For PBMCs and $CD8^+$ T cells separately, differential gene expression test for differences between all pairs of samples specified for the condition (infected vs. negative control group) using Wald test was performed. Therefore, four pairwise comparisons were made: (i) infected vs. negative control group at 0 dpi, (ii) infected vs. negative control group at 7 dpi, (iii) infected vs. negative control group at 14 dpi, and (iv) infected vs. negative control group at 21 dpi. To define differentially expressed genes (DEGs), the following set of criteria was used: fold-change > |2|, maximum of the average reads per kilobase per million mapped reads (RPKM) > 1.5 and a false discovery rate (FDR) corrected p-value < 0.01. Marker genes were identified by comparing infected to negative control group and selecting genes with non-overlapping expression ranges at time points starting from 7 dpi. The R packages ggplot2 (version 3.4.0), ggvenn (version 0.1.9) and pheatmap (version 1.0.12) were used for plotting, Venn diagrams and heatmaps visualization, respectively (R software version 4.2.2, R Core Team, GNU General Public License).

2.5 Time-series clustering of gene expression data

The Mfuzz R package (version 4.2) was employed for noise-robust soft clustering of gene expression data of two group samples (PBMCs and $CD8^+$ T cells) along time series. For that purpose, DEGs were preselected that were differentially expressed in at least one pairwise comparison between infected and negative control groups at one time point. For the time-series clustering, the average of gene expression at each time point was used. The genes belonging to the core clusters were defined with membership value over 0.7 (α-threshold).

2.6 Functional enrichment analysis

Gene ontology – Biological processes (GO-BP) and Kyoto Encyclopedia of Genes and Genomes (KEGG) enrichment analysis were conducted for genes involved in time-series clustering using the ClueGO v.2.5.9 plug-in in the software environment Cytoscape 3.9.1. version (https://cytoscape.org) (35). The analysis was performed based on GO data for *Sus scrofa*. For the selection of significant GO terms and KEGG pathways, the following cut-off thresholds were used: gene count ≥ 2 genes per term, two-sided hypergeometric statistical testing corrected with the Bonferroni step-down method (p < 0.05) and a Kappa score of 0.4.

2.7 Genetic network analysis

Protein-protein interaction networks were generated using the Search Tool for the Retrieval of Interacting Genes (STRING Version 11.5: http://string-db.org) to find direct or indirect associations between proteins. To explore the potential protein relationships among DEGs, default settings of STRING (Network type: full STRING network; required score: medium confidence (0.400); FDR stringency: medium (5 percent)) were applied.

2.8 Gene set enrichment analysis

GSEA was performed to identify differentially regulated gene sets between experimental groups. Specifically, we analyzed the expression data of $CD8^+$ T cells from the PRRSV-infected group at 21 dpi compared to the control group using the GSEA software version 4.3.2 (36, 37) from Broad Institute and gene sets obtained from the Molecular Signatures Database (MSigDB) (38). The analysis was performed using two "c7.immunesigdb.v2023.1.Hs.symbols.gmt" and "h.all.v2023.1. Hs.symbols.gmt" MsigDB gene sets, conducting 1000 permutations and the "gene_set" option as permutation type and a significance threshold of FDR of less than 0.05. To match the MSigDB gene set human symbols, we converted porcine gene names into their human orthologs using the HGNC Comparison of Orthology Predictions (HCOP) tool from HUGO Gene Nomenclature Committee (https://www.genenames.org/tools/hcop/) prior to analysis.

2.9 Quantification of PRRSV RNA

After thawing serum samples at room temperature, they were vortexed for 10 seconds and centrifuged at 16 000 x g for one minute. Hereafter 140 µL of supernatant was extracted employing the QIAamp Viral RNA Mini QIAcube Kit in a QIAcube (Qiagen, Hilden, Germany). The RT-qPCRs were performed using Luna® Universal One-Step RT-qPCR Kit (New England BioLabs) on a qTower³ G Real-time PCR cycler (Analytik Jena GmbH, Jena, Germany). Primers (sense: 5´-TTTATTCTCGACTCCATCCAACC-3´, antisense: 5´-TTTATTCTCGACTCCATCCAACC-3´) and probe (FAM-5'-TCTTCTTGTGASCACGATTCGCCG-3'-BHQ1) were designed to amplify a 98 bp fragment of the PRRSV1´s conserved ORF1a region. PCR cycling conditions were 55˚C for 10 minutes, then 95˚C for 1 minute, followed by 45 cycles of 95˚C for 10 seconds and 60˚C for 30 seconds (data collection step). Moreover, 10^5, 10^6 and 10^7 genomic equivalents (GE)/µL containing dilutions of a cloned AUT15-33 DNA standard were tested side by side with the samples for absolute quantification. The samples were considered positive if the RT-qPCR demonstrated more than 10^4 copies/mL sample. Blanks consisting of sample-free extracts, which were produced simultaneously to each extraction process as well as no template controls served as negative controls. As a part of a multiplex approach beta-actin mRNA RT-qPCR described by Toussaint et al. (39) was performed for each sample extract to exclude PCR inhibiting substances.

2.10 Flow cytometry staining

Isolated PBMCs were transferred into a microtiter plate (Nerbe Plus, Winsen, Germany) and stained using a 4-step procedure. For each panel, primary monoclonal antibodies (mAbs) and secondary reagents used are listed in Table 1. Incubation steps were conducted at 4°C for 20 minutes, followed by two washes with cold PBS

TABLE 1 Antibodies and secondary reagents used for flow cytometry staining.

Marker	Clone	Isotype	Source	Labelling	Fluorophore
CD8 T cells					
CD3	BB23-8E6-8C8	IgG2b	BD biosciences	Direct	PerCP-Cy5.5
CD8α	11/295/33	IgG2a	In-house	Indirect[A]	BV421
Perforin	δ-G9	IgG2b	eBioscience	Direct	PE
CD8 T subsets					
CD8β	PPT23	IgG1	In-house	Indirect[A]	BV421
CD27	b30c7	IgG1	In-house	Direct	AlexaFluor647
Perforin	δ-G9	IgG2b	eBioscience	Direct	PE

[A]Streptavidin-BV421, Biolegend.

supplemented with 10% (v/v) porcine plasma (in-house preparation) for 4 min at 400 x g and 4°C. Surface antigens were stained with mAbs followed by incubation with secondary reagents. While blocking free binding sites of the isotype-specific secondary antibodies with whole mouse IgG molecules (2 µg per sample, ChromPure, Jackson ImmunoResearch, West Grove, PA, USA), we applied Fixable Viability Dye eFluor 506 (Thermo Fisher Scientific) diluted in PBS, and then washed with cold PBS. Cells were further fixed and permeabilized using a FoxP3 fixation/permeabilization kit (eBioscience) before performing an intracellular staining for perforin. Finally, staining for intracellular antigens was performed using directly conjugated mAbs. Following two wash steps, PBMCs were resuspended in permeabilization buffer. The cell measurements were conducted on a CytoFLEX LX (Beckman Coulter GmbH, Krefeld, Germany) and FACSAria (BD Biosciences). Cytotoxic T cells were quantified over time by evaluating the surface expression of CD3, CD8α, and perforin ($CD3^+CD8\alpha^{high}perforin^+$). On the termination day (21 dpi), $CD8^+$ T-cell subsets were defined as naïve (T_n; $CD8\beta^+CD27^+perforin^-$), intermediate differentiated (T_{inter}; $CD8\beta^+CD27^{dim}perforin^+$), and terminally differentiated cells (T_{term}; $CD8\beta^+CD27^-perforin^{high}$). For the phenotyping a minimum of 300,000 and maximum of 500,000 lymphocytes was recorded for each sample. Data analysis was performed using FlowJo software version 10.8.1 (BD Biosciences).

3 Results

3.1 PRRS viral load

The study investigated viremia to confirm PRRS negative status of gilts prior to experimental infection and to monitor virus replication following infection. No PRRSV RNA was detected in any serum samples collected from the control group or from the infected group collected prior to inoculation on day 0, as determined by qRT-PCR analysis. On 7 dpi and 14 dpi, all infected gilts exhibited viremia. By 21 dpi, persistent viremia was observed in all but one of the infected gilts (Figure 1).

3.2 Data summary and global overview of gene expression

Sequencing 64 libraries generated over 6.02 billion paired-end reads. Each of PBMCs and $CD8^+$ T cells were compared between infected and negative control group at four time points, with four replicates for each, resulting in 32 samples being sequenced for both PBMCs and $CD8^+$ T cells. The percentage of mapping reads to the reference genome was between 92.08% and 94.71% (mean = 93.54%) with approximately 94 million paired-end reads per sample (Supplementary Tables 1, 2). Gene expression data from all samples revealed clear separation between PBMCs and $CD8^+$ T cells. Given this high differentiation, we will describe each of them separately in the following sections.

3.3 Gene expression profile of PBMCs after PRRSV infection

Gene expressions of PBMCs from infected animals were clearly distinct from negative control groups as showed in PCA plot (Figure 2A). Notably, in the PCA plot (Figure 2A), the 0 dpi samples of the infected and negative control groups were observed to be positioned on the same side of the PC1 axis (X-axis), indicating similarities in gene expression at this time point. However, along the PC2 axis (Y-axis), there were subtle differences between samples of the infected and negative control groups at 0 dpi. Although they did not form distinct cluster together, they were the closest groups on the PC2 axis, suggesting shared underlying expression patterns or biological similarities. To define gene expression patterns of PBMCs after PRRSV infection we first looked for differentially expressed genes between infected and negative control group at the different time points (Supplementary Table 3). Using the Wald test for pairwise comparison we identified the highest number of DEGs (n = 277) between infected and negative control group at 7 dpi. The smallest number of DEGs was observed at 0 dpi between infected and negative control group (n = 89). Interestingly, similar numbers of

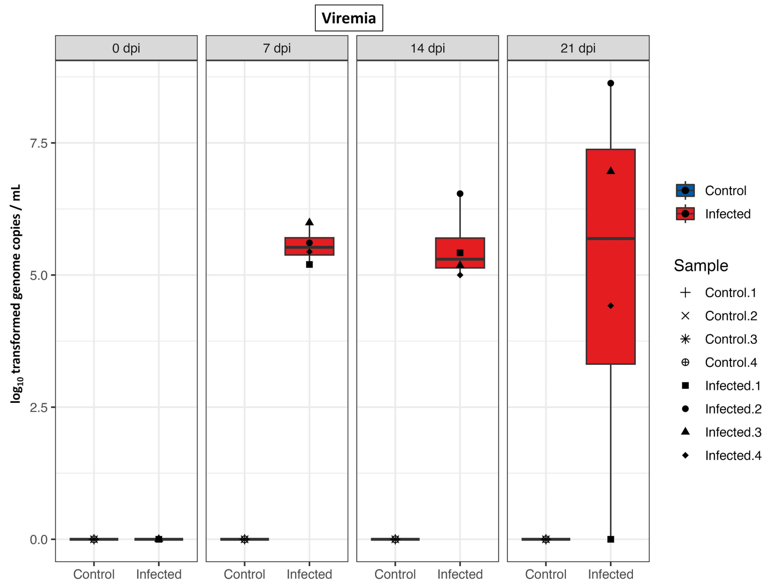

FIGURE 1
PRRS viral load in serum. Boxplots of qRT-PCR results from serum samples (log_{10} genome copies/mL) of control and infected groups at different time points after infection.

DEGs were found between infected and negative control group at 14 dpi (n = 147) and 21 dpi (n = 172).

Venn diagrams were generated using DEGs to represent the overlapping and non-overlapping genes from 0 dpi to 21 dpi in PBMCs and CD8$^+$ T cells, respectively. The Venn diagrams revealed that the largest overlap of DEGs was found between PBMCs from infected animals at 14 and 21 dpi (n = 77), while the intersection of PBMCs from infected animals at 7, 14, and 21 dpi exhibited a smaller overlap (n = 32) (Figure 2B). Additionally, a higher number of DEGs were only expressed in PBMCs from the infected group at 0 dpi (n = 74), 7 dpi (n = 141) and 21 dpi (n = 97). Notably, DEGs in PBMCs of the infected group at 0 dpi were rarely expressed at other time points. In contrast, DEGs in PBMCs at 14 dpi were mostly shared at other time points.

3.4 Gene expression profile of CD8$^+$ T cells after PRRSV infection

PCA plot showed clear separation regarding gene expressions of CD8$^+$ T cells from infected and negative control group for samples belonging to 7 dpi onwards (Figure 3A). We identified the highest number of DEGs (n = 533) between infected and negative control group on the last day after infection (21 dpi). In contrast, the

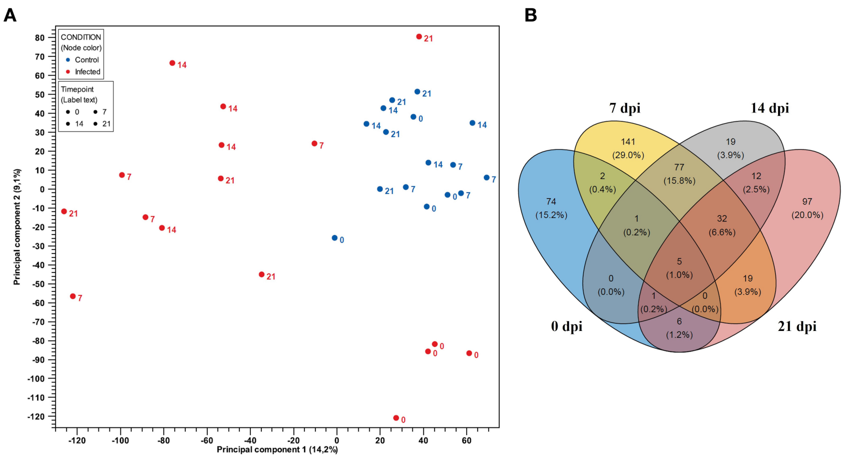

FIGURE 2
(A) PCA plot of expression data derived from 32 PBMCs samples of four PRRSV-infected gilts and four non-infected gilts at four time points. Red color indicates the infected samples, with blue indicating the negative control group. Numbers represent time points (0, 7, 14, and 21 dpi). PC1 explains 14.2% and PC2 explains 9.1% of the observed variance in data. **(B)** Venn diagram showing the overlap of DEGs in PBMCs between the control and PRRSV infected group from 0 dpi to 21 dpi.

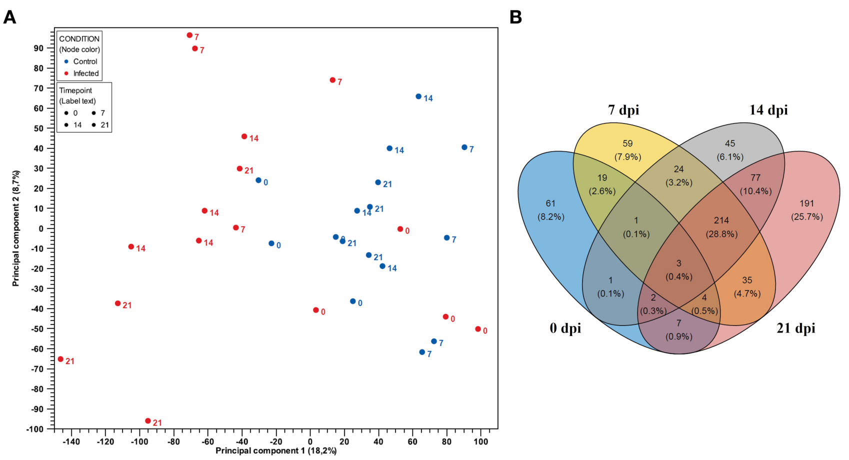

FIGURE 3
(A) PCA plot of expression data derived from 32 CD8$^+$ T cell samples from four PRRSV-infected gilts and from four non-infected gilts. Red color indicates the infected samples, with blue indicating the negative control group. Numbers represent time points (0, 7, 14 and 21 dpi). PC1 explains 18.2% and PC2 explains 8.7% of the observed variance in data. **(B)** Venn diagram showing the overlap of DEGs in CD8$^+$ T cells between the control and PRRSV-infected group from 0 dpi to 21 dpi.

smallest number of DEGs was observed on 0 dpi (n = 98). Interestingly, similar numbers of DEGs were discovered between infected and negative control group at 7 dpi (n = 359) and 14 dpi (n = 367). Furthermore, the Venn diagram (Figure 3B) revealed a high number of unique DEGs at 21 dpi (n = 191). However, we also found a high number of DEGs shared among CD8$^+$ T cells from infected animals at 7 dpi, 14 dpi and 21 dpi (n = 214). In particular, the expression profile of CD8$^+$ T cells of the infected group at 14 dpi shared three times more genes with the expression profile of CD8$^+$ T cells from infected animals at 21 dpi (n = 77) than with the expression profile of CD8$^+$ T cells from infected animals at 7 dpi (n = 24). The DEGs of CD8$^+$ T cells at 0 dpi were mostly unique and intersected to some extent with DEGs of CD8$^+$ T cells of the infected group at dpi 7, suggesting possible changes in the transcriptional profile of CD8$^+$ T cells over time.

3.5 Genetic network analysis of PBMCs and CD8$^+$ T cells during PRRSV infection

To get an overview of the molecular processes involved in the transcriptional response of infected PBMCs and CD8$^+$ T cells, we extracted information about the protein-protein interactions (PPI) of DEG genes from the STRING database and visualized them in the form of networks. After applying MCL clustering on each network, we identified one main cluster for 0 dpi. Cluster 1 contained 13 proteins associated with the blood coagulation and the smooth muscle cell migration. Two clusters were identified for 7 dpi: the first cluster included immune response to virus, innate immune response and regulation of cytokines; the second consisted of proteins enriched for apoptotic processes. Similarly, at 14 dpi, two main clusters were recorded: cluster 1 consisted of 34 proteins enriched for biological processes including immune response to virus, innate immune response and regulation of cytokines, and cluster 2 included 16 proteins linked to the regulation of cell cycle processes. A similar pattern was observed at 21 dpi, with two clusters identified but with different numbers of proteins. Specifically, cluster 1 consisted of 21 proteins associated with the regulation of cell cycle processes, and cluster 2 included 12 proteins involved in biological processes such as the immune response to viruses, innate immunity, and regulation of cytokines (Figures 4A–D).

To construct PPI networks of CD8$^+$ T cells we used DEGs of CD8$^+$ T cells of the infected group at the different time points of infection (Figures 5A–D). For DEGs of 0 dpi, similar to the PBMCs, the main cluster consisted of proteins associated with blood coagulation. PPI analysis of 359 DEGs of the infected group for 7 dpi revealed 5 clusters (Supplementary Table 4). Cluster 1 consisted of 149 proteins linked to regulation of cell cycle processes; cluster 2 was associated with immune response to virus, interferon alpha and beta, and cytokines; cluster 3 consisted of 9 proteins related to chemokine-mediated signaling pathway, inflammatory response, and immune response; cluster 4 and 5 involved 7 and 6 proteins correlated to cell redox homeostasis and chromatin processes, respectively. At 14 dpi, 5 clusters were identified. Similar to 7 dpi, clusters 1 and 2 included proteins related to regulation of cell cycle processes, immune response to virus, interferon alpha and beta, and cytokines; cluster 3 consisted of 23 proteins and was linked to immune response, lymphocyte activation, adaptive immune response, immune effector process, and cytokine-mediated signaling pathway. Both cluster 4 and 5 contained 9 proteins, but with different biological functions associated with it. Cluster 4 was associated with the cytoskeleton organization, whereas cluster 5 was associated with the regulation of oxidoreductase activity. Interestingly, the cluster 6 contained proteins related to the chemokine-mediated signaling pathway, chemotaxis, inflammatory response, and immune response. At 21 dpi, the largest cluster (cluster 1) consisted of 173 proteins involved in the regulation of cell cycle processes. Cluster 2 consisted of proteins associated with the T-cell activation, differentiation, adaptive

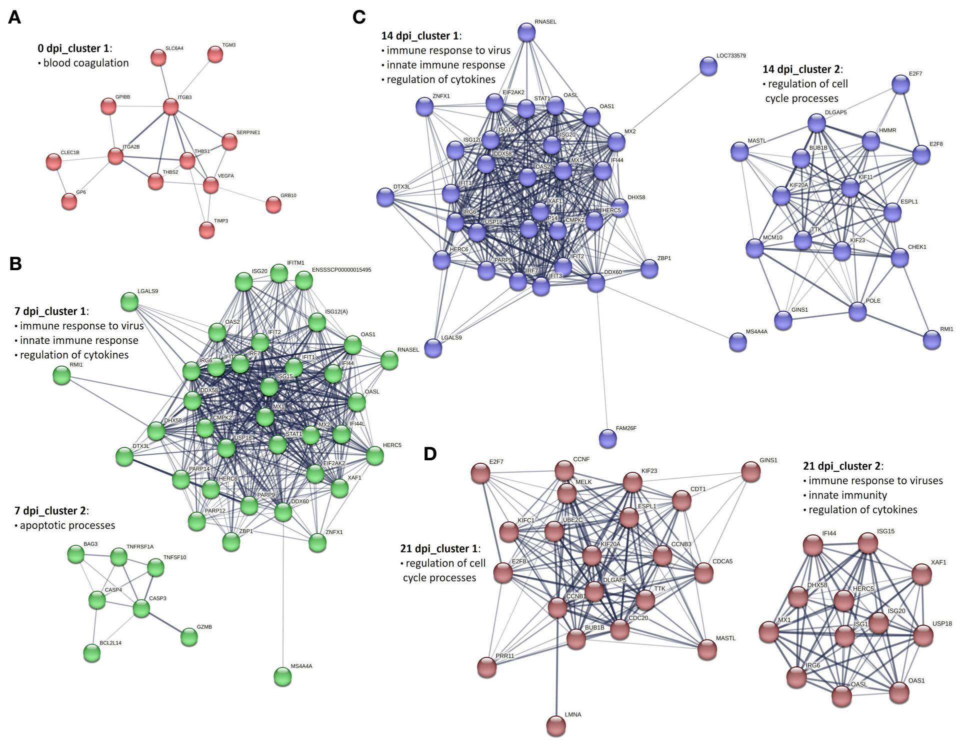

FIGURE 4
Key PPI networks of DEGs in PBMCs from PRRSV-infected animals **(A)** at 0 dpi, **(B)** clusters 1 and 2 at 7 dpi, **(C)** clusters 1 and 2 at 14 dpi, and **(D)** clusters 1 and 2 at 21 dpi.

immune response, regulation of cell killing, and cytokine production. Clusters 3 and 4 were linked to developmental processes and immune response, respectively. Cluster 5 was related to the chemokine-mediated signaling pathway, inflammatory response, immune response, T-cell chemotaxis, and response to cytokines. Both clusters 6 and 8 gathered proteins mostly related to the cell cycle processes. Finally, cluster 7 was specific for the immune response activation and cluster 9 for cytolysis activity (Supplementary Table 4).

3.6 Gene expression changes in PBMCs and CD8$^+$ T cells during PRRSV infection

To gain a deeper understanding of the gene expression changes during PRRSV infection, we further analyzed DEGs at different time points after infection. To visualize these changes, we created heatmaps using DEGs from PBMCs and CD8$^+$ T cells that were differentially expressed in at least one comparison between infected and negative control group at one time point.

For PBMCs from infected animals we found that transcription factor genes *FOSL2* and *CREM* were highly expressed at 0 dpi, while *STAT1*, *PLSCR1*, and *ETV7* were highly expressed at 14 dpi and 21 dpi (Figures 6A–E). It is known that *ETV7* acts as a negative regulator of the type I IFN response, in particular on antiviral interferon-stimulated genes (ISGs) (40). On the other side, the expression of *EGR3*, an early growth response 3 transcription factor that suppresses the T-cell activation and the expression of *IFNGR1* which contributes to the anti-inflammatory effects of type I INFs, was highly upregulated at 21 dpi only (41, 42).

Several genes encoding effector functions including granzymes (*GZMA*, *GZMB*, *GZMK*) and *KLRD1* were increased. Besides 0 dpi, expression of *GZMA* was increased at all other time points. Transcripts of *BCL2L14*, *GZMB* and *KLRD1* were highly upregulated at 7 dpi and 14 dpi. Notably, the apoptotic gene (*ANXA1*) and the heat-shock protein (*HSP90B1*) were markedly upregulated at 7 dpi only. In contrast, another apoptotic gene (*ANXA8*) and granzyme K (*GZMK*) were highly expressed at 21 dpi.

Looking at cytokine genes, we found that only the expression of *IRF7* was significantly upregulated at 7 dpi and 14 dpi. In case of chemokine genes, PBMCs from infected animals showed high expression of chemokine receptors (*CCR1*, *CCR2*), chemokine ligands (*CCL2*, *CCL8*, *CCL9*, *CXCR6*, *CXCL10*, *CXCL13*). Interestingly, *CCL2*, *CCL8*, *CXCL9*, *CXCL13* and *CXCR6* were highly upregulated at dpi 21 only. While chemokine receptors (*CCR1*, *CCR2*) were upregulated at 7 and 14 dpi, the expression of *CXCL10* was increased from 7 dpi to 21 dpi.

We identified a group of genes that encode co-stimulatory and co-inhibitory molecules, including members of the tumor necrosis factor superfamily (TNFSF) and their receptors (TNFRSF). Both *TNFSF10* (TRAIL) and *TNFSF13B* (APRIL) were highly expressed at 7 dpi and 14 dpi. Furthermore, the expression of *TNFAIP6* and *HAVCR2* (TIM3), later known as an inhibitory receptor responsible for CD8 T-cell exhaustion during chronic viral infection (43), were

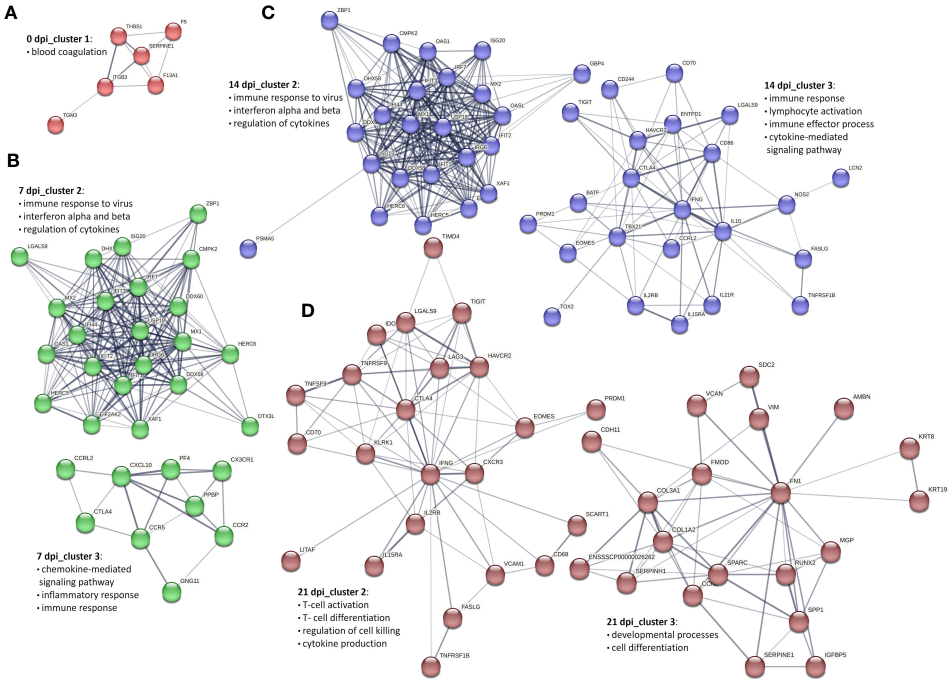

FIGURE 5
Selected PPI networks of DEGs in CD8$^+$ T cells derived from PRRSV-infected animals **(A)** at 0 dpi, **(B)** clusters 2 and 3 at 7 dpi, **(C)** clusters 2 and 3 at 14 dpi, and **(D)** clusters 2 and 3 at 21 dpi.

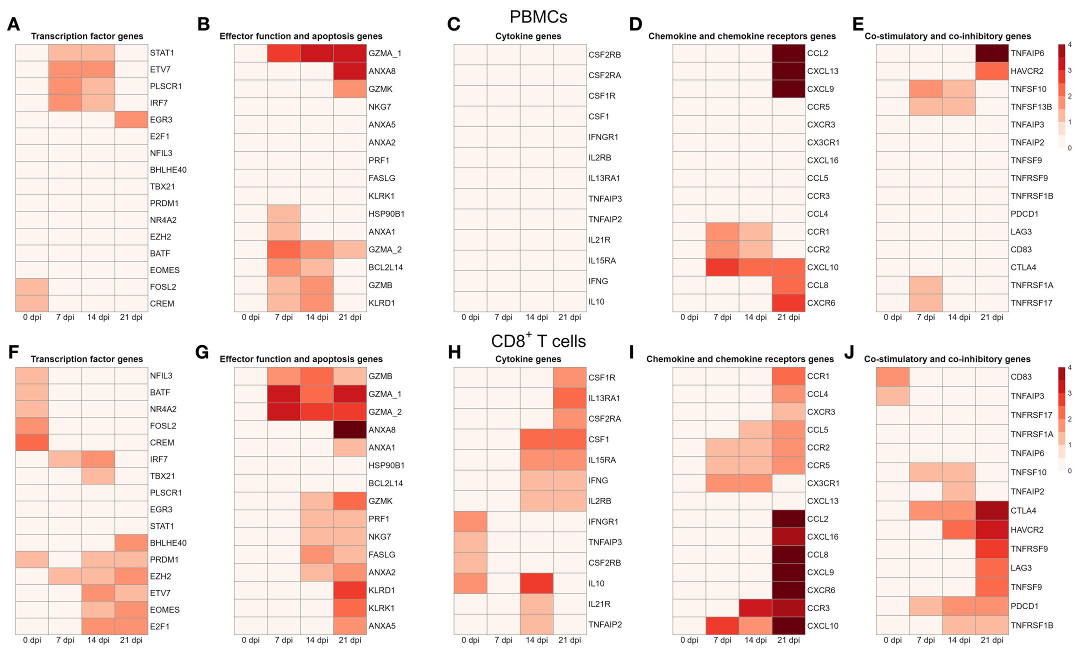

FIGURE 6
Transcription profiles of PBMCs and CD8$^+$ T cells from four infected animals at four time points. All genes shown in the heat maps are differentially expressed genes at least in one material (PBMC or CD8$^+$) and at least in one time point. The heatmap shows the log2 transformed expression data for these selected DEGs in PBMCs: **(A)** for transcription factor genes, **(B)** for genes associated with effector functions and apoptosis, **(C)** for cytokine genes **(D)** for chemokine and chemokine receptor genes, and **(E)** for genes of co-stimulatory and co-inhibitory molecules; in CD8$^+$ T cells: **(F)** for transcription factor genes, **(G)** for genes associated with effector functions and apoptosis, **(H)** for cytokine genes **(I)** for chemokine and chemokine receptor genes, and **(J)** for genes of co-stimulatory and co-inhibitory molecules. A value of 0 indicates that there is no change in gene expression between the infected and negative control groups. As criteria to define DEGs, fold-change > |2| compared to negative control group, maximum of the average RPKM > 1.5 and a false discovery rate corrected p-value < 0.01 (FDR) were used.

increased at 21 dpi only. An opposite expression pattern was observed for *TNFRSF1A* and *TNFRSF17* (BCMA) with expression levels being upregulated at 7 dpi only.

In contrast to PBMCs, we found a higher number of DEGs encoding transcription factors in CD8$^+$ T cells. From transcription factor genes found in PBMCs, only *FOSL2*, *CREM*, and *ETV7* were also upregulated in CD8$^+$ T cells (Figures 6F–J). Similarly to PBMCs, transcription levels of *FOSL2* and *CREM* were increased on 7 dpi only. On the other hand, several genes associated with the late stages of porcine CD8$^+$ T-cell differentiation (44) including *TBX21*, *PRDM1* (Blimp-1) and *EOMES* were highly upregulated in CD8$^+$ T cells upon PRRSV infection. Moreover, all these genes were highly expressed at 14 dpi and 21 dpi. While *BHLHE40* was significantly upregulated at 21 dpi, expression of *NR4A2*, *NFIL3*, and *BATF* was increased at 0 dpi. Previous studies showed that *BHLHE40*, a member of the basic helix-loop-helix TF family, correlates with cytokine and effector/cytolytic molecules production in human and mice (45, 46).

Looking at effector function genes, we found the upregulation of granzymes (*GZMA*, *GZMB*, *GZMK*), perforin (*PRF1*), killer cell lectin like receptors (*KLRK1*, *KLRD1*), and fas ligand (*FASLG*). Generally, the highest expression of these genes was recorded at 21 dpi. From four apoptotic genes (*ANXA1*, *ANXA2*, *ANXA5*, *ANXA8*) found, *ANXA8* showed the strongest upregulation. Interestingly, transcripts of *NKG7*, a natural killer cell granule protein 7 essential for the perforin-dependent cytolytic pathway and expressed in cytotoxic granules of activated CD8$^+$ T cells (47), were highly increased at 14 dpi and 21 dpi. Besides *GZMK*, which was upregulated at 14 and 21 dpi, other granzymes (*GZMB*, *GZMA_1*, *GZMA_2*) were upregulated from 7 dpi to 21 dpi. Both *FASLG* and *PRF1* were highly upregulated at 14 dpi and 21 dpi. Moreover, genes encoding killer cell lectin like receptors (*KLRD1*, *KLRK1*) were upregulated at 21 dpi only.

Contrary to the expression profile of PBMCs, we detected a high expression of several cytokine genes in CD8$^+$ T cells such as *IL10*, *IL2RB* (CD122), *IFNG* (IFN-γ), *IFNGR1* (CD119), and *IRF7*. Also, colony stimulating factors and receptors (*CSF1*, *CSF1R*, *CSF2RA*) were highly upregulated at 14 dpi and 21 dpi. Besides upregulation in expression levels of *IL10* and *IL2RB*, we also found increased expression in other interleukin receptor genes such as *IL21R*, *IL15RA*, and *IL13RA1*. Also, both genes of TNF-induced proteins, *TNFAIP2* and *TNFAIP3* were upregulated in CD8$^+$ T cells.

In comparison to chemokine genes in PBMCs, we found a higher number and markedly higher expressions of chemokine genes in CD8$^+$ T cells derived from PRRSV-infected animals. Moreover, the highest transcript levels of chemokine receptors (*CCR1*, *CCR2*, *CCR3*, *CCR2*, *CCR5*) and chemokines (*CCL2*, *CCL4*, *CCL8*, *CXCR3*, *CXCR6*, *CXCL9*, *CXCL10*, *CXCL16*) were detected at 21 dpi. The *CX3CR1*, a receptor of fractalkine expressed on virus-specific CD8$^+$ T effector cells (48), was upregulated at 7 and 14 dpi. Also, two more chemokine genes, namely *CCR2* and *CCR5*, displayed the same expression pattern. Both *CCR3* and *CCL5* were significantly elevated in CD8$^+$ T cells from PRRSV-infected swine at 14 and 21 dpi. We found a set of genes including *CCR1*, *CCL2*, *CCL4*, *CCL8*, *CXCR3*, *CXCR6*, *CXCL9*, and *CXCL16* highly expressed at 21 dpi only.

In case of co-stimulatory and co-inhibitory molecules, we observed induced expression of *PDCD1* (PD-1) and *CTLA4* from 7 dpi to 21 dpi. Both *HAVCR2* and *TNFRSF1B* were upregulated at 14 dpi and 21 dpi. Furthermore, expressions of *LAG3*, *TNFSF9*, and its receptor *TNFRSF9* (4-1BB) were significantly increased in PRRSV-infected CD8$^+$ T cells at 21 dpi. Expression level of *TNFSF10* (TRAIL) was increased at 7 dpi and 14 dpi, while *CD83* was increased at 0 dpi only.

3.7 Time-series clustering of gene expression data in PBMCs and CD8$^+$ T cells during PRRSV infection

To detect genes with correlated gene expression dynamics during PRRSV infection we performed clustering analysis for the union of 486 DEGs of PBMCs, which were differentially expressed in at least one pairwise comparison between infected and negative control group at one time point. For the time-series clustering, the average of the gene expression at each time point was used. We obtained three gene sets with different expression trends (Figure 7). Genes in cluster 1 (139) had an acute peak at 7 dpi and were then decreasing from 7 dpi to 21 dpi. An upward expression trend for 80 genes in cluster 2 was observed, while a downward expression trend was observed for 56 genes in cluster 3. Furthermore, in cluster 2, expressions of the genes were stable from 0 dpi to 14 dpi, while they increased from 14 to 21 dpi. In contrast to cluster 2, gene expressions in cluster 3 decreased from 0 dpi to 7 dpi and then tended to be stable from 7 dpi to 21 dpi (Supplementary Table 5).

To reveal the biological processes involved in each gene expression cluster, Gene Ontology and KEGG enrichment analyses were performed using ClueGO as described above. The top ten GO terms in each cluster are represented in Figure 8A. Cluster 1 was mainly enriched in processes involved in defense response to virus and innate immune response. Cluster 2 was associated with humoral immune response, complement activation and leukocyte chemotaxis. On the other hand, cluster 3 was enriched in genes involved in blood coagulation and regulation of receptor-mediated endocytosis. KEGG analysis revealed 10 and 12 significantly enriched pathways in cluster 1 and 2, respectively (Figure 9A). Cluster 1 involved genes enriched for influenza A, NOD-like, RIG-I-like, and toll-like receptor signaling pathway. The RIG-I-like receptor signaling pathway, responsible for detecting viral pathogens and generating innate immune responses, contained *CXCL10*, *DHX58*, *IFIH1*, *IRF7*, *ISG15*, and *RIGI* genes. At the same time, the toll-like receptor signaling pathway included *CXCL10*, *IRF7*, *STAT1*, *TLR7* and *TLR8* genes. The genes *C1QA*, *C1QB*, *C1QC*, *C1S*, *C3*, and *C4A* in cluster 2 were predominantly enriched in top ten pathways including *Staphylococcus aureus* infection, pertussis and complement and coagulation cascades. Genes from cluster 3 were not significantly enriched in any KEGG pathway.

The union of 743 DEGs of CD8$^+$ T cells between infected and control animals at each time point were subjected to the time-clustering analysis. With the abovementioned cutoff criteria, four clusters were recorded (Figure 7). Among these, an upward

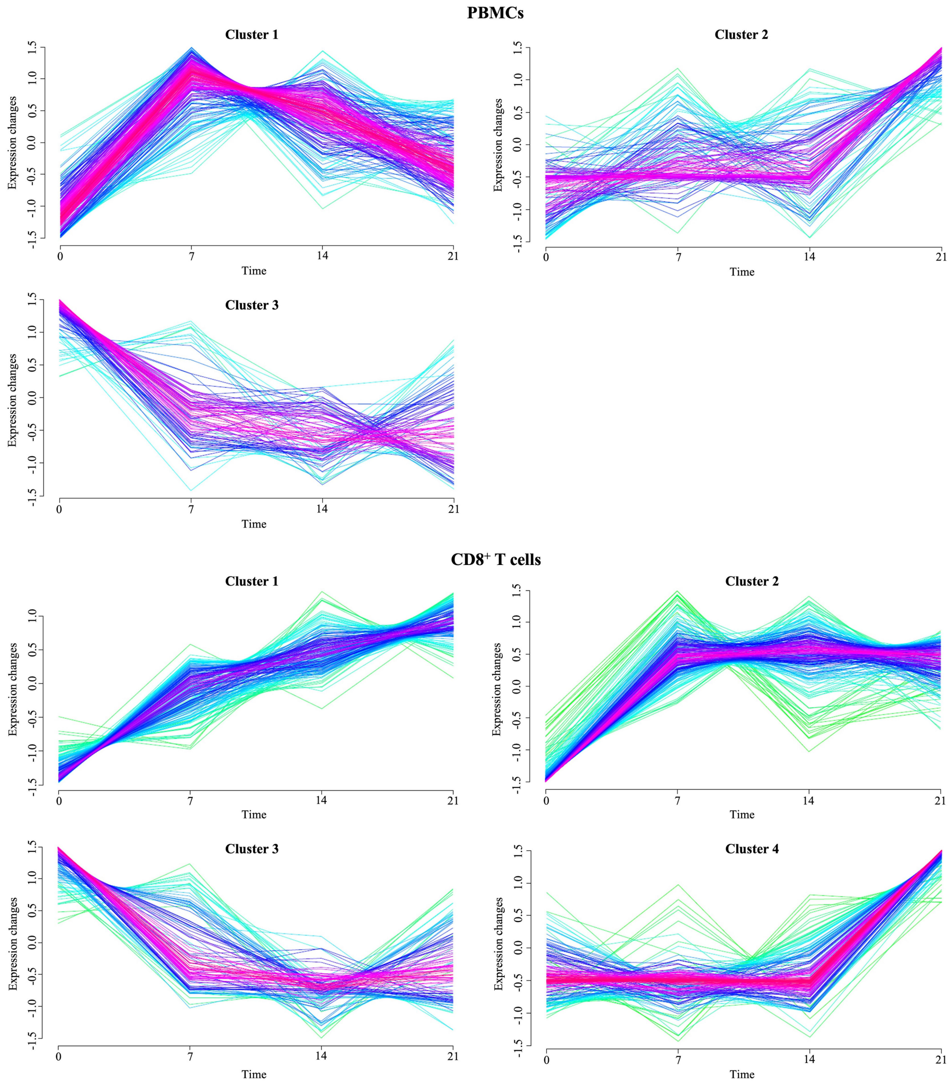

FIGURE 7
Temporal clustering of genes expressed in PBMCs and CD8+ T cells from PRRSV-infected animals. The Y-axis marks the expression changes and X-axis the time points (0, 7, 14 and 21 dpi). Colors indicate membership value, red and purple indicate strong membership (core of a cluster), while green and blue indicate weak membership.

expression trend in cluster 1 (24 genes), cluster 2 (55 genes), and cluster 4 (97 genes) was observed. Conversely, genes involved in cluster 3 (44 genes) showed a downward expression trend from 0 dpi to 7 dpi, with their expression levels stabilizing from 7 dpi to 21 dpi. Both cluster 1 and 4 reached the peak of the gene expression levels at 21 dpi. Genes in cluster 1 were characterized by continuous increase of expression levels from 0 dpi to 21 dpi. In contrast to cluster 1, gene expressions in cluster 4 were stable from 0 dpi to 14 dpi while increasing from 14 dpi to 21 dpi. Finally, cluster 2 grouped genes that primarily increased at 7 dpi and then remained at their plateau expression level from 7 dpi to 21 dpi.

Top ten GO terms for the genes involved in four clusters of CD8+ T cells are listed in Figure 8B. Genes in cluster 1 were enriched in cell cycle process (*AURKB*, *INCENP*), carbohydrate derivative catabolic process (*DUT*, *PNP*), and cyclin-dependent protein serine/threonine kinase inhibitor activity (*CASP3*, *CDKN2C*). Cluster 2 had enriched GO terms in the regulation of mitotic cell cycle, cell cycle checkpoint signaling, and DNA replication. This suggests apparent involvement in cell proliferation. Cluster 3 was enriched in regulation of long-chain fatty acid transport and Fc-epsilon receptor signaling pathway. The genes *CCL2*, *CCL4*, *CCL8*, *CXCL10*, *CXCL16*, *CXCL9*, *CXCR6*, *KLRK1*, *LGMN*, and *RARRES2* from cluster 4 were mostly enriched in top ten GO terms including cell chemotaxis, chemokine activity, and chemokine-mediated signaling pathway. In comparison to the GO enrichment analysis, the KEGG analysis revealed a smaller number of enriched pathways for the four clusters (Figure 9B). Genes involved in cluster 1 were not significantly enriched in any KEGG pathway. Cluster 2 contained *POLE*, *POLE2*, *RPA3*, *BLM*, *BRCA1*, *MCM6*, and *RFC4* which were enriched in DNA replication and repair, as well as the p53 signaling pathway. Genes in cluster 3 were enriched in asthma and bladder cancer pathways only. Similarly to cluster 3 of PBMCs, cluster 4 of CD8+ T cells was enriched in *Staphylococcus aureus* infection,

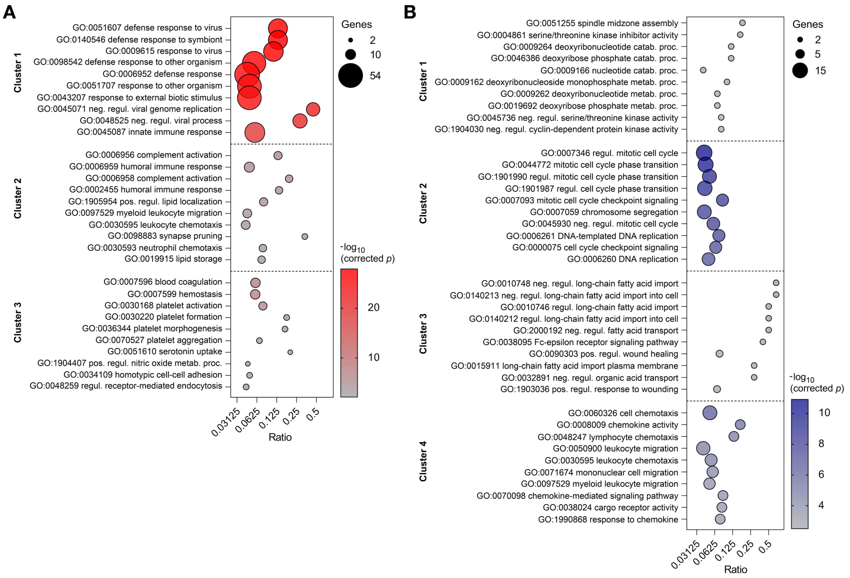

FIGURE 8
Top ten enriched GO terms in three clusters of PBMC **(A)** and four clusters of CD8$^+$ T cells **(B)**. GO terms are listed in descending order of corrected p-value. The size of the bubbles indicates the number of genes enriching the corresponding annotation. Ratio refers to the number of genes found in the dataset relative to the total number of genes associated with the respective GO term.

pertussis, and complement and coagulation cascades. Additionally, it was also enriched in the chemokine signaling and antigen processing and presentation pathways (Supplementary Table 5).

3.8 GSEA of gene expression profile in CD8$^+$ T cells from PRRSV-infected group at 21 dpi

The expression profile of CD8$^+$ T cells from the PRRSV-infected group at 21 dpi showed high levels of effector-associated markers such as *TBX21* (T-bet), *GZMA*, *GZMB*, *GZMK*, *PRF1*, *KLRK1*, *KLRD1*, and *FASLG*. However, these cells also expressed several coinhibitory receptors, including *PDCD1*, *CTLA4*, *LAG3*, and *HAVCR2* (TIM3), as well as the transcription factor *EOMES*. The prolonged expression of these markers is a distinctive feature of exhausted CD8$^+$ T cells (49, 50). To investigate further, GSEA was performed to determine whether expression data of CD8$^+$ T cells from PRRSV-infected group at 21 dpi exhibits statistically significant differences with an *a priori* defined set of genes.

Our findings indicate that CD8$^+$ T cells from PRRSV-infected group at 21 dpi exhibit a gene expression profile that is distinct from exhausted cells. Specifically, we found that genes upregulated in effector CD8$^+$ T cells were enriched in the CD8$^+$ T cells from PRRSV-infected group, while genes associated with T cell exhaustion signatures were downregulated (Supplementary Figure 1). Furthermore, our GSEA of effector CD8$^+$ T cells from PRRSV-infected group revealed significant enrichment of genes

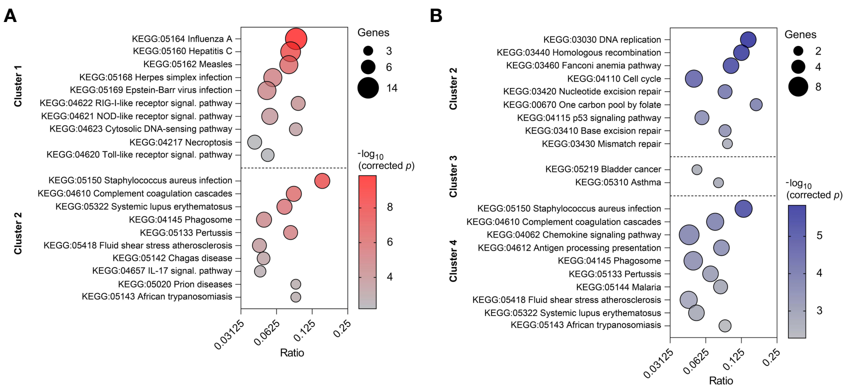

FIGURE 9
Top ten enriched KEGG pathways in two clusters of PBMC **(A)** and three clusters of CD8$^+$ T cells **(B)**. KEGG pathways are listed in descending order of corrected p-value. The size of the bubbles indicates the number of genes enriching the corresponding annotation. Ratio refers to the number of genes found in the dataset relative to the total number of genes associated with the respective KEGG pathway.

10.3389/fimmu.2023.1159970

associated with effector CD8$^+$ T cell state during chronic LCMV infection, while these genes were downregulated in the exhausted state. Notably, the gene expression profile of CD8$^+$ T cells from the PRRSV-infected group showed a significant enrichment in genes upregulated in effector CD8$^+$ T cells at the peak expansion phase (day 8 after LCMV-Armstrong infection) compared to effector CD8$^+$ T cells at the contraction phase (day 15 after LCMV-Armstrong infection), indicating a highly active effector state. As expected, these genes were also significantly enriched in effector CD8$^+$ T cells at the peak expansion phase (day 8 after LCMV-Armstrong infection) compared to memory CD8$^+$ T cells (day 40+ after LCMV-Armstrong infection). GSEA of Hallmark gene sets revealed significant enrichment of CD8$^+$ T cells from the PRRSV-infected group in IFN-α response, IFN-γ response and inflammatory response (Supplementary Figure 2). Moreover, findings showed that gene sets related to cell division and proliferation (E2F targets, G2/M checkpoint, mitotic spindle assembly) as well as effector metabolic programming (glycolysis, MYC targets, mTORC1 complex) were positively enriched in CD8$^+$ T cells from PRRSV-infected group at 21 dpi. Additionally, CD8$^+$ T cells from the PRRSV-infected group at 21 dpi showed significant enrichment in three hallmark gene sets associated with T cell activation, acute phase response, and maintenance of effector CD8$^+$ T cells during infection.

3.9 Temporal quantification of cytotoxic T cell response to PRRSV infection

Characterization of porcine CTLs can be described by the expression of CD3, CD8α and perforin (51). In this study, we investigated the temporal changes of CTLs in response to PRRSV infection, with the aim to provide valuable insights into the role of CTLs in immune response to PRRSV. Here the population of CTLs was defined as CD3$^+$CD8α^{high}perforin$^+$ cells (Figure 10A). Mean frequencies of CD3$^+$CD8α^{high}perforin$^+$ remained stable in control group, while they progressively increased in PRRSV-infected group over time. Notably, during the period from 7 dpi to 21 dpi, average increase of CD3$^+$CD8α^{high}perforin$^+$ was approximately 55% in infected groups compared to the control groups. Also, the highest frequencies of CD3$^+$CD8α^{high}perforin$^+$ in PRRSV-infected group were recorded at 21 dpi (mean = 20.1%) (Figure 10B).

3.10 Differentiation stages of PRRSV-infected CD8β$^+$ T cells

Our current understanding of the differentiation stages that porcine CTLs undergo in response to PRRSV infection is limited. Previous studies showed that we can identify these stages by analyzing the expression of CD8β, CD27, and perforin (44, 51, 52). To gain further understanding of the differentiation process upon PRRSV infection, we investigated the differentiation stages of CTLs by analyzing the phenotypic expression of these three markers at 21 dpi (Figure 11A). Due to technical issues, two animals (one from each group) had to be excluded from the analysis, resulting in a final sample size of 3 animals in the PRRSV-infected group and 3 animals in the control group. The results showed an 62% increase of total CD8β$^+$ T cells in the PRRSV-infected group at 21 dpi, with a mean frequency of 19.2% compared to 11.8% in the control group (Figure 11B). Furthermore, the distribution of three distinct subsets of CD8β$^+$ T cells differed markedly between the control and PRRSV-infected groups. Although the mean frequencies of naïve cells (T_n; CD8β$^+$CD27$^+$perforin$^-$) were comparable between the control and PRRSV-infected groups (mean = 8.5% vs. 8.4%), there were notable differences in the distribution of intermediate differentiated (T_{inter}; CD8β$^+$CD27^{dim}perforin$^+$) and terminally differentiated cells (T_{term}; CD8β$^+$CD27$^-$perforin^{high}) between the two groups. Specifically, in the PRRSV-infected group, we observed a remarkable increase of T_{inter} and T_{term} frequencies, which were over 6.6 and 2.2 times higher than those in the control group, respectively.

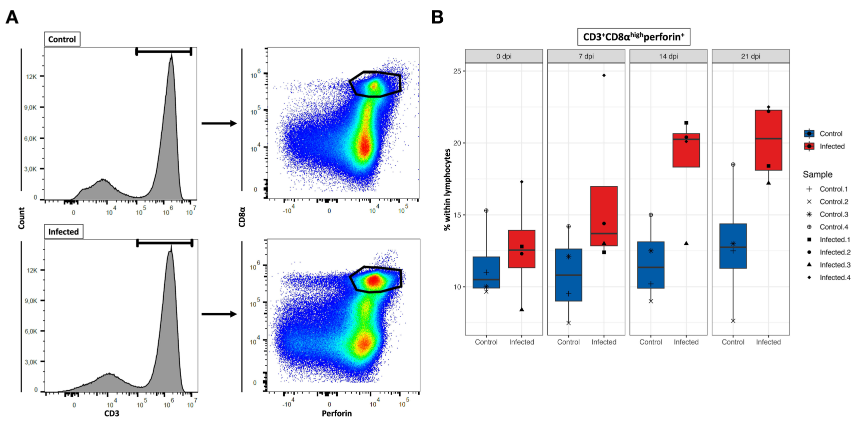

FIGURE 10
Total number of CD8$^+$ T cells at four time points. **(A)** Gating strategy for a representative control and PRRSV-infected animals at 21dpi for the determination of CD8$^+$ T cells. **(B)** Total CD8$^+$ T cells numbers calculated based on the percentages of CD3$^+$CD8α^{high}perforin$^+$ cells in total lymphocytes measured by FCM.

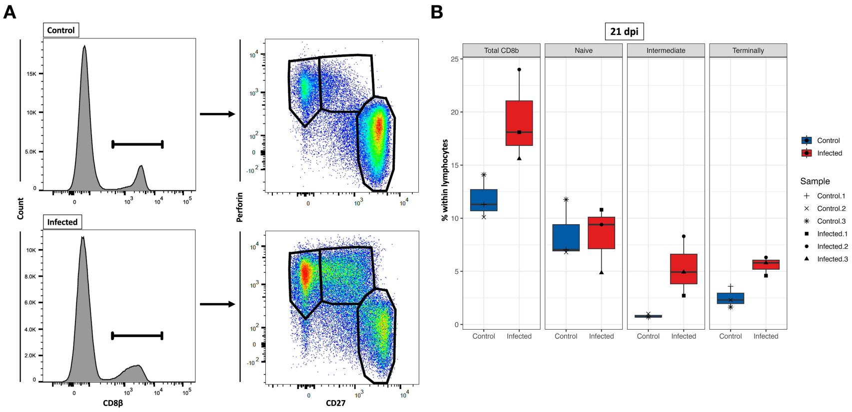

FIGURE 11
Characterization of three CD8β+ T cell subsets at 21 dpi. **(A)** Gating strategy for a representative control and PRRSV-infected animals for the determination of three CD8β+ cell subsets: naïve (T_n; CD8β+CD27+perforin-), intermediate differentiated (T_{inter}; CD8β+CD27dimperforin+), and terminally differentiated cells (T_{term}; CD8β+CD27-perforinhigh). **(B)** T_n (CD8β+CD27+perforin-), T_{inter} (CD8β+CD27dimperforin+), and T_{term} cells (CD8β+CD27-perforinhigh) numbers were calculated based on the percentages of subset in total lymphocytes measured by FCM.

4 Discussion

In this study, we investigated the gene expression profiles of PBMCs and CD8+ T cells after infection with PRRSV strain AUT15-33 over 21 days by identifying the differentially expressed genes and conducting time-course clustering analysis at four time points (0, 7, 14 and 21 dpi) to determine gene expression dynamics of the immune response against PRRSV. To the best of our knowledge, this is the first study which comprehensively describes the time-course of transcriptome responses to PRRSV infection in PBMCs and CD8+ T cells.

The findings of this study highlight significant differences in the gene expression patterns of PBMCs and CD8+ T cells in response to PRRSV infection. The identification of the highest number of DEGs at different time points in each cell type suggests that the immune response is dynamic and time-dependent. The heterogeneous gene expression patterns observed in PBMCs suggest that different immune cell populations within this mixed population may be responding differently to the infection. This is supported by the observation that the majority of DEGs in PBMCs were specific to each time point, indicating a dynamic and time-dependent response to the infection. In contrast, the observation that the number of DEGs in CD8+ T cells increased over time, and that there was more overlap in the DEGs observed at different time points, suggests a more consistent response from this specific cell population. This can be explained by the fact that activated and differentiated CD8+ T cells have a more comparable gene expression profile (44, 52). Overall, these findings underscore the complexity and heterogeneity of the immune response to PRRSV infection, and highlight the importance for a more comprehensive understanding of the dynamics of gene expression in different immune cell populations over time. Such understanding could lead to the identification of potential targets for therapeutic intervention to improve the immune response to PRRSV infection.

PPI network analysis of DEGs in PBMCs and CD8+ T cells provided valuable insights into the complex immune response mechanisms triggered by PRRSV. The key clusters associated with innate and adaptive immune response, regulation of cytokines, and cell cycle processes suggest that a complex interplay of several immune pathways is involved in combating PRRSV. The observation that the innate immune response in PBMCs begins early at 7 dpi and continues at later time points with the involvement of adaptive immunity and regulation of cell cycle processes highlights the importance of an early and coordinated response against PRRSV, given its ability to suppress innate immunity and thereby delay the adaptive immune response (1, 7, 8). The variation in the number of proteins involved in the immune response processes in CD8+ T cells over time suggests that different immune mechanisms come into play at different stages of the infection. The presence of clusters associated with adaptive immune response, immune effector process and cytokine-mediated signaling pathways at 14 dpi and 21 dpi indicates the importance of these pathways in the later stages of the CD8+ T response. The observation of clusters associated with T-cell activation, differentiation, adaptive immune response, regulation of cell killing and cytokine production at 21 dpi further highlights the role of CD8+ T cells in the immune response against PRRSV. Also, the extensive cell cycle processes observed in CD8+ T cells at 21 dpi may reflect their proliferation and differentiation, which are necessary for a robust adaptive immune response against PRRSV.

To better understand changes in immune-related gene expression, we analyzed the most representative genes across five functional categories: transcription factors, effector function and apoptotic genes, cytokine genes, chemokine genes, and co-stimulatory and co-inhibitory genes. Overall, CD8+ T cells had a consistently higher number of DEGs compared to PBMCs. By examining PBMC-specific DEGs in infected group, we can derive genes not directly related to CD8+ T cells, as they are a subset of PBMCs. These include: *STAT1*, *PLSCR1*, *EGR3*, *HSP09B1*, *CXCL13*, *TNFAIP6*, *TNFRSF1A*, and *TNFRSF17*. Previous research showed that PRRSV infection induces expression of *STAT1* and upregulates some proinflammatory cytokines (53). Moreover, *STAT1* is essential in the IFN-α-activated JAK/STAT signaling pathway and it induces expression of IFN-stimulated genes (ISGs) which are important in innate immunity against viral infection (54, 55). Among these, we found three ISGs (*ISG12(A)*, *ISG15*, *ISG20*) significantly upregulated from 7 dpi onwards, in accordance with findings that demonstrate the antiviral activity of ISGs (56–58) and essential role of the heat-shock proteins (HSPs) in signal transduction pathways, which has beneficial effects such as inhibition of virus replication and activation of an antiviral immune response (59). Also, PRRSV-infection is usually accompanied by increased temperature in both young and old pigs (1) and these stress conditions (fever and viral infection) can cause upregulation of the HSPs inside the cell (60). Our findings regarding the *HSP90B1* marker align with a previous study that showed upregulation of this gene in porcine lung after PRRSV infection (30). Interestingly, our analysis also revealed the upregulation of *ETV7* and *EGR3* in PBMCs following PRRSV infection. *ETV7* is a negative regulator of the type I IFN response, particularly on antiviral ISGs (40), while *EGR3* suppresses T-cell activation and the expression of *IFNGR1*, contributing to the anti-inflammatory effects of type I IFNs (41, 42).

During a PRRSV infection, the body's natural defenses against pathogens are weakened. This includes a reduction in the cytotoxic activity of NK cells, which play a key role in the early immune response (7, 61, 62). Based on our assumption that the early cell-mediated immune response to PRRSV in PBMCs at 7 dpi is primarily driven by NK cells (1), our results indicate that this suppression may not be complete, as we observed an upregulation of effector genes such as granzymes (GZMA, GZMB, GZMK), killer lectin like receptor (KLRD1), and BCL2L14 at 7 dpi. These findings can be explained by the crucial role of STAT1 in innate immunity, which is critical for NK cell cytotoxic activity that is independent of IFN signaling (63). It is worth noting that these markers may also be induced by other immune cells, such as $CD8^+$ T cells. However, some of these markers were not expressed in $CD8^+$ T cells, and $CD8^+$ T cells expressed additional markers that are not present in PBMCs.

The results on cytokine and chemokine expression in PBMCs of the present study exhibit a degree of concurrence with the outcomes of the prior research, albeit with some variations. A previous study found that PRRSV-infected gilts showed a significant increase of CCL2 and IFN-α in serum at 2 dpi and 6 dpi, whereas IFN-γ was increased significantly at 2 dpi only. However, other analytes including IL1β, IL8, IL12, IL4 and IL10 did not significantly differ over time (64). Although our study differs in the design and methodology, there may be some commonalities that allow for certain results to be compared. Similar to aforementioned study, the expression of IL1β, IL8, IL12, IL4 and IL10 did not significantly differ over time between PRRSV-infected and control gilts. In contrast, our study revealed a significant upregulation of CCL2 at 21 dpi only, while no significant increases were observed in IFN-α and IFN-γ expression. These differences in expressions can be attributed to a number of factors, such as earlier days of sample collection as well as selected methods of studies. However, our findings align with prior research indicating that PRRSV infection decreases the production of IFN-α (7, 65, 66) and delays the IFN-γ response, while also reducing its effects (65, 67, 68). Notably, PRRSV-infected gilts did not show any IFN-α production, which could be beneficial since high levels of IFN-α have been associated with increased fetal mortality (69). Additionally, our findings regarding IFN-α, IL1β, IL8 and CSF2 are consistent with a previous gene expression study that demonstrated no significant upregulation of these innate markers in animals infected with PRRSV, regardless of whether the infection is persistent or non-persistent (70). Our findings are consistent with another study that showed a downregulation in the expression of Th2 markers (*IL4*, *IL5*, *IL13*, *IL25*) and innate immunity markers (*IL1β*, *IL6*, *IL8*, *IFNα*) in PBMCs isolated from pigs at week 5 after MLV vaccination and subjected to *in vitro* restimulation with PRRSV strain VR-2332 (71). It is known that PRRSV strongly induces upregulation of chemokines such as *CCR1*, *CCR2*, *CCL8*, *CXCL9*, *CXCL10*, *CXCL13*, and *CXCR6* in the lungs of PRRSV-infected animals (30). Our study confirms these previous findings but also shows that the expression of these chemokines varies throughout the entire infection period, with the highest expression observed at 21 dpi. These variations may mirror the complex interplay between PRRSV and the host immune response. Overall, our study shows that PRRSV infection in gilts is associated with alterations in the cytokine and chemokine expression, with some similarities and differences compared to previous research, indicating a potential decrease in IFN-α production, delayed IFN-γ response, downregulation of innate immunity markers, and upregulation of certain chemokines.

Upon virus infection activated naïve $CD8^+$ T cells proliferate and differentiate into virus-specific effector $CD8^+$ T cells that can effectively eliminate virus and virus-infected cells (72). Their effector activity is based on the production of effector cytokines and granule-associated proteases (73–75). When looking at $CD8^+$ T cells only, we observed the upregulation of genes associated with later stages of porcine $CD8^+$ T-cell differentiation along the time-course. For example, transcription factor genes such as *PRDM1* (Blimp-1), *EOMES*, and *TBX21* (*T-bet*) were highly upregulated at 14 dpi and 21 dpi, which fits well with a recent study showing the upregulation of *T-bet* and *EOMES* following PRRSV infection (76). Moreover, genes linked to cytolytic activity including granzymes (*GZMA*, *GZMB*, *GZMK*), perforin (*PRF1*), fas ligand (*FASLG*), killer cell lectin like receptors (*KLRK1*, *KLRD1*), and a natural killer cell granule protein 7 (*NKG7*) were significantly upregulated at later time points (14 and 21 dpi) (47). Notably, the strongest expression was observed at 21 dpi, which further supports the effector function of $CD8^+$ T cells.

Several research papers suggest that expression of co-inhibitory molecules such as *PDCD1* (PD-1), *HAVCR2* (Tim-3), *CTLA4*, and *LAG3* correlates with the activated and more differentiated state of $CD8^+$ T cells in viral infection (77–79). In our study, we found high expression of *PDCD1* (PD-1) and *CTLA4* from 7 dpi to 21 dpi, with the strongest expression at 21 dpi. Furthermore, both *HAVCR2* and *LAG3* showed the highest upregulation at 21 dpi. However, prolonged expression of these markers during chronic infection contributes to the exhaustion of $CD8^+$ T cells (49, 50). To investigate the potential for $CD8^+$ T cell exhaustion during PRRSV infection, we used GSEA to compare gene expression profiles of $CD8^+$ T cells from PRRSV-infected group at 21 dpi with those of exhausted cells. Our GSEA results indicate that $CD8^+$ T cells from PRRSV-infected group at 21 dpi exhibit a gene expression profile that is distinct from exhausted cells. In particular, these cells showed significant enrichment in effector $CD8^+$ T cell gene sets in general as well as during chronic LCMV infection. Upon antigen stimulation, effector $CD8^+$ T cells are known to exhibit a high degree of proliferative capacity as a key feature (80). Also, the metabolic programming of these cells rely on aerobic glycolysis (81, 82), while exhausted $CD8^+$ T cells suppress AKT activation and mTOR activity, resulting in a metabolic switch from glycolysis to fatty acid oxidation (FAO) (83, 84). The positive enrichment of gene sets related to cell division and proliferation in $CD8^+$ T cells from PRRSV-infected group at 21 dpi, suggests that these cells can undergo rapid proliferation in response to viral infection. Moreover, these cells were enriched in gene sets associated with effector metabolic programming, such as glycolysis, MYC targets, and mTORC1 complex, which suggests that they have the necessary metabolic pathways to support their effector function. In addition, the enrichment of hallmark gene sets associated with T cell activation, acute phase response, and maintenance of effector $CD8^+$ T cells during infection, further supports the notion that $CD8^+$ T cells from the PRRSV-infected group at 21 dpi have an activated effector phenotype.

Another distinctive feature of effector $CD8^+$ T cells is the capacity to secrete inflammatory cytokines and chemokines that work together to promote the immune response against viral infections (85). In contrast to gene expression profile of PBMCs derived from PRRSV-infected animals, within $CD8^+$ T cells we found a very strong expression of several cytokine genes (*IL10*, *IL2RB* (CD122), *IFNG* (IFN-γ), *IL21R*, *IL15RA*, *IL13RA1*) at 14 and 21 dpi. Our findings are consistent with a previous study that identified $CD8^+$ T cells as the primary producers of IFN-γ in the lungs of PRRSV-vaccinated animals (86). At the peak of immune response in mice, CD8 T cells are main producers of IL10 at the peripheral sites, whereas they transit to $IL10^-CD8^+$ T cells during later phase (87–89). $IL10^+CD8$ T cells also produce higher amount of granzyme B, IFN-γ and TNF-α than $IL10^-CD8^+$ T cells (89). Our results are consistent with some of these findings, as we observed high expression of IL10 at 14 dpi but not at later time points. However, we found that only GZMB were higher produced, while other granzymes and IFN-γ were more produced at later time point in presumably $IL10^-CD8^+$ T cells. Production of IL10 in $CD8^+$ T cells is directly correlated with level of *PRDM1* expression (Blimp-1) during acute viral infection (90). A previous study demonstrated that Blimp-1 expression in $CD8^+$ T cells might also be induced by other cytokines such as IL21 (91, 92), which is crucial for long-term maintenance of functionality of $CD8^+$ T cell in chronic viral infections such as LCMV in mice (93, 94). In the absence of IL21, CD8 T cells may acquire a more exhausted state, unable to exhibit their cytolytic properties. Our study showed that $CD8^+$ T cells from PRRSV infected animals expressed *IL21R* at 14 dpi only, whereas Blimp-1 was expressed at both 14 dpi and 21 dpi, suggesting possible role of Blimp-1 in regulating the $CD8^+$ T-cell response to PRRSV.

Our study identified a high number of chemokines and chemokine receptors in $CD8^+$ T cells from the PRRSV-infected group. We found that chemokine and chemokine receptor genes such as *CXCR3* and its two ligands (*CXCL9, CXCL10*) were particularly highly expressed at 21 dpi. Together with its ligands, *CXCR3* is known to be highly expressed on activated $CD8^+$ T cells (95). Moreover, *CXCL10* was continuously upregulated from 7 dpi to 21 dpi, which can be explained by the fact that *CXCL10* promotes generation of $CD8^+$ effector cells (96). Interestingly, we found that the transcripts of some genes including *CCR1*, *CCL2*, *CCL4*, *CCL8*, *CXCR3*, *CXCR6*, *CXCL9*, and *CXCL16* were significantly elevated at 21 dpi only. This suggests that these genes may play a role in the later stages of the $CD8^+$ T-cell response to PRRSV. Another interesting finding was the upregulation of *CX3CR1* at 7 and 14 dpi. *CX3CR1* is expressed on virus-specific $CD8^+$ T effector cells (48), which suggests that these cells may be important in the early stages of the immune response to PRRSV.

Upon encountering a virus, naive $CD8^+$ T cells are activated and undergo a process of rapid proliferation and differentiation, resulting in the generation of a heterogeneous pool of effector $CD8^+$ T cells that play a crucial role in the host's immune response against the pathogen (97). Various studies have explored the role of $CD8^+$ T cells in the immune response to PRRSV infection. Peripheral blood $CD8^+$ T cells have been found to proliferate upon restimulation *in vitro* 21 dpi and gain the ability to kill PRRSV-infected macrophages 49 dpi (98). Other studies suggest that $CD8^+$ T cells may play an important role in controlling a PRRSV infection at the site of infection, particularly in the lung and bronchoalveolar lavage (99, 100). Infected pigs have shown a higher percentage of $CD8^+$ T cells and higher levels of IFN-γ-producing cells in their bronchoalveolar lavage fluid compared to control pigs at 5 weeks post-infection (101). PRRSV-specific T cells have also been observed as early as 2 weeks post-infection, but the effectiveness of $CD8^+$ T cells in controlling primary PRRSV infection is still uncertain, as anti-PRRSV-targeted CTLs were only detected after clearance of viremia (98). Nevertheless, recent research has demonstrated that during late gestation $CD8\alpha^{pos}CD27^{dim}$ early effector $CD8\beta^+$ T cells exhibit the strongest response to infection with the two PRRSV-1 strains compared to other investigated lymphocyte subsets (102). Our findings are consistent with these results. Using flow cytometry, we observed a progressive increase in the population of $CD8^+$ T cells characterized by $CD3^+CD8\alpha^{high}perforin^+$ expression following PRRSV infection. This population peaked at 21 days post-infection, indicating an ongoing immune response. Additionally, we observed an increase in total $CD8\beta^+$ T cells in the PRRSV-infected group at 21 dpi, with notable differences in the distribution of intermediate and terminally differentiated cells compared to the control group. These results suggest that the PRRSV infection induces differentiation of CTLs, with a shift towards more differentiated subsets. Taken together, these findings indicate that PRRSV infection leads to a significant expansion and differentiation of CTLs, which could play an important role in controlling the virus. Although our study provided important insights into the role of $CD8^+$ T cells in the immune response to PRRSV infection, we recognize that our analysis was limited by the unavailability of material to use CD8α complementing with CD4 or CD8β markers for time course analysis. Thus, additional studies using alternative markers are warranted to further elucidate the immune response to PRRSV infection.

Our findings demonstrate two key insights about the CD8$^+$ T-cell response to PRRSV infection. First, the general induction of an adaptive immunity through activation of CD8$^+$ T cells, with this response constantly increasing and reaching its peak at 21 dpi. Second, from 14 dpi to 21 dpi CD8$^+$ T cells acquired a more differentiated profile characterized by stronger effector functions and cytolytic activity. To gain insights into the transcriptional regulation of immune-response genes to PRRSV infection, we performed temporal clustering analysis of DEGs in PBMCs and CD8$^+$ T cells from infected animals. In PBMCs, the acute peak at 7 dpi in cluster 1 and the involvement of signaling pathways for innate immune response to viral infection suggest an early activation of host immune defense mechanisms. In their study, Wilkinson et al. found that *CCNB1*, *ISG20*, and *TNFSF10* were upregulated in the whole blood of pregnant gilts at 6 days post-infection with PRRSV-2 (32). Interestingly, these genes were also identified in cluster 1 of our analysis, which also exhibited high expression of *OAS1* and *OAS2*, members of the 2′-5′ oligoadenylate synthetase (OAS) family known to be rapidly induced in response to viral infections (103). In addition, studies in mice have shown that *OAS1* and *OAS2* expression can be enhanced in the lungs after influenza A infection or pathogen-associated molecular pattern stimulation (PAMPs) (104). Cluster 1 also included *OAS2*, *ISG15*, *ISG20*, *USP18* and *MX1*, which were found to be upregulated in the lungs of swine infected with H1N1 swine influenza virus (105). In addition, the *MX1* marker was found to be upregulated in uterine endothelium with adherent placental tissue from PRRSV infected gilts (31). Also, expression of *MX1*, *ISG20*, and *IFIT3* in whole blood from PRRSV-inoculated gilts correlated positively with low fetal mortality at 6 dpi (32). *DDX60*, also present in this cluster, is known to be elevated after viral infection and promotes RIG-I-like receptor-mediated signaling (106). Furthermore, previous studies have demonstrated that the expression levels of ISGs, including *DDX60*, *ISG20*, and *USP18*, were significantly upregulated in whole blood after PRRSV infection (107). Overall, the upregulation of cluster 1 genes in response to PRRSV infections may represent a conserved and critical aspect of the host antiviral response. Cluster 2 increased from 21 dpi and was associated with biological processes such as humoral immune response and complement activation, indicating a crucial role of humoral immunity in response to PRRSV infection. In contrast, the downregulation of genes involved in blood coagulation and receptor-mediated endocytosis in cluster 3 suggests that PRRSV may also evade host immune response by interfering with these biological processes. Supporting evidence from other studies suggests that PRRSV infection involves receptor-mediated endocytosis and replication within host cells (108–110). In particular, infected pigs have been shown to develop a rapid humoral response, but the early development of sub- or non-neutralizing antibodies can enhance viral attachment and internalization through Fc receptor-mediated endocytosis, a phenomenon known as antibody-dependent enhancement (ADE) (111). Moreover, confocal microscopy studies have demonstrated the receptor-mediated endocytosis of PRRSV virions into endosomes (112). Additionally, several studies have highlighted the correlation of blood coagulation and complement cascade pathways with PRRSV infection and vaccination responsiveness (113). These pathways play important roles in the first line of defense against pathogens and the regulation of inflammatory responses (114). Furthermore, early changes in blood transcriptional modules (BTMs) associated with the neutralizing antibody response have included the blood coagulation, platelet activation, and complement activation (29). The KEGG analysis revealed significantly enriched pathways in clusters 1 and 2, with cluster 1 showing involvement in various signaling pathways for innate immune response to viral infection, including RIG-I-like, toll-like and NOD-like receptor pathways, and cluster 2 being associated with pathways involved in bacterial infections such as *Staphylococcus aureus* and *pertussis*. The RIG-I-like receptor signaling pathway is activated by viral infections and initiates an antiviral innate immune response (115, 116). Additionally, the Toll-like and NOD-like receptor signaling pathways, which are also part of pattern recognition receptors (PRRs), play a crucial role in the innate immunity and assist in activation of the adaptive immunity (117). In conclusion, our study suggests that PRRSV infection elicits early activation of host immune defense mechanisms through innate immune response signaling pathways and plays a crucial role in humoral immunity, while also potentially evading host immune response by interfering with genes involved in blood coagulation and receptor-mediated endocytosis.

Time-clustering analysis of DEGs of CD8$^+$ T cells revealed four clusters, which shed light on the molecular processes in CD8$^+$ T cells following PRRSV infection. Genes enriched in cluster 1 and 2 showed that from 7 dpi CD8$^+$ T cell undergo continuous massive cell division and proliferation in response to PRRSV. Notably, the gene *MKI67*, which encodes the marker of proliferation Ki67 (118, 119), was among these genes in cluster 2. In a previous study, we demonstrated that *MKI67* is upregulated in porcine intermediate and terminally differentiated but not in naïve CD8$^+$ T-cell subsets (44). Also, the expression of *MKI67* is in accordance with previous research suggesting that PBMCs of PRRSV-infected animals induce the number of proliferating CTLs after *in vitro* restimulation from 14 dpi (98). Therefore, genes in cluster 2 probably contribute to the early cell transformation of CD8$^+$ T cells after encountering PRRSV. At 7 dpi, cluster 3 revealed downregulated genes necessary for metabolic switching from fatty acid oxidation, which is typical for naïve CD8$^+$ T cells (120). This suggests that CD8$^+$ T cells undergo metabolic reprogramming in response to PRRSV infection. Lastly, cluster 4 showed that CD8$^+$ T cells from 21 dpi increase the chemotaxis and chemokine activity, suggesting a crucial role of these cells in the immune response to PRRSV infection.

In conclusion, our study uncovered the dynamic gene expression patterns of PBMCs and CD8$^+$ T cells during PRRSV infection over the course of 21 days. We observed that the initial innate immune response in PBMCs peaked at 7 dpi, while the adaptive immune response in CD8$^+$ T cells was most prominent at 21 dpi, marked by the generation of highly differentiated CD8$^+$ T cells with potent effector and cytolytic capabilities. Our findings shed light on the complex transcriptional changes and key players involved in the immune response to PRRSV and provide a valuable resource for the identification of biomarkers for PRRSV diagnosis and improved understanding of PRRS pathogenesis.

Data availability statement

The datasets presented in this study can be found in online repositories. The names of the repository/repositories and accession number(s) can be found below: https://www.ncbi.nlm.nih.gov/, PRJNA880682.

Ethics statement

The animal study was reviewed and approved by institutional ethics and animal welfare committee (Vetmeduni Vienna) and the national authority according to §§26ff. of Animal Experiments Act, Tierversuchsgesetz in Austria – TVG 2012 (BMWFW-2021-0.117.108).

Author contributions

EL, AL and AS designed the project. TR provided the virus for the experimental infection. HK performed sample collection. SS and MeS performed lymphocyte isolation. MaS and EL organized magnetic-activated cell sorting. EL performed RNA isolation and quality assessment. RE and EL prepared libraries of the samples. EL performed in-depth bioinformatic analysis. NP advised on the most suitable bioinformatic analysis. EL and AS analyzed the experiments and wrote the manuscript. CP assisted with the interpretation of the data. All authors contributed to the article and approved the submitted version.

Funding

This work was financially supported by intramural funds of the University of Veterinary Medicine Vienna and funds from European PRRS Research Award 2022 of Boehringer Ingelheim.

Conflict of interest

The authors declare that the research was conducted in the absence of any commercial or financial relationships that could be construed as a potential conflict of interest.

Publisher's note

All claims expressed in this article are solely those of the authors and do not necessarily represent those of their affiliated organizations, or those of the publisher, the editors and the reviewers. Any product that may be evaluated in this article, or claim that may be made by its manufacturer, is not guaranteed or endorsed by the publisher.

Supplementary material

The Supplementary Material for this article can be found online at: https://www.frontiersin.org/articles/10.3389/fimmu.2023.1159970/full#supplementary-material

References

1. Lunney JK, Fang Y, Ladinig A, Chen N, Li Y, Rowland B, et al. Porcine reproductive and respiratory syndrome virus (PRRSV): pathogenesis and interaction with the immune system. *Annu Rev Anim Biosci* (2016) 4:129–54. doi: 10.1146/annurev-animal-022114-111025

2. Holtkamp DJ, Kliebenstein JB, Zimmerman JJ, Neumann E, Rotto H, Yoder TK, et al. Economic impact of porcine reproductive and respiratory syndrome virus on U.S. pork producers. *Iowa State University Animal Industry Report* (2012) 9(1). doi: 10.31274/ans_air-180814-28

3. Thanawongnuwech R, Brown GB, Halbur PG, Roth JA, Royer RL, Thacker BJ. Pathogenesis of porcine reproductive and respiratory syndrome virus-induced increase in susceptibility to streptococcus suis infection. *Vet Pathol* (2000) 37:143–52. doi: 10.1354/vp.37-2-143

4. Brockmeier SL, Palmer MV, Bolin SR. Effects of intranasal inoculation of porcine reproductive and respiratory syndrome virus, bordetella bronchiseptica, or a combination of both organisms in pigs. *Am J Vet Res* (2000) 61:892–9. doi: 10.2460/ajvr.2000.61.892

5. Yu J, Wu J, Zhang Y, Guo L, Cong X, Du Y, et al. Concurrent highly pathogenic porcine reproductive and respiratory syndrome virus infection accelerates haemophilus parasuis infection in conventional pigs. *Vet Microbiol* (2012) 158:316–21. doi: 10.1016/j.vetmic.2012.03.001

6. Van Reeth K, Nauwynck H, Pensaert M. Dual infections of feeder pigs with porcine reproductive and respiratory syndrome virus followed by porcine respiratory coronavirus or swine influenza virus: a clinical and virological study. *Vet Microbiol* (1996) 48:325–35. doi: 10.1016/0378-1135(95)00145-X

7. Albina E, Carrat C, Charley B. Short communication: interferon-α response to swine arterivirus (PoAV), the porcine reproductive and respiratory syndrome virus. *J Interf Cytokine Res* (1998) 18:485–90. doi: 10.1089/jir.1998.18.485

8. Renukaradhya GJ, Alekseev K, Jung K, Fang Y, Saif LJ. Porcine reproductive and respiratory syndrome virus–induced immunosuppression exacerbates the inflammatory response to porcine respiratory coronavirus in pigs. *Viral Immunol* (2010) 23:457–66. doi: 10.1089/vim.2010.0051

9. Dwivedi V, Manickam C, Patterson R, Dodson K, Weeman M, Renukaradhya GJ. Intranasal delivery of whole cell lysate of mycobacterium tuberculosis induces protective immune responses to a modified live porcine reproductive and respiratory syndrome virus vaccine in pigs. *Vaccine* (2011) 29:4067–76. doi: 10.1016/j.vaccine.2011.03.005

10. Morgan SB, Graham SP, Salguero FJ, Sánchez Cordón PJ, Mokhtar H, Rebel JMJ, et al. Increased pathogenicity of European porcine reproductive and respiratory syndrome virus is associated with enhanced adaptive responses and viral clearance. *Vet Microbiol* (2013) 163:13–22. doi: 10.1016/j.vetmic.2012.11.024

11. Hanada K, Suzuki Y, Nakane T, Hirose O, Gojobori T. The origin and evolution of porcine reproductive and respiratory syndrome viruses. *Mol Biol Evol* (2005) 22:1024–31. doi: 10.1093/molbev/msi089

12. Cano JP, Dee SA, Murtaugh MP, Pijoan C. Impact of a modified-live porcine reproductive and respiratory syndrome virus vaccine intervention on a population of pigs infected with a heterologous isolate. *Vaccine* (2007) 25:4382–91. doi: 10.1016/j.vaccine.2007.03.031

13. Zuckermann FA, Garcia EA, Luque ID, Christopher-Hennings J, Doster A, Brito M, et al. Assessment of the efficacy of commercial porcine reproductive and respiratory syndrome virus (PRRSV) vaccines based on measurement of serologic response, frequency of gamma-IFN-producing cells and virological parameters of protection upon challenge. *Vet Microbiol* (2007) 123:69–85. doi: 10.1016/j.vetmic.2007.02.009

14. Charerntantanakul W. Porcine reproductive and respiratory syndrome virus vaccines: immunogenicity, efficacy and safety aspects. *World J Virol* (2012) 1:23. doi: 10.5501/wjv.v1.i1.23

15. Díaz I, Darwich L, Pappaterra G, Pujols J, Mateu E. Different European-type vaccines against porcine reproductive and respiratory syndrome virus have different immunological properties and confer different protection to pigs. *Virology* (2006) 351:249–59. doi: 10.1016/j.virol.2006.03.046

16. Charerntantanakul W, Platt R, Roth JA. Effects of porcine reproductive and respiratory syndrome virus-infected antigen-presenting cells on T cell activation and antiviral cytokine production. *Viral Immunol* (2006) 19:646–61. doi: 10.1089/vim.2006.19.646

17. Labarque G, Van RK, Nauwynck H, Drexler C, Van Gucht S, Pensaert M. Impact of genetic diversity of European-type porcine reproductive and respiratory syndrome virus strains on vaccine efficacy. *Vaccine* (2004) 22:4183–90. doi: 10.1016/j.vaccine.2004.05.008

18. Scortti M, Prieto C, Simarro I, Castro JM. Reproductive performance of gilts following vaccination and subsequent heterologous challenge with European strains of porcine reproductive and respiratory syndrome virus. *Theriogenology* (2006) 66:1884–93. doi: 10.1016/j.theriogenology.2006.04.043

19. Mengeling WL, Lager KM, Vorwald AC, Koehler KJ. Strain specificity of the immune response of pigs following vaccination with various strains of porcine reproductive and respiratory syndrome virus. *Vet Microbiol* (2003) 93:13–24. doi: 10.1016/S0378-1135(02)00427-3

20. Borghetti P, Saleri R, Ferrari L, Morganti M, De Angelis E, Franceschi V, et al. Cytokine expression, glucocorticoid and growth hormone changes after porcine reproductive and respiratory syndrome virus (PRRSV-1) infection in vaccinated and unvaccinated naturally exposed pigs. *Comp Immunol Microbiol Infect Dis* (2011) 34:143–55. doi: 10.1016/j.cimid.2010.06.004

21. Martelli P, Gozio S, Ferrari L, Rosina S, De Angelis E, Quintavalla C, et al. Efficacy of a modified live porcine reproductive and respiratory syndrome virus (PRRSV) vaccine in pigs naturally exposed to a heterologous European (Italian cluster) field strain: clinical protection and cell-mediated immunity. *Vaccine* (2009) 27:3788–99. doi: 10.1016/j.vaccine.2009.03.028

22. Bøtner A, Strandbygaard B, Sørensen KJ, Have P, Madsen KG, Madsen ES, et al. Appearance of acute PRRS-like symptoms in sow herds after vaccination with a modified live PRRS vaccine. *Vet Rec* (1997) 141:497–9. doi: 10.1136/vr.141.19.497

23. Wang C, Wu B, Amer S, Luo J, Zhang H, Guo Y, et al. Phylogenetic analysis and molecular characteristics of seven variant Chinese field isolates of PRRSV. *BMC Microbiol* (2010) 10:146. doi: 10.1186/1471-2180-10-146

24. Madsen KG, Hansen CM, Madsen ES, Strandbygaard B, Bøtner A, Sørensen KJ. Sequence analysis of porcine reproductive and respiratory syndrome virus of the American type collected from Danish swine herds. *Arch Virol* (1998) 143:1683–700. doi: 10.1007/s007050050409

25. Wenhui L, Zhongyan W, Guanqun Z, Zhili L, JingYun M, Qingmei X, et al. Complete genome sequence of a novel variant porcine reproductive and respiratory syndrome virus (PRRSV) strain: evidence for recombination between vaccine and wild-type PRRSV strains. *J Virol* (2012) 86:9543–3. doi: 10.1128/JVI.01341-12

26. Nan Y, Wu C, Gu G, Sun W, Zhang Y-J, Zhou E-M. Improved vaccine against PRRSV: current progress and future perspective. *Front Microbiol* (2017) 8:1635. doi: 10.3389/fmicb.2017.01635

27. Leifert JA, Whitton LJ. Immune responses to DNA vaccines: induction of CD8 T cells. In: *Madame curie bioscience database*. Austin (TX: Landes Bioscience (2013).

28. Butler JE, Lager KM, Golde W, Faaberg KS, Sinkora M, Loving C, et al. Porcine reproductive and respiratory syndrome (PRRS): an immune dysregulatory pandemic. *Immunol Res* (2014) 59:81–108. doi: 10.1007/s12026-014-8549-5

29. Bocard LV, Kick AR, Hug C, Lischer HEL, Käser T, Summerfield A. Systems immunology analyses following porcine respiratory and reproductive syndrome virus infection and vaccination. *Front Immunol* (2021) 12:779747. doi: 10.3389/fimmu.2021.779747

30. Xiao S, Jia J, Mo D, Wang Q, Qin L, He Z, et al. Understanding PRRSV infection in porcine lung based on genome-wide transcriptome response identified by deep sequencing. *PloS One* (2010) 5:e11377. doi: 10.1371/journal.pone.0011377

31. Wilkinson JM, Bao H, Ladinig A, Hong L, Stothard P, Lunney JK, et al. Genome-wide analysis of the transcriptional response to porcine reproductive and respiratory syndrome virus infection at the maternal/fetal interface and in the fetus. *BMC Genomics* (2016) 17:383. doi: 10.1186/s12864-016-2720-4

32. Wilkinson JM, Ladinig A, Bao H, Kommadath A, Stothard P, Lunney JK, et al. Differences in whole blood gene expression associated with infection time-course and extent of fetal mortality in a reproductive model of type 2 porcine reproductive and respiratory syndrome virus (PRRSV) infection. *PloS One* (2016) 11:e0153615. doi: 10.1371/journal.pone.0153615

33. Sinn LJ, Klingler E, Lamp B, Brunthaler R, Weissenböck H, Rümenapf T, et al. Emergence of a virulent porcine reproductive and respiratory syndrome virus (PRRSV) 1 strain in lower Austria. *Porc Heal Manag* (2016) 2:28. doi: 10.1186/s40813-016-0044-z

34. Duerlinger S, Knecht C, Sawyer S, Balka G, Zaruba M, Ruemenapf T, et al. Efficacy of a modified live porcine reproductive and respiratory syndrome virus 1 (PRRSV-1) vaccine against experimental infection with PRRSV AUT15-33 in weaned piglets. *Vaccines* (2022) 10:934. doi: 10.3390/vaccines10060934

35. Bindea G, Mlecnik B, Hackl H, Charoentong P, Tosolini M, Kirilovsky A, et al. ClueGO: a cytoscape plug-in to decipher functionally grouped gene ontology and pathway annotation networks. *Bioinformatics* (2009) 25:1091–3. doi: 10.1093/bioinformatics/btp101

36. Subramanian A, Tamayo P, Mootha VK, Mukherjee S, Ebert BL, Gillette MA, et al. Gene set enrichment analysis: a knowledge-based approach for interpreting genome-wide expression profiles. *Proc Natl Acad Sci* (2005) 102:15545–50. doi: 10.1073/pnas.0506580102

37. Mootha VK, Lindgren CM, Eriksson K-F, Subramanian A, Sihag S, Lehar J, et al. PGC-1α-responsive genes involved in oxidative phosphorylation are coordinately downregulated in human diabetes. *Nat Genet* (2003) 34:267–73. doi: 10.1038/ng1180

38. Liberzon A, Subramanian A, Pinchback R, Thorvaldsdóttir H, Tamayo P, Mesirov JP. Molecular signatures database (MSigDB) 3.0. *Bioinformatics* (2011) 27:1739–40. doi: 10.1093/bioinformatics/btr260

39. Toussaint JF, Sailleau C, Breard E, Zientara S, De Clercq K. Bluetongue virus detection by two real-time RT-qPCRs targeting two different genomic segments. *J Virol Methods* (2007) 140:115–23. doi: 10.1016/j.jviromet.2006.11.007

40. Froggatt HM, Harding AT, Chaparian RR, Heaton NS. ETV7 limits antiviral gene expression and control of influenza viruses. *Sci Signal* (2021) 14(691). doi: 10.1126/scisignal.abe1194

41. Safford M, Collins S, Lutz MA, Allen A, Huang C-T, Kowalski J, et al. Egr-2 and egr-3 are negative regulators of T cell activation. *Nat Immunol* (2005) 6:472–80. doi: 10.1038/ni1193

42. Kearney SJ, Delgado C, Eshleman EM, Hill KK, O'Connor BP, Lenz LL. Type I IFNs downregulate myeloid cell IFN-γ receptor by inducing recruitment of an early growth response 3/NGFI-a binding protein 1 complex that silences ifngr1 transcription. *J Immunol* (2013) 191:3384–92. doi: 10.4049/jimmunol.1203510

43. Jin H-T, Anderson AC, Tan WG, West EE, Ha S-J, Araki K, et al. Cooperation of Tim-3 and PD-1 in CD8 T-cell exhaustion during chronic viral infection. *Proc Natl Acad Sci* (2010) 107:14733–8. doi: 10.1073/pnas.1009731107

44. Lagumdzic E, Pernold C, Viano M, Olgiati S, Schmitt MW, Mair KH, et al. Transcriptome profiling of porcine naïve, intermediate and terminally differentiated CD8+ T cells. *Front Immunol* (2022) 13:849922. doi: 10.3389/fimmu.2022.849922

45. Salmon AJ, Shavkunov AS, Miao Q, Jarjour NN, Keshari S, Esaulova E, et al. BHLHE40 regulates the T-cell effector function required for tumor microenvironment remodeling and immune checkpoint therapy efficacy. *Cancer Immunol Res* (2022) 10:597–611. doi: 10.1158/2326-6066.CIR-21-0129

46. Cook ME, Jarjour NN, Lin C-C, Edelson BT. Transcription factor Bhlhe40 in immunity and autoimmunity. *Trends Immunol* (2020) 41:1023–36. doi: 10.1016/j.it.2020.09.002

47. Morikawa Y, Murakami M, Kondo H, Nemoto N, Iwabuchi K, Eshima K. Natural killer cell group 7 sequence in cytotoxic cells optimizes exocytosis of lytic granules essential for the perforin-dependent, but not fas ligand–dependent, cytolytic pathway. *ImmunoHorizons* (2021) 5:234–45. doi: 10.4049/immunohorizons.2100029

48. Gerlach C, Moseman EA, Loughhead SM, Alvarez D, Zwijnenburg AJ, Waanders L, et al. The chemokine receptor CX3CR1 defines three antigen-experienced CD8 T cell subsets with distinct roles in immune surveillance and homeostasis. *Immunity* (2016) 45:1270–84. doi: 10.1016/j.immuni.2016.10.018

49. Seo W, Jerin C, Nishikawa H. Transcriptional regulatory network for the establishment of CD8+ T cell exhaustion. *Exp Mol Med* (2021) 53:202–9. doi: 10.1038/s12276-021-00568-0

50. Li J, He Y, Hao J, Ni L, Dong C. High levels of eomes promote exhaustion of anti-tumor CD8+ T cells. *Front Immunol* (2018) 9:2981. doi: 10.3389/fimmu.2018.02981

51. Talker SC, Käser T, Reutner K, Sedlak C, Mair KH, Koinig H, et al. Phenotypic maturation of porcine NK- and T-cell subsets. *Dev Comp Immunol* (2013) 40:51–68. doi: 10.1016/j.dci.2013.01.003

52. Pernold CPS, Lagumdzic E, Stadler M, Mair KH, Jäckel S, Schmitt MW, et al. Characterization of the immune system of ellegaard göttingen minipigs - an important large animal model in experimental medicine. *Front Immunol* (2022) 13:1003986. doi: 10.3389/fimmu.2022.1003986

53. Yu Y, Wang R, Nan Y, Zhang L, Zhang Y. Induction of STAT1 phosphorylation at serine 727 and expression of proinflammatory cytokines by porcine reproductive and respiratory syndrome virus. *PloS One* (2013) 8:e61967. doi: 10.1371/journal.pone.0061967

54. Darnell JE, Kerr lan M, Stark GR. Jak-STAT pathways and transcriptional activation in response to IFNs and other extracellular signaling proteins. *Science* (1994) 264:1415–21. doi: 10.1126/science.8197455

55. Schindler C, Darnell JE. TRANSCRIPTIONAL RESPONSES TO POLYPEPTIDE LIGANDS: the JAK-STAT pathway. *Annu Rev Biochem* (1995) 64:621–52. doi: 10.1146/annurev.bi.64.070195.003201

56. Degols G, Eldin P, Mechti N. ISG20, an actor of the innate immune response. *Biochimie* (2007) 89:831–5. doi: 10.1016/j.biochi.2007.03.006

57. Xue B, Yang D, Wang J, Xu Y, Wang X, Qin Y, et al. ISG12a restricts hepatitis c virus infection through the ubiquitination-dependent degradation pathway. *J Virol* (2016) 90:6832–45. doi: 10.1128/JVI.00352-16

58. Morales DJ, Lenschow DJ. The antiviral activities of ISG15. *J Mol Biol* (2013) 425:4995–5008. doi: 10.1016/j.jmb.2013.09.041

59. Santoro MG, Amici C, Rossi A. Role of heat shock proteins in viral infection. In: Pockley AG, Calderwood SK, Santoro MG, editors. *Prokaryotic and eukaryotic heat schock proteins in infectious disease*, vol. Vol. 4 . Dordrecht: Springer Netherlands (2009). p. 51–84. doi: 10.1007/978-90-481-2976-8_3

60. van Eden W, van der Zee R, Prakken B. Heat-shock proteins induce T-cell regulation of chronic inflammation. *Nat Rev Immunol* (2005) 5:318–30. doi: 10.1038/nri1593

61. Dwivedi V, Manickam C, Patterson R, Dodson K, Murtaugh M, Torrelles JB, et al. Cross-protective immunity to porcine reproductive and respiratory syndrome virus by intranasal delivery of a live virus vaccine with a potent adjuvant. *Vaccine* (2011) 29:4058–66. doi: 10.1016/j.vaccine.2011.03.006

62. Dwivedi V, Manickam C, Binjawadagi B, Linhares D, Murtaugh MP, Renukaradhya GJ. Evaluation of immune responses to porcine reproductive and respiratory syndrome virus in pigs during early stage of infection under farm conditions. *Virol J* (2012) 9:45. doi: 10.1186/1743-422X-9-45

63. Lee C-K, Rao DT, Gertner R, Gimeno R, Frey AB, Levy DE. Distinct requirements for IFNs and STAT1 in NK cell function. *J Immunol* (2000) 165:3571–7. doi: 10.4049/jimmunol.165.7.3571

64. Ladinig A, Lunney JK, Souza CJ, Ashley C, Plastow G, Harding JC. Cytokine profiles in pregnant gilts experimentally infected with porcine reproductive and respiratory syndrome virus and relationships with viral load and fetal outcome. *Vet Res* (2014) 45:113. doi: 10.1186/s13567-014-0113-8

65. Murtaugh MP, Xiao Z, Zuckermann F. Immunological responses of swine to porcine reproductive and respiratory syndrome virus infection. *Viral Immunol* (2002) 15:533–47. doi: 10.1089/088282402320914485

66. Jung K, Renukaradhya GJ, Alekseev KP, Fang Y, Tang Y, Saif LJ. Porcine reproductive and respiratory syndrome virus modifies innate immunity and alters disease outcome in pigs subsequently infected with porcine respiratory coronavirus: implications for respiratory viral co-infections. *J Gen Virol* (2009) 90:2713–23. doi: 10.1099/vir.0.014001-0

67. Molina RM, Cha S-H, Chittick W, Lawson S, Murtaugh MP, Nelson EA, et al. Immune response against porcine reproductive and respiratory syndrome virus during acute and chronic infection. *Vet Immunol Immunopathol* (2008) 126:283–92. doi: 10.1016/j.vetimm.2008.08.002

68. Xiao Z, Batista L, Dee S, Halbur P, Murtaugh MP. The level of virus-specific T-cell and macrophage recruitment in porcine reproductive and respiratory syndrome virus infection in pigs is independent of virus load. *J Virol* (2004) 78:5923–33. doi: 10.1128/JVI.78.11.5923-5933.2004

69. Ladinig A, Detmer SE, Clarke K, Ashley C, Rowland RRR, Lunney JK, et al. Pathogenicity of three type 2 porcine reproductive and respiratory syndrome virus strains in experimentally inoculated pregnant gilts. *Virus Res* (2015) 203:24–35. doi: 10.1016/j.virusres.2015.03.005

70. Lunney JK, Fritz ER, Reecy JM, Kuhar D, Prucnal E, Molina R, et al. Interleukin-8, interleukin-1β, and interferon-γ levels are linked to PRRS virus clearance. *Viral Immunol* (2010) 23:127–34. doi: 10.1089/vim.2009.0087

71. Royaee AR, Husmann RJ, Dawson HD, Calzada-Nova G, Schnitzlein WM, Zuckermann FA, et al. Deciphering the involvement of innate immune factors in the development of the host response to PRRSV vaccination. *Vet Immunol Immunopathol* (2004) 102:199–216. doi: 10.1016/j.vetimm.2004.09.018

72. Lawrence CW, Braciale TJ. Activation, differentiation, and migration of naive virus-specific CD8+ T cells during pulmonary influenza virus infection. *J Immunol* (2004) 173:1209–18. doi: 10.4049/jimmunol.173.2.1209

73. Kägi D, Ledermann B, Bürki K, Zinkernagel RM, Hengartner H. Molecular mechanisms of lymphocyte-mediated cytotoxicity and their role in immunological protection and pathogenesis in vivo. *Annu Rev Immunol* (1996) 14:207–32. doi: 10.1146/annurev.immunol.14.1.207

74. Wong P, Pamer EG. CD8 T cell responses to infectious pathogens. *Annu Rev Immunol* (2003) 21:29–70. doi: 10.1146/annurev.immunol.21.120601.141114

75. Harty JT, Tvinnereim AR, White DW. CD8+ T cell effector mechanisms in resistance to infection. *Annu Rev Immunol* (2000) 18:275–308. doi: 10.1146/annurev.immunol.18.1.275

76. Ruedas-Torres I, Gómez-Laguna J, Sánchez-Carvajal JM, Larenas-Muñoz F, Barranco I, Pallarés FJ, et al. Activation of T-bet, FOXP3, and EOMES in target organs from piglets infected with the virulent PRRSV-1 Lena strain. *Front Immunol* (2021) 12:773146. doi: 10.3389/fimmu.2021.773146

77. Kuchroo VK, Anderson AC, Petrovas C. Coinhibitory receptors and CD8 T cell exhaustion in chronic infections. *Curr Opin HIV AIDS* (2014) 9:439–45. doi: 10.1097/COH.0000000000000088

78. McCoy KD, Le Gros G. The role of CTLA-4 in the regulation of T cell immune responses. *Immunol Cell Biol* (1999) 77:1–10. doi: 10.1046/j.1440-1711.1999.00795.x

79. Grosso JF, Goldberg MV, Getnet D, Bruno TC, Yen H-R, Pyle KJ, et al. Functionally distinct LAG-3 and PD-1 subsets on activated and chronically stimulated CD8 T cells. *J Immunol* (2009) 182:6659–69. doi: 10.4049/jimmunol.0804211

80. Doering TA, Crawford A, Angelosanto JM, Paley MA, Ziegler CG, Wherry EJ. Network analysis reveals centrally connected genes and pathways involved in CD8+ T cell exhaustion versus memory. *Immunity* (2012) 37:1130–44. doi: 10.1016/j.immuni.2012.08.021

81. Blagih J, Coulombe F, Vincent EE, Dupuy F, Galicia-Vázquez G, Yurchenko E, et al. The energy sensor AMPK regulates T cell metabolic adaptation and effector responses in vivo. *Immunity* (2015) 42:41–54. doi: 10.1016/j.immuni.2014.12.030

82. Wang R, Dillon CP, Shi LZ, Milasta S, Carter R, Finkelstein D, et al. The transcription factor myc controls metabolic reprogramming upon T lymphocyte activation. *Immunity* (2011) 35:871–82. doi: 10.1016/j.immuni.2011.09.021

83. MacIver NJ, Michalek RD, Rathmell JC. Metabolic regulation of T lymphocytes. *Annu Rev Immunol* (2013) 31:259–83. doi: 10.1146/annurev-immunol-032712-095956

84. Zhang Y, Kurupati R, Liu L, Zhou XY, Zhang G, Hudaihed A, et al. Enhancing CD8+ T cell fatty acid catabolism within a metabolically challenging tumor microenvironment increases the efficacy of melanoma immunotherapy. *Cancer Cell* (2017) 32:377–391.e9. doi: 10.1016/j.ccell.2017.08.004

85. Zhang N, Bevan MJ. CD8+ T cells: foot soldiers of the immune system. *Immunity* (2011) 35:161–8. doi: 10.1016/j.immuni.2011.07.010

86. Kick AR, Wolfe ZC, Amaral AF, Cortes LM, Almond GW, Crisci E, et al. Maternal autogenous inactivated virus vaccination boosts immunity to PRRSV in piglets. *Vaccines* (2021) 9:106. doi: 10.3390/vaccines9020106

87. Palmer EM, Holbrook BC, Arimilli S, Parks GD, Alexander-Miller MA. IFNγ-producing, virus-specific CD8+ effector cells acquire the ability to produce IL-10 as a result of entry into the infected lung environment. *Virology* (2010) 404:225–30. doi: 10.1016/j.virol.2010.05.004

88. Sun J, Madan R, Karp CL, Braciale TJ. Effector T cells control lung inflammation during acute influenza virus infection by producing IL-10. *Nat Med* (2009) 15:277–84. doi: 10.1038/nm.1929

89. Trandem K, Zhao J, Fleming E, Perlman S. Highly activated cytotoxic CD8 T cells express protective IL-10 at the peak of coronavirus-induced encephalitis. *J Immunol* (2011) 186:3642–52. doi: 10.4049/jimmunol.1003292

90. Sun J, Dodd H, Moser EK, Sharma R, Braciale TJ. CD4+ T cell help and innate-derived IL-27 induce blimp-1-dependent IL-10 production by antiviral CTLs. *Nat Immunol* (2011) 12:327–34. doi: 10.1038/ni.1996

91. Gong D, Malek TR. Cytokine-dependent blimp-1 expression in activated T cells inhibits IL-2 production. *J Immunol* (2007) 178:242–52. doi: 10.4049/jimmunol.178.1.242

92. Kwon H, Thierry-Mieg D, Thierry-Mieg J, Kim H-P, Oh J, Tunyaplin C, et al. Analysis of interleukin-21-Induced Prdm1 gene regulation reveals functional cooperation of STAT3 and IRF4 transcription factors. *Immunity* (2009) 31:941–52. doi: 10.1016/j.immuni.2009.10.008

93. Fröhlich A, Kisielow J, Schmitz I, Freigang S, Shamshiev AT, Weber J, et al. IL-21R on T cells is critical for sustained functionality and control of chronic viral infection. *Science* (2009) 324:1576–80. doi: 10.1126/science.1172815

94. Elsaesser H, Sauer K, Brooks DG. IL-21 is required to control chronic viral infection. *Science* (2009) 324:1569–72. doi: 10.1126/science.1174182

95. Groom JR, Luster AD. CXCR3 ligands: redundant, collaborative and antagonistic functions. *Immunol Cell Biol* (2011) 89:207–15. doi: 10.1038/icb.2010.158

96. Peperzak V, Veraar EAM, Xiao Y, Bąbała N, Thiadens K, Brugmans M, et al. CD8+ T cells produce the chemokine CXCL10 in response to CD27/CD70 costimulation to promote generation of the CD8+ effector T cell pool. *J Immunol* (2013) 191:3025–36. doi: 10.4049/jimmunol.1202222

97. Kolumam GA, Thomas S, Thompson LJ, Sprent J, Murali-Krishna K. Type I interferons act directly on CD8 T cells to allow clonal expansion and memory formation in response to viral infection. *J Exp Med* (2005) 202:637–50. doi: 10.1084/jem.20050821

98. Costers S, Lefebvre DJ, Goddeeris B, Delputte PL, Nauwynck HJ. Functional impairment of PRRSV-specific peripheral CD3 + CD8 high cells. *Vet Res* (2009) 40:46. doi: 10.1051/vetres/2009029

99. Kick A, Amaral A, Cortes L, Fogle J, Crisci E, Almond G, et al. The T-cell response to type 2 porcine reproductive and respiratory syndrome virus (PRRSV). *Viruses* (2019) 11:796. doi: 10.3390/v11090796

100. Nazki S, Khatun A, Jeong C-G, Mattoo S ul S, Gu S, Lee S-I, et al. Evaluation of local and systemic immune responses in pigs experimentally challenged with porcine reproductive and respiratory syndrome virus. *Vet Res* (2020) 51:66. doi: 10.1186/s13567-020-00789-7

101. Weesendorp E, Rebel JMJ, Popma-De Graaf DJ, Fijten HPD, Stockhofe-Zurwieden N. Lung pathogenicity of European genotype 3 strain porcine reproductive and respiratory syndrome virus (PRRSV) differs from that of subtype 1 strains. *Vet Microbiol* (2014) 174:127–38. doi: 10.1016/j.vetmic.2014.09.010

102. Stas MR, Kreutzmann H, Stadler J, Sassu EL, Mair KH, Koch M, et al. Influence of PRRSV-1 vaccination and infection on mononuclear immune cells at the maternal-fetal interface. *Front Immunol* (2022) 13:1055048. doi: 10.3389/fimmu.2022.1055048

103. Melchjorsen J, Kristiansen H, Christiansen R, Rintahaka J, Matikainen S, Paludan SR, et al. Differential regulation of the OASL and OAS1 genes in response to viral infections. *J Interf Cytokine Res* (2009) 29:199–208. doi: 10.1089/jir.2008.0050

104. Zhou Y, Kang M-J, Jha BK, Silverman RH, Lee CG, Elias JA. Role of ribonuclease l in viral pathogen-associated molecular Pattern/Influenza virus and cigarette smoke–induced inflammation and remodeling. *J Immunol* (2013) 191:2637–46. doi: 10.4049/jimmunol.1300082

105. Li Y, Zhou H, Wen Z, Wu S, Huang C, Jia G, et al. Transcription analysis on response of swine lung to H1N1 swine influenza virus. *BMC Genomics* (2011) 12:398. doi: 10.1186/1471-2164-12-398

106. Miyashita M, Oshiumi H, Matsumoto M, Seya T. DDX60, a DEXD/H box helicase, is a novel antiviral factor promoting RIG-I-Like receptor-mediated signaling. *Mol Cell Biol* (2011) 31:3802–19. doi: 10.1128/MCB.01368-10

107. Schroyen M, Steibel JP, Koltes JE, Choi I, Raney NE, Eisley C, et al. Whole blood microarray analysis of pigs showing extreme phenotypes after a porcine reproductive and respiratory syndrome virus infection. *BMC Genomics* (2015) 16:516. doi: 10.1186/s12864-015-1741-8

108. Shi C, Liu Y, Ding Y, Zhang Y, Zhang J. PRRSV receptors and their roles in virus infection. *Arch Microbiol* (2015) 197:503–12. doi: 10.1007/s00203-015-1088-1

109. Zhang Y, Zhang K, Zheng H, Liu C, Jiang Y, Du N, et al. Development of a monoclonal antibody against porcine CD163 SRCR5 domain which partially blocks infection of PRRSV. *Front Vet Sci* (2020) 7:597843. doi: 10.3389/fvets.2020.597843

110. Kreutz LC, Ackermann MR. Porcine reproductive and respiratory syndrome virus enters cells through a low pH-dependent endocytic pathway. *Virus Res* (1996) 42:137–47. doi: 10.1016/0168-1702(96)01313-5

111. Zhang Y, Zhou Y, Yang Q, Mu C, Duan E, Chen J, et al. Ligation of fc gamma receptor IIB enhances levels of antiviral cytokine in response to PRRSV infection in vitro. *Vet Microbiol* (2012) 160:473–80. doi: 10.1016/j.vetmic.2012.06.021

112. Nauwynck HJ, Duan X, Favoreel HW, Van Oostveldt P, Pensaert MB. Entry of porcine reproductive and respiratory syndrome virus into porcine alveolar macrophages via receptor-mediated endocytosis. *J Gen Virol* (1999) 80:297–305. doi: 10.1099/0022-1317-80-2-297

113. Oikonomopoulou K, Ricklin D, Ward PA, Lambris JD. Interactions between coagulation and complement–their role in inflammation. *Semin Immunopathol* (2012) 34:151–65. doi: 10.1007/s00281-011-0280-x

114. Yang T, Zhang F, Zhai L, He W, Tan Z, Sun Y, et al. Transcriptome of porcine PBMCs over two generations reveals key genes and pathways associated with variable antibody responses post PRRSV vaccination. *Sci Rep* (2018) 8:2460. doi: 10.1038/s41598-018-20701-w

115. Yoneyama M, Kikuchi M, Natsukawa T, Shinobu N, Imaizumi T, Miyagishi M, et al. The RNA helicase RIG-I has an essential function in double-stranded RNA-induced innate antiviral responses. *Nat Immunol* (2004) 5:730–7. doi: 10.1038/ni1087

116. Yoneyama M, Kikuchi M, Matsumoto K, Imaizumi T, Miyagishi M, Taira K, et al. Shared and unique functions of the DExD/H-box helicases RIG-I, MDA5, and LGP2 in antiviral innate immunity. *J Immunol* (2005) 175:2851–8. doi: 10.4049/jimmunol.175.5.2851

117. Li D, Wu M. Pattern recognition receptors in health and diseases. *Signal Transduct Target Ther* (2021) 6:291. doi: 10.1038/s41392-021-00687-0

118. Motamedi M, Xu L, Elahi S. Correlation of transferrin receptor (CD71) with Ki67 expression on stimulated human and mouse T cells: the kinetics of expression of T cell activation markers. *J Immunol Methods* (2016) 437:43–52. doi: 10.1016/j.jim.2016.08.002

119. Hamann D, Roos MT, van Lier RA. Faces and phases of human CD8+ T-cell development. *Immunol Today* (1999) 20:177–80. doi: 10.1016/S0167-5699(99)01444-9

120. Gupta SS, Wang J, Chen M. Metabolic reprogramming in CD8+ T cells during acute viral infections. *Front Immunol* (2020) 11:1013. doi: 10.3389/fimmu.2020.01013

4. Discussion

The aim of this work was to extend our current knowledge of the porcine $CD8^+$ T-cell subsets by investigating their phenotype and transcriptional profile in greater detail. Our investigation encompassed the analysis of $CD8^+$ T-cell subsets under different conditions, including *ex vivo* samples, *in vitro* stimulation, and in the context of a virus infection. Through these comprehensive analyses, we aimed to shed light on the unique features and functional dynamics of porcine $CD8^+$ T-cell subsets. Generally, CTLs are defined by their expression of the CD8 heterodimer, specifically showing a $CD4^-CD8\alpha^{high}CD8\beta^+$ phenotype (83) and demonstrate perforin production (51). Previous studies indicated that expression of CD27 decreases along the differentiation stages of $CD8^+$ T cells, while the expression of perforin increases (53). In the mice CD11a marker allows the distinction between $CD8^+$ T-cell subpopulations, where low and high expressions correlate with naïve and antigen-experienced $CD8^+$ T-cell subpopulations, respectively (27,84,85). In providing effective defence against viral and bacterial infections, the adaptive immune system relies on the vital contribution of $CD8^+$ T cells. As mentioned before, CTLs play a significant role in adaptive immune response to PRRSV infection (68–75). However, characteristics of their exact profile, time point and magnitude of their involvement in combating this viral disease remains unresolved.

In the first research project, with a total of 72 samples from six animals, we employed surface-antigen based cell sorting and transcriptome analysis using next-generation sequencing (NGS) technologies. Our research focused on the gene signatures of three $CD8^+$ T-cell subsets postulated as: naïve (T_n; $CD8\beta^+CD27^+CD11a^{low}$), intermediate differentiated (T_{inter}; $CD8\beta^+CD27^{dim}CD11a^+$), and terminally differentiated cells (T_{term}; $CD8\beta^+CD27^-CD11a^{high}$). The results obtained from this research project were published in the journal Frontiers in Immunology (Lagumdzic et al. 2022). In the second research project, we investigated the transcriptomes of PBMCs and $CD8^+$ T cells in PRRSV-infected gilts at different time points after infection with PRRSV strain AUT15-33. This study included a total of 64 samples from eight one-year old gilts. To enhance our investigation, we employed a multi-faceted approach that included time-series clustering analysis, protein-protein interaction (PPI) networks, extensive gene ontology (GO) enrichment, pathway analysis, and gene set enrichment analysis (GSEA), while also measuring viral loads in serum and conducting flow cytometry analyses. The outcomes of this research project were documented and published in the journal Frontiers in Immunology (Lagumdzic et al. 2023).

4.1. Transcriptional profiles of three phenotypically defined CD8⁺ T-cell subsets

Extensive research in both mice and human has demonstrated that upon activation $CD8^+$ T cells differentiate into distinct subsets, each characterized by specific transcriptional profiles (86–89). In line with these findings, our differential gene expression analysis revealed significant differences in porcine *ex vivo* $CD8^+$ T-cell subsets. Furthermore, we identified the highest number of differently expressed genes (DEGs) between naïve (T_n; $CD8\beta^+CD27^+CD11a^{low}$) and terminally differentiated cells (T_{term}; $CD8\beta^+CD27^-CD11a^{high}$), with 575 and 709 DEGs observed, respectively. Specially, T_n exhibited a distinct gene expression profile characterized by the presence of important transcription factors *LEF1*, *BACH2*, *TCF7* (TCF1), *SATB1*, *ZEB1* and *BCL2*. These genes are known to be associated with early stages of T-cell differentiation and play key roles in maintaining the quiescent state of naïve T cell (90–92). Additionally, T_n showed the high upregulation of genes encoding lymph node homing receptor molecules such as *CCR7*, *SELL* (CD62L) and *CCR9*. Moreover, *S1PR1*, a sphingosine-1-Phosphate Receptor 1, which is critical for lymphocyte trafficking and known to be highly upregulated in human naïve T cells, was also elevated in the porcine T_n (93). Both *S1PR1* and *SELL* (CD62L), promoted by the zinc-finger transcription factor *KLF2*, are essential for the recirculation of naïve T cells (94,95). Furthermore, the observed downregulation of *S1PR1* along T-cell differentiation (96) is consistent with our findings of this marker in the porcine T_{inter} and T_{term}. Additionally, T_n showed high expression of *MYB*, which enforce cell stemness and restrain terminal T-cell differentiation (97). In more detail, MYB regulates $CD8^+$ T-cell differentiation by activating *TCF7* and *BCL2* while repressing expression of *ZEB2*, a gene known to act as a major driver of $CD8^+$ T cell terminal differentiation (98,99). These findings are in accordance with our results which show that T_n express *MYB*, *TCF7* and *BCL2*, while conversely, T_{inter} and T_{term} lacked their expression and showed an upregulation of *ZEB2*, suggesting a more differentiated state. Similarly, *FOXP1*, another critical regulator of naïve $CD8^+$ T quiescence, which represses key pathways in both metabolism and cell cycle progression (100), was highly upregulated in T_n. Additionally, our study highlights the upregulation of CD27, CCR7, and CD28 in porcine T_n cells, mirroring the pattern observed in the human T_n subset characterized by the four-dimensional model of T-cell differentiation stages (47).

On the other hand, both the T_{inter} and T_{term} demonstrated a distinct gene expression signature characterized by the upregulation of key transcription factors involved in driving the differentiation into terminally effector cells. Notably, this included *TBX21* (T-bet), *PRDM1* (Blimp-1), *ZEB2*, *ZNF683* (Hobit), *ID2*, and *STAT4*, which play crucial roles in driving the differentiation and functional specialization of effector T cells (91,101,102). Specifically, T-bet act as a 'master regulator' of cell-mediated immunity, regulating the expression of genes encoding effector molecules in CTLs, such as IFN-γ, perforin, and granzyme B (103). Moreover, expression of CX3CR1, a marker of effector T-cell differentiation, was significantly elevated in the T_{inter} and T_{term}. An increase in CX3CR1 expression during $CD8^+$ T-cell differentiation was first noted by Gerlach et al., revealing the existence of three distinct effector $CD8^+$ subpopulations characterized as $CX3CR1^-$, $CX3CR1^{int}$ and $CX3CR1^{hi}$ cells. Furthermore, the $CD8^+CX3CR1^{hi}$ cells were characterized by a $CD27^-$ and $CD127^-$ phenotype, predominantly expressing KLRG1. These cells also contained the lowest number of IL-2 producing cells and showed at least a 50% higher expression of T-bet compared to $CD8^+CX3CR1^-$ and $CD8^+CX3CR1^{int}$

cells (104), reminiscent of the typical terminally differentiated effector $CD8^+$ cells (28,31,105,106). These findings strongly align with our results obtained from porcine T_n, T_{inter} and T_{term} cells.

In mice, naïve $CD8^+$ T cells are characterized as $CD11a^{low}CD44^{low}CD27^+KLRG^-CD62L^+CD122^-$ cells, whereas terminally differentiated effector cells can be identified by their $CD11a^{high}CD44^{high}CD27^-KLRG^+CD62L^-CD122^-$ phenotype (47,107). Notably, our findings in porcine T_n and T_{term} cells align well with these established profiles, except for the expression of CD122 (*IL2RB*). The enhanced expression of CD122, the receptor responsible for cellular responsiveness to IL-15, can be attributed to the high levels of T-bet (*TBX21*), since T-bet is necessary for the induction and maintenance of the $CD122^{hi}$ state within $CD8^+$ T cells (103). A previous study demonstrated that *ITGA4* (CD49d) is absent in naïve $CD8^+$ T cells in mice, while it is highly expressed in more differentiated and antigen-experienced subsets associated with higher cytolytic effector status, such as $CD8^+$ effector T cells, central and effector memory $CD8^+$ T cells (108–110). Consistent with these findings, we also observed a high expression of *ITGA4* in T_{inter} and T_{term} cells, further supporting the concept of increased *ITGA4* (CD49d) expression in differentiated $CD8^+$ T-cell subsets. Furthermore, T_{inter} and T_{term} cells exhibited an upregulation of other markers for antigen-experienced cells (84,110), including *ITGAL* (CD11a) and *MKI67* (Ki67), suggesting their potential expansion as a result of antigen exposure.

Following the expansion phase, $CD8^+$ T cells with prior antigen exposure undergo differentiation into two distinct subsets: short-lived effector cells (SLEC) and memory precursor effector cells (MPEC), distinguished by their differential expression of CD127 and KLRG1 markers (28,31). In our study, we observed distinct expression patterns of *IL7R* (CD127) and *KLRG1* in the porcine T_{inter} and T_{term} cells. Particularly, T_{inter} showed significantly higher expression of *IL7R* (CD127) compared to T_{term}, while the expression of *KLRG1* was over three times higher in T_{term} than in T_{inter}. This indicates that T_{inter} may represent porcine MPECs, characterized by high *IL7R* expression, while T_{term} may correspond to SLECs, characterized by elevated *KLRG1* expression. As mentioned before, $CD8^+$ T cells efficiently eliminate infected or abnormal cells through cytotoxic mechanisms, including the release of cytotoxic granules and induction of apoptosis. They also produce cytokines such as IFN-γ and TNF-α with antimicrobial and antitumor effects (6–11). Thus, our analysis demonstrated significant upregulation of genes associated with cytolytic activity in the T_{term} and to a lesser extent in T_{inter}. Notably, *GNLY*, *PRF1* (perforin), *GZMB*, *FASL*, *IFNG*, and *TNF* exhibited the highest level of upregulation in T_{term}, followed by T_{inter}. Furthermore, our data confirmed the absence of these key cytolytic genes in *ex vivo* T_n cells. We also observed higher expression of the co-inhibitory molecule *PDCD1* (PD-1) in T_{inter} and T_{term} compared to T_n. The higher expression of *PDCD1* in T_{inter} and T_{term} suggests their tendency for SLEC formation and their highly activated state as observed in previous research (101,111). These findings highlight distinct cytolytic signatures within three distinct porcine $CD8^+$ T-cell subsets and provide valuable insights into their functional characteristics. In contrast to T_n cells, our analysis revealed a downregulation of CD27, CD28, and CCR7 genes in the T_{term}. Conversely, T_{inter} showed expression of CD27 and CD28, but lacked CCR7 expression. Considering the four-dimensional model established in humans, these expression patterns suggest that T_{inter} in swine may represent early differentiated $CD8^+$ T cells, defined by the $CD27^+CD28^+CCR7^-$ profile.

Our study aimed to understand the immunological roles and functions of genes in *ex vivo* $CD8^+$ T-cell subsets. Through GO term enrichment analysis, we uncovered distinct patterns of upregulated DEGs in these subsets. T_{term} showed upregulated genes associated with lymphocyte activation in immune response, while T_n exhibited genes linked to T-cell differentiation, T-cell receptor signalling, and V(D)J recombination. In T_{inter}, upregulated genes were related to T-cell differentiation, cytokine production, and αβ T-cell differentiation. Notably, T_{inter} had a higher proportion of genes involved in the regulation of T-cell differentiation compared to T_{term}. Additionally, the KEGG pathway analysis revealed unique enrichment patterns in the T_n, T_{inter}, and T_{term} subsets. T_{term} exhibited enrichment in immune-related pathways, particularly chemokine and T-cell receptor signalling, emphasizing its active immune response. T_n displayed enrichment in immune-related pathways along with metabolic and MAPK signalling pathways, suggesting its involvement in diverse cellular functions. While the number of immune-related pathways involved in DEGs was similar between T_n and T_{term} subsets, we observed a higher representation of DEGs in these pathways in the T_{term}. In contrast, the comparison between T_{inter} and T_{term} subsets showed the lowest number of KEGG pathways represented by DEGs, indicating a closer similarity in gene expression profiles between T_{inter} and T_{term} subsets.

Taken together, these findings provide insights into the specific gene expression profiles and functional characteristics of each $CD8^+$ T-cell subset, enhancing our understanding of the dynamic nature of T-cell responses in the porcine immune system. The identification of enriched pathways and biological processes associated with each subset sheds light on the specific gene regulatory networks operating within each subset, offering valuable insights into the molecular mechanisms underlying their distinct functions. Overall, these results underscore the differences in gene expression profiles among *ex vivo* $CD8^+$ T-cell subsets, with the most pronounced distinction observed between T_n and T_{term} subsets and a smaller distinction between T_{inter} and T_{term} subsets.

4.2. Gene signatures of three *in vitro* stimulated $CD8^+$ T-cell subsets

The stimulation of three $CD8^+$ T-cell subsets with ConA and PMA/ionomycin revealed distinct gene expression patterns and heterogeneity among the subsets. PMA/ionomycin stimulation resulted in a higher number of upregulated DEGs compared to ConA. PCA analysis showed separate clustering of T_n, T_{inter}, and T_{term} subsets, indicating their distinct gene expression profiles. Among PMA/ionomycin-stimulated subsets, T_{term}

demonstrated the highest number of upregulated DEGs, followed by T_{inter} and T_n. Interestingly, despite the separate clustering, there were a significant number of shared DEGs among the PMA/ionomycin-stimulated subsets, suggesting some degree of similarity in cellular properties. In contrast, ConA stimulation resulted in a smaller number of DEGs, with T_n showing the highest number, followed by T_{inter} and T_{term}.

Following PMA/ionomycin stimulation, all three subsets exhibited overexpression of *IFNG* (IFN-γ) and *TNF*, indicating their activation. Porcine T_n and T_{inter} subsets displayed high expression of *IL2* and its receptor chains *IL2RA* (CD25) and *IL2RG* (CD132), as well as *IRF7*, upon PMA/ionomycin stimulation. This suggests their involvement in terminal effector differentiation and memory development of $CD8^+$ T cells (112). Furthermore, expression of *IL4*, *IL17A*, *IL18RAP*, and *IL22* was induced specifically in PMA/ionomycin-stimulated T_{inter}. Notably, both mouse and human $CD8^+$ T cells have shown ability to produce the IL17A and IL22 (113). Conversely, *IL12RB1*, *IL27RA*, and *ILF3* were exclusively expressed in T_{term}. A previous study in mice demonstrated that IL27 maintains proliferation potential and is required to sustain *IRF1* expression in rapidly dividing $CD8^+$ T cells (114). Both *IL6ST* and *ILF2* were similarly increased in all three subsets upon PMA/ionomycin stimulation. Notably, the highest expression of *IL4R*, *IL15RA*, and *IRF1* was observed in T_n, followed by T_{inter} and T_{term}. Additionally, genes encoding TNF-induced proteins, *TNFAIP2*, *TNFAIP3*, and *TNFAIP8*, were highly expressed in $CD8^+$ T-cell subsets following PMA/ionomycin stimulation. *TNFAIP2* and *TNFAIP3*, known to inhibit the canonical NF-kB signalling pathway and negatively affect cytokine production (115,116), exhibited the highest expression in T_n. *TNFAIP3*, in addition to its functions, restricts MAP kinases and $CD8^+$ T-cell proliferation and is highly expressed in naïve T cells (117).

Chemokines and their receptors play a crucial role in guiding T cells to specific locations during immune responses. PMA/ionomycin stimulation resulted in stronger induction of genes associated with chemokines compared to ConA stimulation, with shared and subset-specific expression profiles observed. The inflammatory chemokines *CCL4* and *XCL1* are consistently upregulated in all three subsets following both stimulations, suggesting their essential role in T-cell activation and migration. In a previous single-cell sequencing study, *CCL4* was highly expressed in $CD8^+$ T cells and was associated with biological functions such as the cell cycle. Importantly, *CCL4* expression showed a significant correlation with the expression of CTL markers, including CD8 and Granzyme B (118,119). On the other hand, *XCL1* is found to be highly expressed in activated $CD8^+$ T cells in blood and plays a significant role in promoting an efficient cytotoxic immune response. It acts by attracting XCR1-expressing dendritic cells (DCs). This XCL1-XCR1 interaction facilitates antigen presentation from DCs to $CD8^+$ T cells, promoting the proliferation and differentiation of $CD8^+$ T cells (120,121). Notably, PMA/ionomycin-stimulated T_{inter} showed a significant increase in the expression of *CCL20*, *CXCL8*, and *CXCL10*, known as interferon-inducible ligands of *CXCR3* (122). Following PMA/ionomycin stimulation, high upregulation of *CCL5* (RANTES) and *CXCL16* was observed in all three $CD8^+$ T-cell subsets, while T_{inter} and T_{term} increased expression levels of *CCL1*, highlighting their role in immune response and T-cell activation.

The transition from naïve to activated effector T cells involves metabolic adjustments to support specific cellular functions (123). PMA/ionomycin stimulation induced a stronger upregulation of genes associated with T-cell metabolism compared to ConA. During T-cell activation, the upregulation of branched-chain amino acid transaminase (BCAT) and glutamate-cysteine ligase catalytic subunit (GCLC) is observed. Later is crucial for the synthesis of glutathione, an antioxidant that helps protect activated T cells from oxidative stress and plays essential role in maintaining glycolysis and supporting T-cell proliferation (124–126). Also, activated T cells express the aerobic glycolysis–supporting enzyme lactate dehydrogenase A (LDHA), which maintains high amounts of acetyl–coenzyme A and promotes IFN-γ expression (127). Moreover, LDHA initiates metabolic switching to aerobic glycolysis that ensures clonal proliferation, differentiation, and immune effects of activated effector T cells (128). To that end, upon PMA/ionomycin stimulation, porcine T_n and T_{inter} upregulated *BCAT1* and *GCLC*, while T_{term} elevated *LDHA* and *TPI1* transcripts. The differential expression of metabolic genes among three $CD8^+$ T-cell subsets, emphasize the heterogeneity in their metabolic profiles and functional characteristics. The observed upregulation of *HIF1A*, *SLC7A5*, *SLC1A5*, *HK2*, *MYC*, and *ID2* in specific subsets suggests their involvement in the metabolic adaptations necessary for T-cell activation and effector functions. Furthermore, these findings enhance our understanding of the metabolic requirements of $CD8^+$ T-cell subsets and provide insights into their functional characteristics.

Our investigation into the impact of stimulation on transcription factor gene expression in $CD8^+$ T-cell subsets revealed distinct patterns. PMA/ionomycin stimulation led to the upregulation of several transcription factors associated with terminally differentiated effector cells, including *BATF*, *BATF3*, *EZH2*, *MYC*, and *TBX21*, across all subsets. Notably, T_n showed the highest upregulation of *TBX21*, which encodes T-bet, a master regulator of cytotoxic T-cell development (129). The expression of *BATF* during chronic infection is essential for both the optimal persistence of CD8 T cells and their anti-viral effector function. Moreover, *BATF* plays a critical role in sustaining CD8 T-cell response by cooperating with *IRF4* to preserve the expression of *PRDM1* (Blimp-1), an essential transcription factor for CD8 T-cell effector function and maintenance (130). The upregulation of *IRF4* was observed in all three subsets following PMA/ionomycin and ConA stimulations, with the highest expression in PMA/ionomycin-stimulated T_n, followed by T_{inter} and T_{term}. This is consistent with previous studies in mice, suggesting the contribution of *IRF4* to expansion, maintenance of effector functions, and memory formation of CTL (131). The expression of *IRF8* showed similarity among $CD8^+$ T-cell subsets stimulated with PMA/ionomycin, while ConA stimulation induced lower expression in T_{inter} and T_{term}. Furthermore, PMA/ionomycin stimulation resulted in the upregulation of *FOXO1*, *FOXP1*, *PRDM1* (Blimp-1), *SATB1*, and *SREBF2* in T_{inter} and T_{term}, indicating their involvement in T-cell activation and differentiation. Blimp-1, encoded by *PRDM1,* plays a crucial role in activated T cells by promoting IL10 production and contributing to the function of cytotoxic T cells. Specifically, Blimp-1 is essential for the formation of SLECs, as evidenced by its higher expression in SLECs compared to MPECs (132). Interestingly, both T_{inter} and T_{term} showed high expression of *IL10* after PMA/ionomycin stimulation. On the other hand, ConA stimulation induced specific upregulation of *EOMES* and *ID3* in T_n. Eomes is upregulated in effector $CD8^+$ T cells and plays a critical role in T-bet-independent IFN-γ induction in $CD8^+$ T cells (133). On a different note, $ID3^{hi}CD8^+$ T effector cells have a higher propensity to differentiate into long-lived memory cells, while $ID3^{lo}CD8^+$ T effector cells are more prone to becoming short-lived effector cells early after infection (134). The expression of EGR family transcription factors (*EGR1*, *EGR2*, and *EGR3*) and *NAB2*, a coactivator and corepressor of T-cell function, gradually increased along the differentiation subsets. Additionally, *NR4A2* and *NR4A3*, members of the *NR4A* family known for their role in acute and chronic $CD8^+$ T-cell response (135), were highly expressed, with the highest levels observed in T_{term}.

Notably, the expression of *BCL2* was observed in T_n and T_{inter}, indicating their reliance on *BCL2* for survival (136). *MYB*, a transcription factor known for promoting the formation of stem-like memory cells and restraining terminal effector differentiation by regulating the expression of *BCL2* and *TCF7*, as well as inhibiting *ZEB2* (137), was strongly expressed in T_n but not in T_{inter} or T_{term}. *BACH2*, a transcriptional repressor of terminal differentiation (138,139), was upregulated in T_n and T_{inter} following PMA/ionomycin stimulation. Moreover, the expression of *ZEB1* and *TCF3* was induced in T_{inter} and T_{term}, respectively, upon PMA/ionomycin stimulation. The PMA/ionomycin stimulation induced high expression of *STAT1* in all subsets, while *STAT4* upregulation was observed in T_{inter} and T_{term}. These transcription factors play important roles in clonal expansion and effector maturation of $CD8^+$ T cells, with *STAT1* involved in type I IFN-dependent expansion and *STAT4* contributing to IL-12-mediated proliferation (140,141). PMA/ionomycin stimulation induced high expression of *BCL6* in T_n and T_{term}, while *ID2*, a transcriptional regulator upregulated during the effector phase (142), was upregulated in all subsets.

We also investigated the genes associated with effector functions in $CD8^+$ T-cell subsets upon stimulation with ConA and PMA/ionomycin. PMA/ionomycin stimulation induced a much stronger upregulation of genes compared to ConA, indicating its higher potency in inducing gene expression changes in $CD8^+$ T-cell subsets. Our findings revealed several important insights. First, stimulation with PMA/ionomycin resulted in a notable similarity in the gene expression profiles of the $CD8^+$ T-cell subsets, as indicated by the high number of shared DEGs. This convergence suggests a common activation state induced by the stimulation, leading to substantial changes in gene expression across all three subsets. Second, despite the overall similarity in gene expression profiles following PMA/ionomycin stimulation, we observed distinct differences among the $CD8^+$ T-cell subsets. T_n exhibited upregulation of genes associated with T-cell activation and differentiation but did not fully acquire the gene expression profile of mature effector cells. Notably, T_n also showed upregulation of several genes linked to early stages of differentiation, such as *BACH2* and *BCL6*, which have been found to negatively correlate with IFN-γ, TNF-α, and granzyme B expression in effector $CD8^+$ T cells (139,143). In contrast, T_{term} and T_{inter} demonstrated a higher expression of genes linked to late-stage differentiation and effector functions. Generally, our results suggest that T_n may require additional time or assistance from other cells to reach their full cytotoxic potential compared to T_{inter} and T_{term}. This is supported by their upregulation of genes associated with early stages of differentiation and the absence of genes involved in effector functions, such as *GNLY*, *PRF1*, *GZMB*, and *FASL*. Therefore, the distinct gene expression profiles among the three porcine $CD8^+$ T-cell subsets indicate their functional heterogeneity and different capacities for cytotoxicity and effector functions.

Additionally, the GO term and KEGG pathway analyses provided robust evidence for the distinct functional characteristics of the $CD8^+$ T-cell subsets upon stimulation.

PMA/ionomycin-stimulated T_n exhibited enrichment in GO terms related to the regulation of T-cell activation, while T_{inter} and T_{term} showed enrichment in terms associated with leukocyte differentiation and lymphocyte activation. KEGG pathway analysis further supported these findings, with T_{inter} and T_{term} exhibiting a higher number of DEGs enriched in immune-related pathways compared to T_n. Additionally, T_{inter} showed the highest enrichment of DEGs in the T-cell receptor signalling pathway, while T_n had the highest number of immune-related pathways enriched upon ConA stimulation.

Our study reveals valuable insights into the gene expression dynamics and functional heterogeneity of $CD8^+$ T-cell subsets during stimulation. PMA/ionomycin induces a stronger cytolytic T-cell response compared to ConA, with T_{inter} and T_{term} showing a more pronounced and early response. T_n exhibits a partial activation with upregulated genes associated with early differentiation. These findings enhance our understanding of immune responses and highlight the distinct characteristics of $CD8^+$ T-cell subsets.

4.3. Temporal quantification and differentiation stages of cytotoxic T-cell response to PRRSV infection

Investigating $CD8^+$ T cells in the context of PRRSV infection is crucial due to the disease's global prevalence, economic losses, and its ability to suppress the immune system, leading to higher susceptibility to secondary infections. Studying the role of $CD8^+$ T cells in the immune response to PRRSV can provide insights into their cytolytic activity and their potential as targets for intervention strategies. Additionally, given the variability in CTL activity observed in previous studies and the need for innovative approaches, there is a demand for fresh perspectives in the analysis of CTLs in PRRSV-infected swine. Therefore, in this study, we conducted a comprehensive investigation of the immune response to PRRSV infection by analysing a total of 64 samples collected from eight one-year-old gilts. $CD8^+$ T cells were obtained from four PRRSV-infected gilts and four non-infected gilts. The infection was induced at 85 gestation day through intranasal administration of PRRSV strain AUT15-33 and blood samples were collected at multiple time points, including prior to infection (day 0) and at days 7, 14, and approximately 21 post-infection (dpi). Viremia analysis confirmed the PRRS negative status of the gilts before infection and demonstrated virus replication following infection. No PRRSV RNA was detected in serum samples collected prior to inoculation on day 0. However, all infected gilts exhibited viremia at 7 and 14 dpi. By 21 dpi, persistent viremia was observed in all but one of the infected gilts.

In this study, we investigated the temporal dynamics of CTLs response to PRRSV infection, aiming to gain insights into the immune response against the virus. CTLs were characterized as $CD3^+CD8\alpha^{high}perforin^+$ cells, representing an activated and cytotoxic phenotype (53). We observed a progressive increase in the frequencies of CTLs in the PRRSV-infected group compared to the control group. Importantly, the highest frequencies of these activated and cytotoxic CTLs were observed at 21 dpi. These findings indicate that PRRSV infection elicits a robust CTL response, characterized by the expansion of activated cytotoxic T cells.

Based on these findings, we aimed to delve deeper into the poorly understood differentiation process of CTLs in the context of PRRSV infection. In our study, we aimed to shed light on these differentiation processes by analysing the phenotypic expression of CD8β, CD27, and perforin markers at 21 dpi. The total frequency of $CD8\beta^+$ T cells showed a significant increase of 62% in the PRRSV-infected group compared to the control group at 21 dpi. This suggests an expansion of $CD8\beta^+$ T cells during PRRSV infection, indicating their active involvement in the immune response against the virus. Further examination of specific $CD8\beta^+$ T cell subsets revealed distinct distribution patterns between the control and PRRSV-infected groups. While the frequencies of naïve cells (T_n; $CD8\beta^+CD27^+perforin^-$) were comparable between the two groups, indicating the relative stability of this subset, remarkable differences were observed in the intermediate (T_{inter}; $CD8\beta^{+}CD27^{dim}perforin^{+}$) and terminally differentiated cells (T_{term}; $CD8\beta^{+}CD27^{-}perforin^{high}$).

Notably, the frequencies of both T_{inter} and T_{term} subsets were significantly higher in the PRRSV-infected group compared to the control group. The increase in T_{inter} frequencies was more than 6.6-fold, while T_{term} frequencies were 2.2 times higher in the PRRSV-infected group. These findings suggest that the PRRSV infection promotes the differentiation of $CD8^{+}$ T cells into more activated and cytotoxic subsets.

4.4. Gene expression profile of $CD8^{+}$ T cells after PRRSV infection

In our study, we conducted a comprehensive analysis of gene expression in $CD8^{+}$ T cells from both the infected and negative control groups. PCA plot clearly demonstrated distinct separation, indicating significant differences in gene expression profiles between the two groups following PRRSV infection. We identified a varying number of DEGs at different time points post-infection. Interestingly, the highest number of DEGs (533) was observed at 21 dpi, indicating substantial transcriptional changes in $CD8^{+}$ T cells at this later time point. In contrast, the smallest number of DEGs (98) was observed at day 0. Notably, comparable numbers of DEGs were found at 7 dpi (359) and 14 dpi (367), suggesting a robust transcriptional response during the early phase of infection.

Furthermore, the Venn diagram analysis revealed a significant number of unique DEGs at 21 dpi, indicating distinct gene expression patterns specific to this time point. Additionally, a considerable number of DEGs (214) were shared among $CD8^{+}$ T cells from infected animals at 7 dpi, 14 dpi, and 21 dpi, suggesting common transcriptional changes across these time points. Importantly, the expression profiles of $CD8^{+}$ T cells at 14 dpi shared a greater number of genes with those at 21 dpi than with those at 7 dpi, indicating a progressive shift in gene expression during the infection progression.

The observed differences in DEGs at different time points and the progressive shift in gene expression profiles indicate a dynamic and evolving immune response.

Our analysis of protein-protein interaction (PPI) networks in $CD8^+$ T cells during different time points of PRRSV infection revealed distinct clusters associated with specific biological processes and immune responses. At 7 dpi, the clusters primarily involved regulation of cell cycle processes, immune response to virus, interferon signalling, and cytokine production. This suggests the activation of antiviral immune mechanisms and early immune response in $CD8^+$ T cells. At 14 dpi, the identified clusters included immune response, lymphocyte activation, adaptive immune response, cytokine-mediated signalling and cell cycle. These findings indicate the ongoing immune activation, differentiation, and effector functions of $CD8^+$ T cells at this stage of infection. By 21 dpi, $CD8^+$ T cells demonstrated a predominant cluster involved in the regulation of cell cycle processes, highlighting their proliferation and expansion. Additionally, clusters associated with T-cell activation, differentiation, adaptive immune response, cytolysis activity and cytokine production were observed, indicating the persistence and involvement of $CD8^+$ T cells in the late stage of PRRSV infection.

Upon virus infection, activated naïve $CD8^+$ T cells undergo proliferation and differentiation into virus-specific effector $CD8^+$ T cells, which play a crucial role in eliminating virus-infected cells. The effector activity of $CD8^+$ T cells relies on the production of effector cytokines and granule-associated proteases. In our study, we observed the upregulation of genes associated with the later stages of porcine $CD8^+$ T-cell differentiation during the time-course of PRRSV infection. Transcription factors *PRDM1* (Blimp-1), *EOMES*, and *TBX21* (T-bet) were highly expressed at 14 dpi and 21 dpi, consistent with previous findings highlighting their involvement in the immune response to PRRSV. Additionally, genes involved in cytolytic activity, including granzymes, perforin, fas ligand, killer cell lectin-like receptors, and *NKG7*, were significantly upregulated at 14 dpi and 21 dpi, with the highest expression observed at 21 dpi, indicating the activation of cytotoxic and target cell elimination mechanisms.

Our study revealed a robust upregulation of chemokines and chemokine receptors in $CD8^+$ T cells from PRRSV-infected animals. Specifically, we observed a significant increase in the expression of *CXCR3* and its ligands *CXCL9* and *CXCL10* at 21 dpi, indicating their potential involvement in the activation of $CD8^+$ T cells (144). Moreover, the continuous upregulation of *CXCL10* throughout the infection period suggests its role in promoting the generation of $CD8^+$ effector cells (145). Additionally, we found that the expression of *CCR1*, *CCL2*, *CCL4*, *CCL8*, *CXCR3*, *CXCR6*, *CXCL9*, and *CXCL16* was significantly elevated exclusively at 21 dpi, suggesting their importance in the later stages of the $CD8^+$ T-cell response. Furthermore, the upregulation of *CX3CR1* at 7 and 14 dpi highlights its potential role in the early immune response mediated by virus-specific effector $CD8^+$ T cells. These findings suggest that chemokines play a crucial role in the recruitment and activation of $CD8^+$ T cells during PRRSV infection.

Our study demonstrated a strong expression of cytokine genes, including *IL10*, *IL2RB* (CD122), *IFNG* (IFN-γ), *IL21R*, *IL15RA*, and *IL13RA1*, in $CD8^+$ T cells at 14 and 21 dpi, indicating their crucial role in the immune response against PRRSV infection. These findings align with previous studies highlighting $CD8^+$ T cells as primary producers of IFN-γ in PRRSV-vaccinated animals (75) and the importance of IL10 expression during acute viral infection (146–148). Interestingly, we observed a differential expression pattern among granzymes and IFN-γ, with higher production of GZMB and IFN-γ at later time points, potentially in $IL10^-CD8^+$ T cells. The production of IL10 in $CD8^+$ T cells was correlated with *PRDM1* expression (Blimp-1) (149), and the presence of IL21 was found to play a crucial role in maintaining $CD8^+$ T cell functionality during chronic viral infections (150–153). In our study, we observed the expression of *IL21R* at 14 dpi only, while *PRDM1* (Blimp-1) was expressed at both 14 and 21 dpi, suggesting a potential role for Blimp-1 in regulating the $CD8^+$ T-cell response to PRRSV. Collectively, these findings highlight the contribution of CD8$^+$ T cells in producing inflammatory cytokines critical for mounting an effective immune response against PRRSV.

Co-inhibitory molecules such as *PDCD1* (PD-1), *HAVCR2* (Tim-3), *CTLA4*, and *LAG3* have been implicated in the regulation of activated and differentiated CD8$^+$ T cells during viral infections (154–157). During PRRSV infection, there was a gradual upregulation of co-inhibitory molecules (*PDCD1*, *CTLA4*, *HAVCR2*, *LAG3*) in CD8$^+$ T cells, with the highest expression observed at 21 dpi, suggesting the involvement of immune checkpoint pathways in modulating CD8$^+$ T cell function. To further investigate potential exhaustion signals in CD8$^+$ T cells at 21 dpi, we performed gene set enrichment analysis (GSEA). Our analysis further supported the effector state of CD8$^+$ T cells at 21 dpi, showing significant enrichment of gene sets associated with effector CD8$^+$ T cells, IFN-α and IFN-γ responses, inflammatory response, T cell activation, acute phase response, and maintenance of effector CD8$^+$ T cells during infection. This suggests that CD8$^+$ T cells in PRRSV-infected animals are highly functional and actively engaged in immune responses. Moreover, the enrichment of gene sets related to cell division, proliferation, and metabolic programming indicates that CD8$^+$ T cells at 21 dpi are actively proliferating and undergoing metabolic changes to support their effector functions.

4.5. Temporal gene expression clustering in CD8$^+$ T cells during PRRSV infection

Our comprehensive gene expression profiling uncovered important aspects of the CD8$^+$ T-cell response to PRRSV infection. We made two significant observations: Firstly, there is a progressive and robust activation of CD8$^+$ T cells, culminating in peak activity at 21 dpi, which indicates the successful induction of adaptive immunity. Secondly, during the later stages of infection (14 to 21 dpi), CD8$^+$ T cells undergo a process of differentiation, characterized by heightened effector functions and enhanced cytolytic activity. However, to unravel the underlying transcriptional regulatory mechanisms driving these immune responses, we employed temporal clustering analysis of DEGs in $CD8^+$ T cells from PRRSV-infected animals.

The time-clustering analysis of DEGs in $CD8^+$ T cells during PRRSV infection identified four distinct clusters that provide insights into the molecular processes underlying $CD8^+$ T cell responses. Cluster 1 and cluster 2 genes showed continuous upregulation from 7 dpi, indicating a robust cell division and proliferation response. Cluster 1 included genes such as *AURKB*, known to be associated with cell division processes in $CD8^+$ T cells (158). Notably, cluster 2 included genes such as *MKI67*, *CHEK1*, and *BLM*, which are known to be expressed in dividing cells and play important roles in cell proliferation (159,160). This aligns with previous findings of *MKI67* upregulation in differentiated $CD8^+$ T cell subsets (161) and the proliferation of CTLs in PRRSV-infected animals (71). Furthermore, genes in cluster 1 were enriched in processes related to the cell cycle, carbohydrate derivative catabolism, and cyclin-dependent protein kinase inhibitor activity, while cluster 2 genes were associated with the regulation of mitotic cell cycle, cell cycle checkpoint signalling, and DNA replication. Therefore, these genes likely contribute to early $CD8^+$ T cell transformation upon encountering PRRSV.

Cluster 3 genes were found to be enriched in the regulation of long-chain fatty acid transport and the Fc-epsilon receptor signalling pathway. Interestingly, these genes showed downregulation at 7 dpi, indicating a metabolic switch from fatty acid oxidation, which is characteristic of naïve $CD8^+$ T cells (162). This indicates that $CD8^+$ T cells undergo metabolic reprogramming in response to PRRSV infection.

Lastly, cluster 4 revealed upregulated genes associated with chemotaxis and chemokine activity at 21 dpi, suggesting an important role for $CD8^+$ T cells in the immune response against PRRSV. Genes such as *CCL2*, *CCL4*, *CCL8*, *CXCL10*, *CXCL16*, *CXCL9*, *CXCR6*, *KLRK1*, *LGMN*, and *RARRES2* in cluster 4 were particularly enriched in GO terms related to cell chemotaxis, chemokine activity, and chemokine-mediated signalling pathways. These findings highlight the importance of chemotaxis and chemokine-mediated interactions in the recruitment and activation of $CD8^+$ T cells during the immune response to PRRSV. Overall, these findings highlight the dynamic molecular changes in $CD8^+$ T cells during PRRSV infection, including cell proliferation, metabolic reprogramming, and chemotaxis- and chemokine-related processes. Understanding these molecular processes can provide valuable insights into the immune response and potential targets for controlling PRRSV infection.

4.6. Conclusions

In conclusion, our PhD work has significantly advanced our understanding of the porcine $CD8^+$ T-cell subsets and their interaction with PRRSV. Through comprehensive transcriptomics analysis, we elucidated the gene signatures associated with the differentiation stages of three porcine $CD8^+$ T-cell subsets, providing valuable insights into their immunological roles and functions.

In our first study, we successfully analysed the transcriptomes of porcine $CD8\beta^+$ T-cell subsets, specifically focusing on the differentiation stages defined phenotypically by the CD11a/CD27 expression pattern. Through our research, we successfully characterized three distinct subsets: naïve (T_n; $CD8\beta^+CD27^+CD11a^{low}$), intermediate ($T_{inter}$; $CD8\beta^+CD27^{dim}CD11a^+$), and terminally differentiated cells (T_{term}; $CD8\beta^+CD27^-CD11a^{high}$). By employing NGS, we obtained comprehensive transcriptional profiles of these subsets in both *ex vivo* conditions and following *in vitro* stimulation with ConA and PMA/ionomycin. We observed distinct gene expression signatures among T_n, T_{inter}, and T_{term}, with genes associated with cell proliferation, T-cell differentiation, and cytolytic activity being highly expressed in specific subsets. Specifically, our findings revealed significant differences in gene expression between the T_n and T_{term}, indicating their distinct differentiation stages and functional roles. Genes associated with early stages of $CD8^+$ T-cell differentiation (90–92), such as *IL7-R*, *CCR7*, *SELL*, *TCF7*, *LEF1*, *BACH2*, *SATB1*, *ZEB1*, and *BCL2*, were highly expressed in the T_n. On the other hand, genes related to late stages of $CD8^+$ T-cell differentiation (91,101,102), including *KLRG1*, *TBX21*, *PRDM1*, *CX3CR1*, *ZEB2*, *ZNF683*, *BATF*, *EZH2*, and *ID2*, were predominantly expressed in the T_{term}. The T_{inter} exhibited a gene expression profile more closely resembling the later stages of T-cell differentiation. Furthermore, we observed that genes associated with cytolytic activity, such as *GNLY*, *PRF1*, *GZMB*, *FASL*, *IFNG*, and *TNF*, were highly expressed in both T_{term} and T_{inter}. In contrast, the T_n displayed minimal expression of these cytolytic genes, even after *in vitro* stimulation. In summary, our study delivers a comprehensive analysis of the transcriptional profiles of three distinct differentiation stages within porcine $CD8^+$ T-cell subsets. Moreover, our findings offer a valuable resource for identifying candidate markers that can be utilized to further characterize porcine immune cell subsets with greater precision.

In the second study, we provided comprehensive insights into the temporal dynamics, differentiation stages, gene expression profiles, and functional characteristics of $CD8^+$ T cells during PRRSV infection. Through our investigation, we have made significant findings. Firstly, we observed a progressive increase in the frequencies of cytotoxic $CD8^+$ T cells, with the highest levels observed at 21 dpi, indicating a robust CTL response to PRRSV infection. Secondly, the differentiation analysis of $CD8^+$ T cells revealed a significant expansion of intermediate (T_{inter}) and terminally differentiated (T_{term}) subsets in the PRRSV-infected group compared to the control group. This suggests that PRRSV infection promotes the differentiation of $CD8^+$ T cells into more activated and cytotoxic subsets. Thirdly, gene expression analysis identified DEGs at multiple time points post-infection. The highest number of DEGs was observed at 21 dpi, indicating substantial transcriptional changes in $CD8^+$ T cells at this later time point. Furthermore, our temporal clustering analysis of DEGs in $CD8^+$ T cells revealed four distinct clusters associated with specific biological processes and immune responses. These clusters represented cell division and proliferation, metabolic reprogramming, chemotaxis, and chemokine activity. This indicates the dynamic and coordinated regulation of $CD8^+$ T cell responses during PRRSV infection.

The enrichment of specific biological processes, such as cell cycle regulation, immune response to virus, interferon signalling, cytokine production, and immune checkpoint pathways, further supports the involvement of $CD8^+$ T cells in antiviral immunity and immune regulation during PRRSV infection. Overall, our findings enhance our understanding of the dynamic changes in $CD8^+$ T cells during PRRSV infection, including their expansion, differentiation, gene expression profiles, and functional properties. These insights provide valuable knowledge for the development of targeted strategies to control PRRSV infection, including the design of vaccines, therapeutics, and diagnostic markers. Further investigations are warranted to elucidate the functional significance of the identified genes and pathways, as well as to explore the long-term immune response and potential correlates of protection.

4.7. Outlook

The comprehensive transcriptomics data generated in our studies pave the way for further investigations and future directions in porcine immunology research. To validate the findings and gain a more comprehensive understanding of the immune response and the functional roles of specific genes in porcine $CD8^+$ T cells, additional assays can be employed.

Validation of protein expression levels can be performed using flow cytometry, allowing for a correlation between gene expression and protein abundance at the single-cell level. Functional assays such as cytotoxicity assays, including impedance-based assays, can assess the impact of these genes on the cytolytic activity of $CD8^+$ T subsets in real-time (163), providing insights into their cytotoxic potential. Furthermore, cytokine production assays can evaluate the effect of these genes on effector molecule

production by $CD8^+$ T subsets. Knockdown or overexpression studies can further elucidate the functional roles of specific genes in porcine $CD8^+$ T cell responses.
Co-culture experiments with target cells or antigen-presenting cells can shed light on the direct interaction and functional consequences of $CD8^+$ T subsets expressing the identified genes. *In vivo* studies using animal models infected with relevant pathogens can validate the functional significance of these genes in the context of infection, providing valuable information on their contribution to the immune response.

In addition to bulk RNA sequencing, single-cell sequencing can provide a more detailed understanding of the heterogeneity within $CD8^+$ T-cell subsets and their responses to antigen. This approach enables the identification of rare cell populations and novel immune-regulatory mechanisms, uncovering cell-to-cell variations in gene expression and functional states. Single-cell transcriptomics overcomes limitations of flow cytometry-based assays, allowing for analysis in tissues with limited cell yields or when specific antibodies are unavailable. It also facilitates the detection of low-abundance transcripts, making it particularly valuable for studying rare cell types or dynamic processes. Integration of transcriptomic data with other omics data, such as proteomics or epigenomics, further enhances the comprehensive analysis of cellular functions (164).

To gain deeper insights into the dynamics of immune cell populations and gene expression changes following infection, longitudinal studies tracking the immune response over an extended period or with more time points would be beneficial. These studies can identify critical time points, immune markers, and potential intervention strategies for controlling infections with PRRSV or other pathogens.

By incorporating these complementary methods and assays, we can further validate and expand our understanding of the immune response in porcine $CD8^+$ T cells, unravel the functional significance of specific genes, and explore novel immune regulatory mechanisms.

5. References

1. Marshall JS, Warrington R, Watson W, Kim HL. An introduction to immunology and immunopathology. Allergy, Asthma Clin Immunol (2018) 14(S2):49. doi: 10.1186/s13223-018-0278-1
2. Bonilla FA, Oettgen HC. Adaptive immunity. J Allergy Clin Immunol (2010) 125(2):S33–40. doi: 10.1016/j.jaci.2009.09.017
3. Tsimberidou A-M, Van Morris K, Vo HH, Eck S, Lin Y-F, Rivas JM, et al. T-cell receptor-based therapy: an innovative therapeutic approach for solid tumors. J Hematol Oncol (2021) 14(1):102. doi: 10.1186/s13045-021-01115-0
4. Huang D, Miller M, Ashok B, Jain S, Peppas NA. CRISPR/Cas systems to overcome challenges in developing the next generation of T cells for cancer therapy. Adv Drug Deliv Rev (2020) 158:17–35. doi: 10.1016/j.addr.2020.07.015
5. Zhang N, Bevan MJ. CD8+ T Cells: Foot Soldiers of the Immune System. Immunity (2011) 35(2):161–8. doi: 10.1016/j.immuni.2011.07.010
6. Sigal LJ. Activation of CD8 T Lymphocytes during Viral Infections. In: Encyclopedia of Immunobiology Elsevier (2016). p. 286–90. doi: 10.1016/B978-0-12-374279-7.14009-3
7. Berke G. The Binding and Lysis of Target Cells by Cytotoxic Lymphocytes: Molecular and Cellular Aspects. Annu Rev Immunol (1994) 12(1):735–73. doi: 10.1146/annurev.iy.12.040194.003511
8. Clark WR, Walsh CM, Glass AA, Hayashi F, Matloubian M, Ahmed R. Molecular Pathways of CTL-mediated Cytotoxicity. Immunol Rev (1995) 146(1):33–44. doi: 10.1111/j.1600-065X.1995.tb00682.x
9. Kägi D, Ledermann B, Bürki K, Seiler P, Odermatt B, Olsen KJ, et al. Cytotoxicity mediated by T cells and natural killer cells is greatly impaired in perforin-deficient mice. Nature (1994) 369(6475):31–7. doi: 10.1038/369031a0
10. Badovinac VP, Tvinnereim AR, Harty JT. Regulation of Antigen-Specific CD8 + T Cell Homeostasis by Perforin and Interferon-γ. Science (2000) 290(5495):1354–7. doi: 10.1126/science.290.5495.1354
11. Harty JT, Tvinnereim AR, White DW. CD8+ T Cell Effector Mechanisms in Resistance to Infection. Annu Rev Immunol (2000) 18(1):275–308. doi:

10.1146/annurev.immunol.18.1.275

12. Germain RN. T-cell development and the CD4–CD8 lineage decision. Nat Rev Immunol (2002) 2(5):309–22. doi: 10.1038/nri798
13. Deftos ML, Bevan MJ. Notch signaling in T cell development. Curr Opin Immunol (2000) 12(2):166–72. doi: 10.1016/S0952-7915(99)00067-9
14. Godfrey DI, Kennedy J, Suda T, Zlotnik A. A developmental pathway involving four phenotypically and functionally distinct subsets of CD3-CD4-CD8- triple-negative adult mouse thymocytes defined by CD44 and CD25 expression. J Immunol (1993) 150(10):4244–52. doi: 10.4049/jimmunol.150.10.4244
15. Allman D, Sambandam A, Kim S, Miller JP, Pagan A, Well D, et al. Thymopoiesis independent of common lymphoid progenitors. Nat Immunol. (2003) 4(2):168–74. doi: 10.1038/ni878
16. Bhandoola A, Sambandam A, Allman D, Meraz A, Schwarz B. Early T Lineage Progenitors: New Insights, but Old Questions Remain. J Immunol. (2003) 171(11):5653–8. doi: 10.4049/jimmunol.171.11.5653
17. Borowski C, Li X, Aifantis I, Gounari F, von Boehmer H. Pre-TCRα and TCRα Are Not Interchangeable Partners of TCRβ during T Lymphocyte Development. J Exp Med. (2004) 199(5):607–15. doi: 10.1084/jem.20031973
18. Hernandez JB, Newton RH, Walsh CM. Life and death in the thymus—cell death signaling during T cell development. Curr Opin Cell Biol (2010) 22(6):865–71. doi: 10.1016/j.ceb.2010.08.003
19. Hosokawa H, Rothenberg E V. Cytokines, Transcription Factors, and the Initiation of T-Cell Development. Cold Spring Harb Perspect Biol. (2018) 10(5):a028621. doi: 10.1101/cshperspect.a028621
20. Robey E, Fowlkes BJ. Selective Events in T Cell Development. Annu Rev Immunol (1994) 12(1):675–705. doi: 10.1146/annurev.iy.12.040194.003331
21. von Boehmer H, Teh HS, Kisielow P. The thymus selects the useful, neglects the useless and destroys the harmful. Immunol Today (1989) 10(2):57–61. doi: 10.1016/0167-5699(89)90307-1
22. Matzinger P, Guerder S. Does T-cell tolerance require a dedicated antigen-presenting cell? Nature (1989) 338(6210):74–6. doi: 10.1038/338074a0

23. Kishimoto H, Sprent J. Negative Selection in the Thymus Includes Semimature T Cells. J Exp Med. (1997) 185(2):263–72. doi: 10.1084/jem.185.2.263
24. Anderson MS, Venanzi ES, Klein L, Chen Z, Berzins SP, Turley SJ, et al. Projection of an Immunological Self Shadow Within the Thymus by the Aire Protein. Science (2002) 298(5597):1395–401. doi: 10.1126/science.1075958
25. Matloubian M, Lo CG, Cinamon G, Lesneski MJ, Xu Y, Brinkmann V, et al. Lymphocyte egress from thymus and peripheral lymphoid organs is dependent on S1P receptor 1. Nature (2004) 427(6972):355–60. doi: 10.1038/nature02284
26. Zachariah MA, Cyster JG. Neural Crest–Derived Pericytes Promote Egress of Mature Thymocytes at the Corticomedullary Junction. Science (2010) 328(5982):1129–35. doi: 10.1126/science.1188222
27. Cossarizza A, Chang H, Radbruch A, Abrignani S, Addo R, Akdis M, et al. Guidelines for the use of flow cytometry and cell sorting in immunological studies (third edition). Eur J Immunol (2021) 51(12):2708–3145. doi: 10.1002/eji.202170126
28. Kaech SM, Tan JT, Wherry EJ, Konieczny BT, Surh CD, Ahmed R. Selective expression of the interleukin 7 receptor identifies effector CD8 T cells that give rise to long-lived memory cells. Nat Immunol (2003) 4(12):1191–8. doi: 10.1038/ni1009
29. Huster KM, Busch V, Schiemann M, Linkemann K, Kerksiek KM, Wagner H, et al. Selective expression of IL-7 receptor on memory T cells identifies early CD40L-dependent generation of distinct CD8 + memory T cell subsets. Proc Natl Acad Sci (2004) 101(15):5610–5. doi: 10.1073/pnas.0308054101
30. Schluns KS, Kieper WC, Jameson SC, Lefrançois L. Interleukin-7 mediates the homeostasis of naïve and memory CD8 T cells in vivo. Nat Immunol (2000) 1(5):426–32. doi: 10.1038/80868
31. Joshi NS, Cui W, Chandele A, Lee HK, Urso DR, Hagman J, et al. Inflammation Directs Memory Precursor and Short-Lived Effector CD8+ T Cell Fates via the Graded Expression of T-bet Transcription Factor. Immunity (2007) 27(2):281–95. doi: 10.1016/j.immuni.2007.07.010
32. Chung HK, McDonald B, Kaech SM. The architectural design of CD8+ T cell responses in acute and chronic infection: Parallel structures with divergent fates. J Exp Med (2021) 218(4). doi: 10.1084/jem.20201730

33. Kaech SM, Wherry EJ, Ahmed R. Effector and memory T-cell differentiation: implications for vaccine development. Nat Rev Immunol. (2002) 2(4):251–62. doi: 10.1038/nri778
34. Gattinoni L, Speiser DE, Lichterfeld M, Bonini C. T memory stem cells in health and disease. Nat Med. (2017) 23(1):18–27. doi: 10.1038/nm.4241
35. Lugli E, Gattinoni L, Roberto A, Mavilio D, Price DA, Restifo NP, et al. Identification, isolation and in vitro expansion of human and nonhuman primate T stem cell memory cells. Nat Protoc (2013) 8(1):33–42. doi: 10.1038/nprot.2012.143
36. Gattinoni L, Lugli E, Ji Y, Pos Z, Paulos CM, Quigley MF, et al. A human memory T cell subset with stem cell–like properties. Nat Med (2011) 17(10):1290–7. doi: 10.1038/nm.2446
37. Sallusto F, Lenig D, Förster R, Lipp M, Lanzavecchia A. Two subsets of memory T lymphocytes with distinct homing potentials and effector functions. Nature (1999) 401(6754):708–12. doi: 10.1038/44385
38. Rutishauser RL, Martins GA, Kalachikov S, Chandele A, Parish IA, Meffre E, et al. Transcriptional Repressor Blimp-1 Promotes CD8+ T Cell Terminal Differentiation and Represses the Acquisition of Central Memory T Cell Properties. Immunity (2009) 31(2):296–308. doi: 10.1016/j.immuni.2009.05.014
39. Martin MD, Badovinac VP. Defining Memory CD8 T Cell. Front Immunol (2018) 9. doi: 10.3389/fimmu.2018.02692
40. Wherry EJ, Teichgräber V, Becker TC, Masopust D, Kaech SM, Antia R, et al. Lineage relationship and protective immunity of memory CD8 T cell subsets. Nat Immunol (2003) 4(3):225–34. doi: 10.1038/ni889
41. Mahnke YD, Brodie TM, Sallusto F, Roederer M, Lugli E. The who's who of T-cell differentiation: Human memory T-cell subsets. Eur J Immunol (2013) 43(11):2797–809. doi: 10.1002/eji.201343751
42. Appay V, van Lier RAW, Sallusto F, Roederer M. Phenotype and function of human T lymphocyte subsets: Consensus and issues. Cytom Part A (2008) 73A(11):975–83. doi: 10.1002/cyto.a.20643
43. Romero P, Zippelius A, Kurth I, Pittet MJ, Touvrey C, Iancu EM, et al. Four Functionally Distinct Populations of Human Effector-Memory CD8+ T Lymphocytes. J Immunol (2007) 178(7):4112–9. doi: 10.4049/jimmunol.178.7.4112

44. Pangrazzi L, Naismith E, Meryk A, Keller M, Jenewein B, Trieb K, et al. Increased IL-15 Production and Accumulation of Highly Differentiated CD8+ Effector/Memory T Cells in the Bone Marrow of Persons with Cytomegalovirus. Front Immunol (2017) 8. doi: 10.3389/fimmu.2017.00715
45. Weekes MP, Wills MR, Mynard K, Hicks R, Sissons JGP, Carmichael AJ. Large clonal expansions of human virus-specific memory cytotoxic T lymphocytes within the CD57 + CD28 - CD8 + T-cell population. Immunology (1999) 98(3):443–9. doi: 10.1046/j.1365-2567.1999.00901.x
46. Pabst R. The pig as a model for immunology research. Cell Tissue Res (2020) 380(2):287–304. doi: 10.1007/s00441-020-03206-9
47. Cossarizza A, Chang H, Radbruch A, Acs A, Adam D, Adam-Klages S, et al. Guidelines for the use of flow cytometry and cell sorting in immunological studies (second edition). Eur J Immunol (2019) 49(10):1457–973. doi: 10.1002/eji.201970107
48. Overgaard NH, Fan TM, Schachtschneider KM, Principe DR, Schook LB, Jungersen G. Of Mice, Dogs, Pigs, and Men: Choosing the Appropriate Model for Immuno-Oncology Research. ILAR J (2018) 59(3):247–62. doi: 10.1093/ilar/ily014
49. Pauly T, Elbers K, Konig M, Lengsfeld T, Saalmuller A, Thiel H-J. Classical swine fever virus-specific cytotoxic T lymphocytes and identification of a T cell epitope. J Gen Virol (1995) 76(12):3039–49. doi: 10.1099/0022-1317-76-12-3039
50. Saalmüller A, Pauly T, Höhlich B-J, Pfaff E. Characterization of porcine T lymphocytes and their immune response against viral antigens. J Biotechnol (1999) 73(2–3):223–33. doi: 10.1016/S0168-1656(99)00140-6
51. Denyer MS, Wileman TE, Stirling CMA, Zuber B, Takamatsu H-H. Perforin expression can define CD8 positive lymphocyte subsets in pigs allowing phenotypic and functional analysis of Natural Killer, Cytotoxic T, Natural Killer T and MHC un-restricted cytotoxic T-cells. Vet Immunol Immunopathol (2006) 110(3–4):279–92. doi: 10.1016/j.vetimm.2005.10.005
52. Pauly T, Weiland E, Hirt W, Dreyer-Bux C, Maurer S, Summerfield A, et al. Differentiation between MHC-restricted and non-MHC-restricted porcine cytolytic T lymphocytes. Immunology (1996) 88(2):238–46. doi: 10.1111/j.1365-2567.1996.tb00010.x
53. Talker SC, Käser T, Reutner K, Sedlak C, Mair KH, Koinig H, et al. Phenotypic maturation

of porcine NK- and T-cell subsets. Dev Comp Immunol (2013) 40(1):51–68. doi: 10.1016/j.dci.2013.01.003

54. Moreno S, Álvarez B, Martínez P, Uenishi H, Revilla C, Ezquerra A, et al. Analysis of chemokine receptor CCR7 expression on porcine blood T lymphocytes using a CCL19-Fc fusion protein. Dev Comp Immunol (2013) 39(3):207–13. doi: 10.1016/j.dci.2012.11.010
55. Reutner K, Leitner J, Essler SE, Witter K, Patzl M, Steinberger P, et al. Porcine CD27: Identification, expression and functional aspects in lymphocyte subsets in swine. Dev Comp Immunol (2012) 38(2):321–31. doi: 10.1016/j.dci.2012.06.011
56. Martini V, Edmans M, Gubbins S, Jayaraman S, Paudyal B, Morgan S, et al. Spatial, temporal and molecular dynamics of swine influenza virus-specific CD8 tissue resident memory T cells. Mucosal Immunol (2022) 15(3):428–42. doi: 10.1038/s41385-021-00478-4
57. Rodríguez-Gómez IM, Talker SC, Käser T, Stadler M, Hammer SE, Saalmüller A, et al. Expression of T-bet, Eomesodermin and GATA-3 in porcine αβ T cells. Dev Comp Immunol (2016) 60:115–26. doi: 10.1016/j.dci.2016.02.022
58. Gerner W, Mair KH, Schmidt S. Local and Systemic T Cell Immunity in Fighting Pig Viral and Bacterial Infections. Annu Rev Anim Biosci (2022) 10(1):349–72. doi: 10.1146/annurev-animal-013120-044226
59. Zhao F-R, Xie Y-L, Liu Z-Z, Shao J-J, Li S-F, Zhang Y-G, et al. Transcriptomic analysis of porcine PBMCs in response to FMDV infection. Acta Trop (2017) 173(March):69–75. doi: 10.1016/j.actatropica.2017.05.009
60. Yang T, Zhang F, Zhai L, He W, Tan Z, Sun Y, et al. Transcriptome of Porcine PBMCs over Two Generations Reveals Key Genes and Pathways Associated with Variable Antibody Responses post PRRSV Vaccination. Sci Rep (2018) 8(1):2460. doi: 10.1038/s41598-018-20701-w
61. Zhang J, Zheng Y, Xia X-Q, Chen Q, Bade SA, Yoon K-J, et al. High-throughput whole genome sequencing of Porcine reproductive and respiratory syndrome virus from cell culture materials and clinical specimens using next-generation sequencing technology. J Vet Diagnostic Investig (2017) 29(1):41–50. doi: 10.1177/1040638716673404
62. Lunney JK, Fang Y, Ladinig A, Chen N, Li Y, Rowland B, et al. Porcine Reproductive and Respiratory Syndrome Virus (PRRSV): Pathogenesis and Interaction with the Immune

System. Annu Rev Anim Biosci. (2016) 4(1):129–54. doi: 10.1146/annurev-animal-022114-111025

63. Thanawongnuwech R, Brown GB, Halbur PG, Roth JA, Royer RL, Thacker BJ. Pathogenesis of Porcine Reproductive and Respiratory Syndrome Virus-induced Increase in Susceptibility to Streptococcus suis Infection. Vet Pathol (2000) 37(2):143–52. doi: 10.1354/vp.37-2-143

64. Brockmeier SL, Palmer M V., Bolin SR. Effects of intranasal inoculation of porcine reproductive and respiratory syndrome virus, Bordetella bronchiseptica, or a combination of both organisms in pigs. Am J Vet Res (2000) 61(8):892–9. doi: 10.2460/ajvr.2000.61.892

65. Yu J, Wu J, Zhang Y, Guo L, Cong X, Du Y, et al. Concurrent highly pathogenic porcine reproductive and respiratory syndrome virus infection accelerates Haemophilus parasuis infection in conventional pigs. Vet Microbiol (2012) 158(3–4):316–21. doi: 10.1016/j.vetmic.2012.03.001

66. Van Reeth K, Nauwynck H, Pensaert M. Dual infections of feeder pigs with porcine reproductive and respiratory syndrome virus followed by porcine respiratory coronavirus or swine influenza virus: a clinical and virological study. Vet Microbiol (1996) 48(3–4):325–35. doi: 10.1016/0378-1135(95)00145-X

67. Kolumam GA, Thomas S, Thompson LJ, Sprent J, Murali-Krishna K. Type I interferons act directly on CD8 T cells to allow clonal expansion and memory formation in response to viral infection. J Exp Med (2005) 202(5):637–50. doi: 10.1084/jem.20050821

68. Bautista EM, Molitor TW. Cell-Mediated Immunity to Porcine Reproductive and Respiratory Syndrome Virus in Swine. Viral Immunol (1997) 10(2):83–94. doi: 10.1089/vim.1997.10.83

69. López Fuertes L, Doménech N, Alvarez B, Ezquerra A, Domínguez J, Castro J., et al. Analysis of cellular immune response in pigs recovered from porcine respiratory and reproductive syndrome infection. Virus Res (1999) 64(1):33–42. doi: 10.1016/S0168-1702(99)00073-8

70. Meier WA, Galeota J, Osorio FA, Husmann RJ, Schnitzlein WM, Zuckermann FA. Gradual development of the interferon-γ response of swine to porcine reproductive and respiratory syndrome virus infection or vaccination. Virology (2003) 309(1):18–31. doi:

10.1016/S0042-6822(03)00009-6

71. Costers S, Lefebvre DJ, Goddeeris B, Delputte PL, Nauwynck HJ. Functional impairment of PRRSV-specific peripheral CD3 + CD8 high cells. Vet Res (2009) 40(5):46. doi: 10.1051/vetres/2009029
72. Mokhtar H, Pedrera M, Frossard J-P, Biffar L, Hammer SE, Kvisgaard LK, et al. The Non-structural Protein 5 and Matrix Protein Are Antigenic Targets of T Cell Immunity to Genotype 1 Porcine Reproductive and Respiratory Syndrome Viruses. Front Immunol (2016) 7. doi: 10.3389/fimmu.2016.00040
73. Ferrari L, Martelli P, Saleri R, De Angelis E, Cavalli V, Bresaola M, et al. Lymphocyte activation as cytokine gene expression and secretion is related to the porcine reproductive and respiratory syndrome virus (PRRSV) isolate after in vitro homologous and heterologous recall of peripheral blood mononuclear cells (PBMC) from pigs. Vet Immunol Immunopathol (2013) 151(3–4):193–206. doi: 10.1016/j.vetimm.2012.11.006
74. Kick A, Amaral A, Cortes L, Fogle J, Crisci E, Almond G, et al. The T-Cell Response to Type 2 Porcine Reproductive and Respiratory Syndrome Virus (PRRSV). Viruses (2019) 11(9):796. doi: 10.3390/v11090796
75. Kick AR, Wolfe ZC, Amaral AF, Cortes LM, Almond GW, Crisci E, et al. Maternal Autogenous Inactivated Virus Vaccination Boosts Immunity to PRRSV in Piglets. Vaccines (2021) 9(2):106. doi: 10.3390/vaccines9020106
76. De Bruin MGM, De Visser YE, Kimman TG, Bianchi ATJ. Time course of the porcine cellular and humoral immune responses in vivo against pseudorabies virus after inoculation and challenge: significance of in vitro antigenic restimulation. Vet Immunol Immunopathol (1998) 65(1):75–87. doi: 10.1016/S0165-2427(98)00175-5
77. Even C, Rowland RR, Plagemann PG. Cytotoxic T cells are elicited during acute infection of mice with lactate dehydrogenase-elevating virus but disappear during the chronic phase of infection. J Virol (1995) 69(9):5666–76. doi: 10.1128/jvi.69.9.5666-5676.1995
78. Weesendorp E, Morgan S, Stockhofe-Zurwieden N, Graaf DJP-D, Graham SP, Rebel JMJ. Comparative analysis of immune responses following experimental infection of pigs with European porcine reproductive and respiratory syndrome virus strains of differing virulence. Vet Microbiol (2013) 163(1–2):1–12. doi: 10.1016/j.vetmic.2012.09.013
79. Weesendorp E, Rebel JMJ, Popma-De Graaf DJ, Fijten HPD, Stockhofe-Zurwieden N.

Lung pathogenicity of European genotype 3 strain porcine reproductive and respiratory syndrome virus (PRRSV) differs from that of subtype 1 strains. Vet Microbiol (2014) 174(1–2):127–38. doi: 10.1016/j.vetmic.2014.09.010

80. Stas MR, Kreutzmann H, Stadler J, Sassu EL, Mair KH, Koch M, et al. Influence of PRRSV-1 vaccination and infection on mononuclear immune cells at the maternal-fetal interface. Front Immunol (2022) 13. doi: 10.3389/fimmu.2022.1055048

81. Butler JE, Lager KM, Golde W, Faaberg KS, Sinkora M, Loving C, et al. Porcine reproductive and respiratory syndrome (PRRS): an immune dysregulatory pandemic. Immunol Res (2014) 59(1–3):81–108. doi: 10.1007/s12026-014-8549-5

82. Loving CL, Osorio FA, Murtaugh MP, Zuckermann FA. Innate and adaptive immunity against Porcine Reproductive and Respiratory Syndrome Virus. Vet Immunol Immunopathol (2015) 167(1–2):1–14. doi: 10.1016/j.vetimm.2015.07.003

83. Yang H, Parkhouse RME. Phenotypic classification of porcine lymphocyte subpopulations in blood and lymphoid tissues. Immunology (1996) 89(1):76–83. doi: 10.1046/j.1365-2567.1996.d01-705.x

84. Masopust D, Murali-Krishna K, Ahmed R. Quantitating the Magnitude of the Lymphocytic Choriomeningitis Virus-Specific CD8 T-Cell Response: It Is Even Bigger than We Thought. J Virol (2007) 81(4):2002–11. doi: 10.1128/JVI.01459-06

85. Bose TO, Pham Q-M, Jellison ER, Mouries J, Ballantyne CM, Lefrançois L. CD11a Regulates Effector CD8 T Cell Differentiation and Central Memory Development in Response to Infection with Listeria monocytogenes. Flynn JL, editor. Infect Immun (2013) 81(4):1140–51. doi: 10.1128/IAI.00749-12

86. Mold JE, Modolo L, Hård J, Zamboni M, Larsson AJM, Stenudd M, et al. Divergent clonal differentiation trajectories establish CD8+ memory T cell heterogeneity during acute viral infections in humans. Cell Rep (2021) 35(8):109174. doi: 10.1016/j.celrep.2021.109174

87. Lu J, Ahmad R, Nguyen T, Cifello J, Hemani H, Li J, et al. Heterogeneity and transcriptome changes of human CD8+ T cells across nine decades of life. Nat Commun (2022) 13(1):5128. doi: 10.1038/s41467-022-32869-x

88. Kakaradov B, Arsenio J, Widjaja CE, He Z, Aigner S, Metz PJ, et al. Early transcriptional and epigenetic regulation of CD8+ T cell differentiation revealed by single-cell RNA sequencing. Nat Immunol (2017) 18(4):422–32. doi: 10.1038/ni.3688

89. McLane LM, Abdel-Hakeem MS, Wherry EJ. CD8 T Cell Exhaustion During Chronic Viral Infection and Cancer. Annu Rev Immunol (2019) 37(1):457–95. doi: 10.1146/annurev-immunol-041015-055318

90. Tsukumo S -i., Unno M, Muto A, Takeuchi A, Kometani K, Kurosaki T, et al. Bach2 maintains T cells in a naive state by suppressing effector memory-related genes. Proc Natl Acad Sci (2013) 110(26):10735–40. doi: 10.1073/pnas.1306691110

91. Kaech SM, Cui W. Transcriptional control of effector and memory CD8+ T cell differentiation. Nat Rev Immunol (2012) 12(11):749–61. doi: 10.1038/nri3307

92. Bennett TJ, Udupa VA V., Turner SJ. Running to Stand Still: Naive CD8+ T Cells Actively Maintain a Program of Quiescence. Int J Mol Sci (2020) 21(24):9773. doi: 10.3390/ijms21249773

93. Drouillard A, Neyra A, Mathieu A-L, Marçais A, Wencker M, Marvel J, et al. Human Naive and Memory T Cells Display Opposite Migratory Responses to Sphingosine-1 Phosphate. J Immunol (2018) 200(2):551–7. doi: 10.4049/jimmunol.1701278

94. Carlson CM, Endrizzi BT, Wu J, Ding X, Weinreich MA, Walsh ER, et al. Kruppel-like factor 2 regulates thymocyte and T-cell migration. Nature (2006) 442(7100):299–302. doi: 10.1038/nature04882

95. Bai A, Hu H, Yeung M, Chen J. Krüppel-Like Factor 2 Controls T Cell Trafficking by Activating L-Selectin (CD62L) and Sphingosine-1-Phosphate Receptor 1 Transcription. J Immunol (2007) 178(12):7632–9. doi: 10.4049/jimmunol.178.12.7632

96. Skon CN, Lee J-Y, Anderson KG, Masopust D, Hogquist KA, Jameson SC. Transcriptional downregulation of S1pr1 is required for the establishment of resident memory CD8+ T cells. Nat Immunol (2013) 14(12):1285–93. doi: 10.1038/ni.2745

97. Gautam S, Fioravanti J, Zhu W, Le Gall JB, Brohawn P, Lacey NE, et al. The transcription factor c-Myb regulates CD8+ T cell stemness and antitumor immunity. Nat Immunol (2019) 20(3):337–49. doi: 10.1038/s41590-018-0311-z

98. Omilusik KD, Best JA, Yu B, Goossens S, Weidemann A, Nguyen J V., et al. Transcriptional repressor ZEB2 promotes terminal differentiation of CD8+ effector and memory T cell populations during infection. J Exp Med (2015) 212(12):2027–39. doi: 10.1084/jem.20150194

99. Dominguez CX, Amezquita RA, Guan T, Marshall HD, Joshi NS, Kleinstein SH, et al. The

transcription factors ZEB2 and T-bet cooperate to program cytotoxic T cell terminal differentiation in response to LCMV viral infection. J Exp Med (2015) 212(12):2041–56. doi: 10.1084/jem.20150186

100. Wei H, Geng J, Shi B, Liu Z, Wang Y-H, Stevens AC, et al. Cutting Edge: Foxp1 Controls Naive CD8+ T Cell Quiescence by Simultaneously Repressing Key Pathways in Cellular Metabolism and Cell Cycle Progression. J Immunol (2016) 196(9):3537–41. doi: 10.4049/jimmunol.1501896

101. Chen Y, Zander R, Khatun A, Schauder DM, Cui W. Transcriptional and Epigenetic Regulation of Effector and Memory CD8 T Cell Differentiation. Front Immunol (2018) 9:2826. doi: 10.3389/fimmu.2018.02826

102. Rutishauser RL, Kaech SM. Generating diversity: transcriptional regulation of effector and memory CD8 + T-cell differentiation. Immunol Rev (2010) 235(1):219–33. doi: 10.1111/j.0105-2896.2010.00901.x

103. Intlekofer AM, Takemoto N, Wherry EJ, Longworth SA, Northrup JT, Palanivel VR, et al. Effector and memory CD8+ T cell fate coupled by T-bet and eomesodermin. Nat Immunol (2005) 6(12):1236–44. doi: 10.1038/ni1268

104. Gerlach C, Moseman EA, Loughhead SM, Alvarez D, Zwijnenburg AJ, Waanders L, et al. The Chemokine Receptor CX3CR1 Defines Three Antigen-Experienced CD8 T Cell Subsets with Distinct Roles in Immune Surveillance and Homeostasis. Immunity (2016) 45(6):1270–84. doi: 10.1016/j.immuni.2016.10.018

105. Sarkar S, Kalia V, Haining WN, Konieczny BT, Subramaniam S, Ahmed R. Functional and genomic profiling of effector CD8 T cell subsets with distinct memory fates. J Exp Med (2008) 205(3):625–40. doi: 10.1084/jem.20071641

106. Voehringer D, Blaser C, Brawand P, Raulet DH, Hanke T, Pircher H. Viral Infections Induce Abundant Numbers of Senescent CD8 T Cells. J Immunol (2001) 167(9):4838–43. doi: 10.4049/jimmunol.167.9.4838

107. Jiang Y, Li Y, Zhu B. T-cell exhaustion in the tumor microenvironment. Cell Death Dis (2015) 6(6):e1792–e1792. doi: 10.1038/cddis.2015.162

108. Christiaansen AF, Dixit UG, Coler RN, Marie Beckmann A, Reed SG, Winokur PL, et al. CD11a and CD49d enhance the detection of antigen-specific T cells following human vaccination. Vaccine (2017) 35(33):4255–61. doi: 10.1016/j.vaccine.2017.06.013

109. Oh J, Magnuson A, Benoist C, Pittet MJ, Weissleder R. Age-related tumor growth in mice is related to integrin α 4 in CD8+ T cells. JCI Insight (2018) 3(21). doi: 10.1172/jci.insight.122961

110. Huang H, Li S, Zhang Y, Han X, Jia B, Liu H, et al. CD8 + T Cell Immune Response in Immunocompetent Mice during Zika Virus Infection. Diamond MS, editor. J Virol (2017) 91(22). doi: 10.1128/JVI.00900-17

111. Ahn E, Araki K, Hashimoto M, Li W, Riley JL, Cheung J, et al. Role of PD-1 during effector CD8 T cell differentiation. Proc Natl Acad Sci (2018) 115(18):4749–54. doi: 10.1073/pnas.1718217115

112. Kalia V, Sarkar S. Regulation of Effector and Memory CD8 T Cell Differentiation by IL-2—A Balancing Act. Front Immunol (2018) 9(December):2987. doi: 10.3389/fimmu.2018.02987

113. Srenathan U, Steel K, Taams LS. IL-17+ CD8+ T cells: Differentiation, phenotype and role in inflammatory disease. Immunol Lett (2016) 178:20–6. doi: 10.1016/j.imlet.2016.05.001

114. Huang Z, Zak J, Pratumchai I, Shaabani N, Vartabedian VF, Nguyen N, et al. IL-27 promotes the expansion of self-renewing CD8+ T cells in persistent viral infection. J Exp Med (2019) 216(8):1791–808. doi: 10.1084/jem.20190173

115. Jia L, Shi Y, Wen Y, Li W, Feng J, Chen C. The roles of TNFAIP2 in cancers and infectious diseases. J Cell Mol Med (2018) 22(11):5188–95. doi: 10.1111/jcmm.13822

116. Das T, Chen Z, Hendriks RW, Kool M. A20/Tumor Necrosis Factor α-Induced Protein 3 in Immune Cells Controls Development of Autoinflammation and Autoimmunity: Lessons from Mouse Models. Front Immunol (2018) 9(FEB):104. doi: 10.3389/fimmu.2018.00104

117. Just S, Nishanth G, Buchbinder JH, Wang X, Naumann M, Lavrik I, et al. A20 Curtails Primary but Augments Secondary CD8+ T Cell Responses in Intracellular Bacterial Infection. Sci Rep (2016) 6(1):39796. doi: 10.1038/srep39796

118. Liu JY, Li F, Wang LP, Chen XF, Wang D, Cao L, et al. CTL- vs Treg lymphocyte-attracting chemokines, CCL4 and CCL20, are strong reciprocal predictive markers for survival of patients with oesophageal squamous cell carcinoma. Br J Cancer (2015) 113(5):747–55. doi: 10.1038/bjc.2015.290

119. Chen R, Ma L, Jiang C, Zhang S. Expression and potential role of CCL4 in CD8+T cells in NSCLC. Clin Transl Oncol (2022) 24(12):2420–31. doi: 10.1007/s12094-022-02913-9

120. Lei Y, Takahama Y. XCL1 and XCR1 in the immune system. Microbes Infect (2012) 14(3):262–7. doi: 10.1016/j.micinf.2011.10.003
121. Kelner GS, Kennedy J, Bacon KB, Kleyensteuber S, Largaespada DA, Jenkins NA, et al. Lymphotactin: a Cytokine that Represents a New Class of Chemokine. Science (1994) 266(5189):1395–9. doi: 10.1126/science.7973732
122. Groom JR, Luster AD. CXCR3 in T cell function. Exp Cell Res (2011) 317(5):620–31. doi: 10.1016/j.yexcr.2010.12.017
123. Shyer JA, Flavell RA, Bailis W. Metabolic signaling in T cells. Cell Res (2020) 30(8):649–59. doi: 10.1038/s41422-020-0379-5
124. Devadas S, Zaritskaya L, Rhee SG, Oberley L, Williams MS. Discrete Generation of Superoxide and Hydrogen Peroxide by T Cell Receptor Stimulation. J Exp Med (2002) 195(1):59–70. doi: 10.1084/jem.20010659
125. Mak TW, Grusdat M, Duncan GS, Dostert C, Nonnenmacher Y, Cox M, et al. Glutathione Primes T Cell Metabolism for Inflammation. Immunity (2017) 46(4):675–89. doi: 10.1016/j.immuni.2017.03.019
126. Ananieva EA, Patel CH, Drake CH, Powell JD, Hutson SM. Cytosolic Branched Chain Aminotransferase (BCATc) Regulates mTORC1 Signaling and Glycolytic Metabolism in CD4+ T Cells. J Biol Chem (2014) 289(27):18793–804. doi: 10.1074/jbc.M114.554113
127. Peng M, Yin N, Chhangawala S, Xu K, Leslie CS, Li MO. Aerobic glycolysis promotes T helper 1 cell differentiation through an epigenetic mechanism. Science (2016) 354(6311):481–4. doi: 10.1126/science.aaf6284
128. Dai M, Wang L, Yang J, Chen J, Dou X, Chen R, et al. LDHA as a regulator of T cell fate and its mechanisms in disease. Biomed Pharmacother (2023) 158:114164. doi: 10.1016/j.biopha.2022.114164
129. Kallies A, Good-Jacobson KL. Transcription Factor T-bet Orchestrates Lineage Development and Function in the Immune System. Trends Immunol (2017) 38(4):287–97. doi: 10.1016/j.it.2017.02.003
130. Xin G, Schauder DM, Lainez B, Weinstein JS, Dai Z, Chen Y, et al. A Critical Role of IL-21-Induced BATF in Sustaining CD8-T-Cell-Mediated Chronic Viral Control. Cell Rep (2015) 13(6):1118–24. doi: 10.1016/j.celrep.2015.09.069
131. Huber M, Lohoff M. IRF4 at the crossroads of effector T-cell fate decision. Eur J Immunol

(2014) 44(7):1886–95. doi: 10.1002/eji.201344279

132. Fu S-H, Yeh L-T, Chu C-C, Yen BL-J, Sytwu H-K. New insights into Blimp-1 in T lymphocytes: a divergent regulator of cell destiny and effector function. J Biomed Sci (2017) 24(1):49. doi: 10.1186/s12929-017-0354-8

133. Li J, He Y, Hao J, Ni L, Dong C. High Levels of Eomes Promote Exhaustion of Anti-tumor CD8+ T Cells. Front Immunol (2018) 9. doi: 10.3389/fimmu.2018.02981

134. Yang CY, Best JA, Knell J, Yang E, Sheridan AD, Jesionek AK, et al. The transcriptional regulators Id2 and Id3 control the formation of distinct memory CD8+ T cell subsets. Nat Immunol (2011) 12(12):1221–9. doi: 10.1038/ni.2158

135. Collins S, Wolfraim LA, Drake CG, Horton MR, Powell JD. Cutting Edge: TCR-Induced NAB2 Enhances T Cell Function by Coactivating IL-2 Transcription. J Immunol (2006) 177(12):8301–5. doi: 10.4049/jimmunol.177.12.8301

136. Zhan Y, Carrington EM, Zhang Y, Heinzel S, Lew AM. Life and Death of Activated T Cells: How Are They Different from Naïve T Cells? Front Immunol (2017) 8(DEC):1–9. doi: 10.3389/fimmu.2017.01809

137. Gautam S, Fioravanti J, Zhu W, Le Gall JB, Brohawn P, Lacey NE, et al. The transcription factor c-Myb regulates CD8+ T cell stemness and antitumor immunity. Nat Immunol (2019) 20(3):337–49. doi: 10.1038/s41590-018-0311-z

138. Yao C, Lou G, Sun H-W, Zhu Z, Sun Y, Chen Z, et al. BACH2 enforces the transcriptional and epigenetic programs of stem-like CD8+ T cells. Nat Immunol (2021) 22(3):370–80. doi: 10.1038/s41590-021-00868-7

139. Roychoudhuri R, Clever D, Li P, Wakabayashi Y, Quinn KM, Klebanoff CA, et al. BACH2 regulates CD8+ T cell differentiation by controlling access of AP-1 factors to enhancers. Nat Immunol (2016) 17(7):851–60. doi: 10.1038/ni.3441

140. Li Q, Eppolito C, Odunsi K, Shrikant PA. IL-12-Programmed Long-Term CD8 + T Cell Responses Require STAT4. J Immunol (2006) 177(11):7618–25. doi: 10.4049/jimmunol.177.11.7618

141. Quigley M, Huang X, Yang Y. STAT1 Signaling in CD8 T Cells Is Required for Their Clonal Expansion and Memory Formation Following Viral Infection In Vivo. J Immunol (2008) 180(4):2158–64. doi: 10.4049/jimmunol.180.4.2158

142. Cannarile MA, Lind NA, Rivera R, Sheridan AD, Camfield KA, Wu BB, et al.

Transcriptional regulator Id2 mediates CD8+ T cell immunity. Nat Immunol (2006) 7(12):1317–25. doi: 10.1038/ni1403

143. Yoshida K, Sakamoto A, Yamashita K, Arguni E, Horigome S, Arima M, et al. Bcl6 controls granzyme B expression in effector CD8+ T cells. Eur J Immunol (2006) 36(12):3146–56. doi: 10.1002/eji.200636165

144. Groom JR, Luster AD. CXCR3 ligands: redundant, collaborative and antagonistic functions. Immunol Cell Biol (2011) 89(2):207–15. doi: 10.1038/icb.2010.158

145. Peperzak V, Veraar EAM, Xiao Y, Bąbała N, Thiadens K, Brugmans M, et al. CD8+ T Cells Produce the Chemokine CXCL10 in Response to CD27/CD70 Costimulation To Promote Generation of the CD8+ Effector T Cell Pool. J Immunol (2013) 191(6):3025–36. doi: 10.4049/jimmunol.1202222

146. Palmer EM, Holbrook BC, Arimilli S, Parks GD, Alexander-Miller MA. IFNγ-producing, virus-specific CD8+ effector cells acquire the ability to produce IL-10 as a result of entry into the infected lung environment. Virology (2010) 404(2):225–30. doi: 10.1016/j.virol.2010.05.004

147. Trandem K, Zhao J, Fleming E, Perlman S. Highly Activated Cytotoxic CD8 T Cells Express Protective IL-10 at the Peak of Coronavirus-Induced Encephalitis. J Immunol (2011) 186(6):3642–52. doi: 10.4049/jimmunol.1003292

148. Sun J, Madan R, Karp CL, Braciale TJ. Effector T cells control lung inflammation during acute influenza virus infection by producing IL-10. Nat Med (2009) 15(3):277–84. doi: 10.1038/nm.1929

149. Sun J, Dodd H, Moser EK, Sharma R, Braciale TJ. CD4+ T cell help and innate-derived IL-27 induce Blimp-1-dependent IL-10 production by antiviral CTLs. Nat Immunol (2011) 12(4):327–34. doi: 10.1038/ni.1996

150. Elsaesser H, Sauer K, Brooks DG. IL-21 Is Required to Control Chronic Viral Infection. Science (2009) 324(5934):1569–72. doi: 10.1126/science.1174182

151. Fröhlich A, Kisielow J, Schmitz I, Freigang S, Shamshiev AT, Weber J, et al. IL-21R on T Cells Is Critical for Sustained Functionality and Control of Chronic Viral Infection. Science (2009) 324(5934):1576–80. doi: 10.1126/science.1172815

152. Kwon H, Thierry-Mieg D, Thierry-Mieg J, Kim H-P, Oh J, Tunyaplin C, et al. Analysis of Interleukin-21-Induced Prdm1 Gene Regulation Reveals Functional Cooperation of

STAT3 and IRF4 Transcription Factors. Immunity (2009) 31(6):941–52. doi: 10.1016/j.immuni.2009.10.008

153. Gong D, Malek TR. Cytokine-Dependent Blimp-1 Expression in Activated T Cells Inhibits IL-2 Production. J Immunol (2007) 178(1):242–52. doi: 10.4049/jimmunol.178.1.242

154. Grosso JF, Goldberg M V., Getnet D, Bruno TC, Yen H-R, Pyle KJ, et al. Functionally Distinct LAG-3 and PD-1 Subsets on Activated and Chronically Stimulated CD8 T Cells. J Immunol (2009) 182(11):6659–69. doi: 10.4049/jimmunol.0804211

155. McCoy KD, Le Gros G. The role of CTLA-4 in the regulation of T cell immune responses. Immunol Cell Biol (1999) 77(1):1–10. doi: 10.1046/j.1440-1711.1999.00795.x

156. Kuchroo VK, Anderson AC, Petrovas C. Coinhibitory receptors and CD8 T cell exhaustion in chronic infections. Curr Opin HIV AIDS (2014) 9(5):439–45. doi: 10.1097/COH.0000000000000088

157. Jin H-T, Anderson AC, Tan WG, West EE, Ha S-J, Araki K, et al. Cooperation of Tim-3 and PD-1 in CD8 T-cell exhaustion during chronic viral infection. Proc Natl Acad Sci (2010) 107(33):14733–8. doi: 10.1073/pnas.1009731107

158. Hudson WH, Gensheimer J, Hashimoto M, Wieland A, Valanparambil RM, Li P, et al. Proliferating Transitory T Cells with an Effector-like Transcriptional Signature Emerge from PD-1+ Stem-like CD8+ T Cells during Chronic Infection. Immunity (2019) 51(6):1043-1058.e4. doi: 10.1016/j.immuni.2019.11.002

159. Chandele A, Sewatanon J, Gunisetty S, Singla M, Onlamoon N, Akondy RS, et al. Characterization of Human CD8 T Cell Responses in Dengue Virus-Infected Patients from India. Diamond MS, editor. J Virol (2016) 90(24):11259–78. doi: 10.1128/JVI.01424-16

160. Babbe H, Chester N, Leder P, Reizis B. The Bloom's Syndrome Helicase Is Critical for Development and Function of the α β T-Cell Lineage. Mol Cell Biol (2007) 27(5):1947–59. doi: 10.1128/MCB.01402-06

161. Lagumdzic E, Pernold C, Viano M, Olgiati S, Schmitt MW, Mair KH, et al. Transcriptome Profiling of Porcine Naïve, Intermediate and Terminally Differentiated CD8+ T Cells. Front Immunol (2022) 13. doi: 10.3389/fimmu.2022.849922

162. Gupta SS, Wang J, Chen M. Metabolic Reprogramming in CD8+ T Cells During Acute Viral Infections. Front Immunol (2020) 11. doi: 10.3389/fimmu.2020.01013

163. Peper JK, Schuster H, Löffler MW, Schmid-Horch B, Rammensee H-G, Stevanović S. An

impedance-based cytotoxicity assay for real-time and label-free assessment of T-cell-mediated killing of adherent cells. J Immunol Methods (2014) 405:192–8. doi: 10.1016/j.jim.2014.01.012

164. Hwang B, Lee JH, Bang D. Single-cell RNA sequencing technologies and bioinformatics pipelines. Exp Mol Med (2018) 50(8):1–14. doi: 10.1038/s12276-018-0071-8